MATHEMATICAL MODELING OF BLOOD FLOW AND HEAT TRANSFER IN THE HUMAN CARDIOVASCULAR SYSTEM

BY

SALIHU, Nasiru Omeiza
PhD/SPS/2017/1028

DEPARTMENT OF MATHEMATICS

FEDERAL UNIVERSITY OF TECHNOLOGY

MINNA

SEPTEMBER, 2023

MATHEMATICAL MODELING OF BLOOD FLOW AND HEAT TRANSFER IN THE HUMAN CARDIOVASCULAR SYSTEM

BY

SALIHU, Nasiru Omeiza
PhD/SPS/2017/1028

A THESIS SUBMITTED TO THE POSTGRADUATE SCHOOL FEDERAL UNIVERSITY OF TECHNOLOGY, MINNA, NIGERIA IN PARTIAL FULFILLMENT OF THE REQUIREMENTS FOR THE AWARD OF THE DEGREE OF DOCTOR OF PHILOSOPHY (PhD) IN MATHEMATICS

SEPTEMBER, 2023

DECLARATION

I hereby declare that this thesis titled: "**Mathematical Modeling of Blood Flow and Heat Transfer in the Human Cardiovascular System**" is a collection of my original research work and it has not been presented for any other qualification anywhere. Information from other sources (published or unpublished) has been duly acknowledged.

SALIHU, Nasiru Omeiza
PhD/SPS/2017/1028
FEDERAL UNIVERSITY OF TECHNOLOGY,
MINNA, NIGERIA

...……
SIGNATURE/DATE

CERTIFICATION

The thesis titled: "**Mathematical Modeling of Blood Flow and Heat Transfer in the Human Cardiovascular System**" by SALIHU, Nasiru Omeiza, (PhD/SPS/2017/1028) meets the regulations governing the award of the degree of Doctor of Philosophy of the Federal University of Technology, Minna and it is approved for its contribution to scientific knowledge and literary presentation.

Prof. Y. M. Aiyesimi ----------
MAJOR SUPERVISOR Signature & Date

Prof. M. Jiya ----------
CO- SUPERVISOR Signature & Date

Prof. G. A. Bolarin ----------
CO- SUPERVISOR Signature & Date

Prof. A. I. Enagi ----------
HEAD OF DEPARTMENT Signature & Date

Prof. M. Jiya ----------
DEAN, SCHOOL OF PHYSICAL SCIENCES Signature & Date

Prof. O. K. Abubakre ----------
DEAN, POSTGRADUATE SCHOOL Signature & Date

DEDICATION

This research work is dedicated to God Almighty, the infinite source of knowledge and wisdom, for his guidance and protection over me.

ACKNOWLEDGEMENTS

All thanks and unending glory to Almighty God, the exalted, who granted me the inspiration and stamina all along to complete this humble work.

I sincerely wish to express my profound gratitude to my Major supervisor, Prof. Y. M. Aiyesimi and my Co-supervisors, Prof. M. Jiya and Prof. G. A. Bolarin for their support and encouragement in making this research work a success. I sincerely want to thank all my teachers at all levels under whom I studied. Without their being teachers, I would not have arrived at where I am today.

I would like to appreciate the effort of Prof. A.I. Enagi (Head of Department), Prof. K. R. Adeboye, Prof. N. I. Akinwande, Prof. Y. A. Yahaya, Prof. U.Y. Abubakar, Prof. D. Hakimi, Prof. M. D. Shehu, Prof. A. A. Mohammed, Prof. R .O. Olayiwola, Prof. A. Ndanusa, Dr. A. T. Cole, Dr. U. Mohammed, Dr. R. O. Jimoh, Dr. S. I. Yusuf, Dr. R. Mohammed, Dr. N. Ngutor, Dr. A. Yusuf, Dr. S.A Somma, Dr. F. A. Oguntolu, Dr. A. Yusuf, Dr. Khadeejah James Audu, Mrs. N. Abdurrahman, Mr. A. C, Ugwu, Mr. Z. Abraham and all other members of staff who contributed greatly to the success of this research work.

My special appreciation also goes to my parents, Mr. & Mrs. Salihu Otaru and other well-wishers for their support. I am immeasurably blessed and fulfilled to have you all.

ABSTRACT

This thesis presents a theoretical study of blood flow and heat transfer in the cardiovascular system of humans undergoing tumor treatment under the action of an externally applied magnetic field. The fluid (blood) medium is assumed to be porous in nature. The variable viscosity of blood depending on hematocrit is taken into account in order to improve the resemblance to the real situation. The temperature-dependent blood thermal conductivity is considered. The transient governing equations for laminar, incompressible and Newtonian fluid and heat transfer are solved by using the Generalized Polynomial Approximation Method (GPAM). The solutions are obtained for flow velocity and heat transfer in both tissue and blood. The computations were done using the Computer Symbolic Algebraic Package MAPLE 17 version and the results are presented graphically. It is observed that the influence of hematocrit, magnetic field, permeability parameter, Reynolds number and Pressure gradient have an important impact on the velocity profile. Moreover, the effect of Peclet number, pressure gradient and perfusion mass flow rate on the tissue and blood temperature profiles has been significantly observed. From the results obtained, it was observed that the flow velocity is at maximum value $\phi(\eta,t)=3.1$ when $\eta=0$ while blood temperature attained maximum values when $\eta=0$ and $t=0.5$. The research revealed that the blood flow velocity tends to zero $\left(\phi(\eta,t)\to 0\right)$ as the Hartmann number varies from 0 to 4.0. This implies that the strength of Lorentz force produced become stronger with an increase in Hartmann number that leads to retardation on the blood's motion and this indicates that to ensure the flow along the artery region is properly controlled, a certain strength of magnetic intensity is required. The research also revealed that at a temperature ratio, $(\alpha=0)$ the blood temperature was minimal while the temperature ratio $(\alpha=-1.0,\ \alpha=1.0)$ resulted in a maximal high blood temperature. This implies that the heat required for tumor treatment can be boosted when blood thermal conductivity depends on tissue temperature. It can be concluded that the flow of blood can be controlled by the application of an external magnetic field.

TABLE OF CONTENTS

LIST OF TABLES

LIST OF FIGURES

CHAPTER ONE

1.0 INTRODUCTION

1.1 Background to the Study

The cardiovascular system is the blood transport mechanism that enables the nutrient transport to the tissues and organs of the body and the removal of various waste and toxic substances (Urquiza *et al*., 2005). It consists of three major components listed as the heart (the system's pump that pump blood around the body), the blood vessel (the delivery routes) and the blood (a fluid that contains the needed oxygen and nutrients for the body and carries the wastes that needed to be removed). Generally, the cardiovascular system comprises of two connected distinct systems: The systemic circulation that provide organs, tissues and cells with blood so that they can get oxygen and other vital substances (Taura *et al*., 2012), the pulmonary circulation where the fresh oxygen we breathe in flows into the blood. Simultaneously, carbon dioxide is being released from the blood.

The major function of cardiovascular system is to support blood flow to all parts of the body for its survival. The function of the arteries is to carry blood away from the heart while the veins take it back to the heart. Used blood is being delivered through the veins from the body back to the heart (Tripathi *et al*., 2017). The blood in the veins has a low content of oxygen as a result of the fact that it has been taken out by the body and a high content of carbon dioxide because the body has absorbed it back into the blood (Bessonov *et al*., 2016). All the veins flow into the superior and inferior vena cava which then flow into the right atrium. The right atrium pushes blood into the right ventricle, and then the right ventricle pushes blood to the pulmonary trunk via the pulmonary arteries into the lungs. Right in the lungs, the blood collects the oxygen that

is breathe in and removes the carbon dioxide that is breathe out (Malatos *et al*., 2016). Away from the lungs, blood flows into the left atrium and is then drives into the left ventricle which then moves this oxygenated blood into the aorta and it is distributed through the other arteries to the rest of the body in order for the body to perform its usual functions. Again, this blood will go back to the heart via the veins and the circulation continues (Gumez *et al*., 2017). Arterioles are the smallest vessels of the arterial system. They serve as the major factor of blood pressure as blood flow to the individual organs. Arterioles have a much smaller diameter than arteries and it provides important opposition to the blood flow (Mohan *et al*., 2012). This opposition creates pressure in circulatory system. Pressure is needed to give adequate flow of blood to all parts of the body. Blood flow to individual organs can be monitored by controlling the diameter of the arterioles (Bali and Awasthi, 2011). Vasodilatation (dilation or relaxation of the arterioles to allow more blood to the area) of an arteriole lowers the opposition and results to an increase in flow through that particular arterioles (Labadin and Ahmadi, 2006).

The examination of heat transfer and blood flow in biological processes demands exact or careful mathematical models. The biological processes normally involve two stages namely solid and liquid (fluid). Thermal ablation therapy is an application of heat transfer and fluid flow in biological processes. Temperature plays an important role with tissue interactions (Aiyesimi and Salihu, 2016). The blood flow in a tissue mainly has a direction from artery to vein passing through the capillary bed, the blood and its surrounding tissues are not in thermal equilibrium when the blood vessel diameter is larger which means the energy equations for tissue and blood in large vessels must be treated one at a time. One of the crucial issues of thermal treatments is blood flow. Blood flow usually drains the free heat from the heating region, which causes

inadequate thermal dose in the targeted volume. This is an important factor needing to be treated carefully in thermal treatments (Shih *et al.,* 2006).

Blood exhibits anomalous viscous properties. The uncertain behavior of blood is normally due to the suspension of particles in plasma. The plasma content in the blood obeys the linear Newtonian model for viscosity (Liu *et al.*, 2022). Nevertheless, blood in its totality is frequently considered as Non-Newtonian fluid, especially when the characteristic dimension of the flow is close to the cell dimension. The practical observations and theoretical analysis of blood flow are very important for the diagnosis of a number of cardiovascular diseases and development of pathological categories in animal and human physiology (Srivastava and Rivastava, 2009). The flow of blood via small diameter tubes is of physiological and clinical significance. As a result of its complexity and uncertainty behaviour, it is always difficult to analyze it. The two types of anomaly are due to low shear and high shear effects (Muhammad and Zuhaila, 2019). When blood flows via larger diameter arteries at high shear rates, it acts like a Newtonian fluid.

1.2 Statement of the Research Problem

The effects of blood flow and heat transfer in the cardiovascular system has not been adequately and mathematically studied to date. One of the motivations to study the blood flow is to understand the conditions that may contribute to cardiovascular diseases (Tripathi *et al*., 2017). The practical observations and mathematical study of these blood flow and heat transfer are very important for the diagnosis of a number of cardiovascular diseases (Khushboo *et al*., 2017). Hence, the needs for this research.

1.3 Significance of the Study

Many cardiovascular diseases like the arterial blockage is one of the leading causes of death worldwide (Perez *et al*., 2017). The partial obstructions of the arteries due to stenosis not only restrain the regular flow of blood but also associated with hardening and thickening of the arterial wall. However, the major cause of this formation of narrowing in a blood vessel is still unknown but it is well confirmed that the fluid dynamical factors play a significant role as to further development of this narrowing in the blood vessel. In the time immemorial, the observation of heat transfer and fluid flow in biological processes demands correct mathematical models. To meet these criteria, many researchers around the world have proposed mathematical models in various dimensions in an attempt to properly describe the heat transfer and fluid flow in biological processes in a heated, vascularized, finite tissue by making a few simplifying assumptions. One of the key issues of thermal treatments is blood flow. Blood flow usually drains the delivered heat from the heating region, which now causes insufficient thermal dose in the targeted volume. This is an important factor to be considered carefully in thermal treatments (Shih *et al*., 2006). In fact, the differential therapeutic effects of thermal treatments between malignant and normal tissue may primarily depend on the vascular characteristics of the tumor (Song *et al.*, 1984). There is need for more research in this area. Therefore, the need for this research work.

1.4 Scope and Limitation of the Study

This research work focus on the mathematical modeling of blood flow and heat transfer impacts in the human cardiovascular system with pulsation and time dependent thermal conductivity. The research is limited to the mathematical study alone.

1.5 Aim and Objectives of the Study

1.5.1 Aim of the Study

The aim of this research is to mathematically analyze the effects of unsteadiness, variable viscosity and variable thermal conductivity on the blood flow and heat transfer in the human cardiovascular system.

1.5.2 Objectives of the Study

The objectives of the study are to:

i. Present mathematical equations governing blood flow and heat transfer in the cardiovascular system of a body undergoing hyperthermia.

ii. Solve the model equations using Olayiwola's Generalized Polynomial Approximation Method (OGPAM).

iii. Provide graphical summaries of the system responses.

iv. Validate the result obtained with the existing literature.

1.6 Definition of Terms

Artery: A stream blood vessel from the heart carrying blood away from the heart paying no attention to oxygenation status.

Axisymmetric Flow: A flow is said to be axisymmetric if the pressure and the cylindrical velocity components are independent of the angular variable.

Boundary Value Problem: This is a differential equation that has all of the conditions specified at different values or more than one value of the independent variable in the equation. The problem $y'' + 2y' = e^x; y(0) = 1, y(1) = 1$ is a boundary value problem because the two subsidiary conditions are given as $x = 0$ and $x = 1$

Blood Flow: This is the movement of blood through a vessel, tissue, or organ.

Blood Vessel: An elastic passage through which blood circulates in the body. The three major types of blood vessel are: the arteries, the capillaries and the tissues/veins.

Cardiovascular System: This is the blood transport mechanism that enables the nutrient transport to the tissues and organs of the body and the removal of various waste and toxic substances.

Capillary: This is any of the small blood vessels that join arteries to veins.

Deoxygenated Blood: This is the blood which has a low level of oxygen saturation in the lung. It is also known as venous blood.

Heat Transfer: This is the movement of thermal energy from one point to another point of different temperature by means of conduction (through direct contact), convection (through fluid movement) or radiation (through electromagnetic waves).

Hematocrit: This is an instrument for analyzing/measuring the percentage by volume of red blood cells and plasma in the blood.

Hyperthermia: The condition of having a body temperature greatly above normal.

Initial Value Problem: This is a differential equation that has all of the conditions specified at the same value of the independent variable in the equation (and that value is at the lower boundary of the domain). The problem $y'' + 2y' = e^x; y(\pi) = 1, y'(\pi) = 2$ is an initial value problem because the two subsidiary conditions are given at $x = \pi$.

Incompressible Flow: An incompressible flow is flow in which the fluid flow density remain unchanged when the pressure changes.

Laminar Flow: This is a flow in which the fluid travels smoothly in regular paths that never interfere with one another. The velocity of the fluid is always constant at any point of the fluid.

Lesion: This is any abnormal change in the tissue of an organism generally caused by disease or trauma including tumours, ulcers, sores and wound.

Mathematical Model: This is a description of a system using mathematical concepts and language.

Mathematical Modeling: This is the process of developing a mathematical model.

Newtonian Fluid: This is a fluid whose viscosity does not change with rate of flow. It is a fluid in which some viscous stresses from its flow at every point in time are linearly proportional to the local strain rate (the rate of change of its deformation over time).

No-slip Boundary Condition: The no-slip boundary condition for viscous fluids assumes that at a solid boundary, the fluid will have zero velocity relative to the boundary.

Nutrient: This is an important substance such as food needed to keep a living thing alive and grow.

Organ: This is a part of the body that performs similar and particular function.

Oxygenated Blood: This is the blood which has been exposed to the high level of oxygen in the lung. It is also called arterial blood.

Porous Medium: This is a medium or material containing pores that are typically filled with a fluid.

Pulmonary Circulation: This is the part of the cardiovascular system which transports deoxygenated blood away from the heart to the lungs and brings back oxygenated blood to the heart.

Pulsatile Flow: This is a flow where the pressure gradient varies periodically with time. Pulsatile flow is also known as womersley flow.

Pulsation: This is a periodically recurring alternate increase and decrease of a quantity (such as pressure, volume, or voltage)

Stenosis: This is an abnormal constriction or narrowing of the diameter of a blood vessel.

Systematic Circulation: This is the part of the cardiovascular system which transports oxygenated blood away from the heart to the body and brings back deoxygenated blood to the heart.

Thermal Conductivity: This is the rate at which heat passes through a specified material, expressed as the amount of heat that flows per unit time through a unit area with a temperature gradient of one degree per unit distance.

Thermal Energy: This is the energy possessed by an object or system due to the movement of particles within the object or the system.

Thermal Lesion: This is defined as tissue injury as a result of application of heat in any form to the internal or external body surfaces.

Tissue: A collection of similar cells that work together to do a unique job.

Vein: A blood vessel that conveys blood from the capillaries back to the heart.

CHAPTER TWO

2.0 LITERATURE REVIEW

2.1 Blood Flow Model

Most of the models such as Haik *et al*. (2001), Womersley (1955), Lightfoot (1974), Sud and Sekhon (1985) and Chaturani and Palanisamy (1991) on blood flow deal with one phase model. Thus, for the fact that blood is a suspension, a two phase model seems to be more suitable. Wagh and Wagh (1992) used Saffman (1962), a model of dusty gas to analyze the effects of the magnetic nature of red blood cells of the blood flow. The reason being that, blood is a liquid suspension having mass and volume concentrations almost the same, however, for dusty gas, the mass and bulk concentrations are quite different. Nayfeh (1966) and Sanyal *et al*. (2007) said two phase model seems to be more suitable for blood flow.

Pries *et al.* (1992) studied the effects of the tube diameter and the hematocrit ratio on the blood viscosity and discovered that for tube diameters greater than 1 mm, the blood viscosity does not depend on the diameter while for tube diameter less than 1 mm, the blood viscosity is highly dependent on the tube diameter. They also recounted that the viscosity increases non-linearly with the hematocrit. Srivastava and Rivastava (2009), Sharan and Popel (2001), Srivastava *et al*. (2007) and Sankar and Lee (2008) have conveyed that for blood flowing through narrow blood vessels, there is an auxiliary layer of plasma and a center region of suspension of all the erythrocytes. Also, the red blood cell is a major bio-magnetic substance and the blood flow may be affected by the magnetic field (Mishra and Verma, 2007). The impact of magnetic field on the blood flow has been studied theoretically by treating blood as an electrically conductive fluid

(Chen, 1985). Believing blood as a magnetic fluid, it may be possible to control the blood pressure and its flow behavior by using a suitable magnetic field. Therefore, such studies have potential for therapeutic use in the diseases of heart, blood and blood vessels (Srivastava *et al*., 2012)

Several researches were carried out by Young (1979), Young and Tsai (1973) to understand the impacts of abnormal narrowing (stenosis) on the flow of blood through arteries. Tu and Deville (1996) studied the pulsatile flow of blood in stenosed arteries. For the fact that blood has complicated rheological qualities, it acts like different fluid model under different biological and structural state. As a result of this condition, MacDonald (1979) observed that vessels of radius greater than 0.025 cm can be considered as a homogeneous Newtonian fluid and in contrary, Caro *et al.* (1978) and Caro (2001) remarked that normal arterial blood flow at high shear rates, blood acts like a Newtonian fluid. Misra and Chakravorty (1986) and Shit and Roy (2012) formulated a mathematical model of the unsteady flow of blood through arteries having abnormal narrowing (stenosis) where blood was handled as a Newtonian viscous incompressible fluid. Some experimental analysis of Liepsch (1986) and Liepsch (2002) discovered that at a low shear rates blood may acts as non-newtonian fluid in large arteries. It is a well-known fact that blood being a suspension of red blood cells in plasma act like a non-Newtonian fluid at a low shear rates as reported in Buchanan *et al*. (2000) and Whitemore (1959). Misra and Shit (2006) and Misra and Shit (2007) studied in two different conditions on the flow of blood through the abnormal narrowing of arteries (stenosis) by handling blood as a non-Newtonian fluid model with or without considering slip effects. Tian *et al*. (2013) investigated on the pulsatile non-Newtonian flow through a stenosed artery with atherosclerosis. Chen *et al*. (2006) studied the non-

Newtonian impacts of blood flow in hemodynamics on distal vascular graft anastomoses. The hemodynamics linked with a single stenotic lesion is seriously affected by the presence of a second lesion. In most conditions, there are observations of the presence of the multiple stenoses such as the patients of angiogram. Misra *et al.* (2008a) performed a theoretical study of the impacts of overlapping stenosis. An experimental analysis of blood flow via an arterial part having overlapping stenoses was made by (Talukder *et al.* 1977). The impacts of multiple stenoses via an arterial stenosis have been efficaciously carried out analytically and numerically by Chakravarty and Mondal (1994) and Layek *et al.* (2009) respectively. Hence, all these analyses are limited to the condition of both the externally applied magnetic field and the porous medium. The impact of magnetic field on the flow of blood has been studied theoretically and practically by many researchers like Varshney *et al.* (2010), Haik *et al.* (2001), Chakeras *et al.* (2003) and Kinouchi *et al.* (1996) on various conditions. Shit and Roy (2017), Misra *et al.* (2011), Misra and Shit (2009) and Misra *et al.* (2008b) studied various flow behaviour of blood in arteries by analysing a Newtonian/non-Newtonian model with a uniform magnetic field. The studies of blood flow via a porous medium have gained serious attention to the medical practitioners as a result of its massive changes in the flow conditions. The capillary endothelium is wrapped by a thin layer lining of the alveoli which has been treated as a porous medium. Dash *et al.* (1996) studied the Brinkman equation to model the flow of blood when there is an accumulation of fatty plaques in the lumen of an arterial part. They treated the clogged segment as a porous medium. Bhargava *et al.* (2007) analysed the transport of pharmaceutical species in laminar, homogeneous, incompressible, magneto-hydrodynamic, pulsating flow via two dimensional channels with a porous wall containing non porous materials. Misra and Shit (2007) and Misra *et al.* (2011)

considered a mathematical model and numerical model for analyzing blood flow via a porous vessel with a magnetic field where the viscosity varies in the radial direction.

Shit and Roy (2017) presented a paper on a theoretical study of blood flow through a tampered and overlapping stenosed artery under the action of an externally applied magnetic field with the blood medium assumed to be porous in nature. The variable viscosity of blood depending on hematocrite (percentage volume of erythrocytes) is taken into account with the equation:

$$\frac{\partial p}{\partial z}-\frac{1}{r}\frac{\partial\left(r\mu(r)\frac{du}{dr}\right)}{\partial r}+\sigma B_0^2 u+\frac{\mu(r)}{k}u=0 \qquad (2.1)$$

2.2 Bioheat Transfer Models

Many researchers have worked on temperature treatments with tissue in order to predict temperatures in a perfuse tissue and they are all very much concerned about a thermal model that can satisfy the following three criteria: the model that satisfy the conservation of energy; the model of heat transfer rate from blood vessels to tissue without following a vessel path; and the model applied to any unheated and heated tissue. To meet these criteria, many researchers around the world have suggested mathematical models in order to properly explain the heat transfer and fluid flow in biological processes in a heated, vascularized, finite tissue by making a few simple assumptions. We will now discuss some key models for considering the impact of large blood vessels.

For more than half a century Pennes (1948) bioheat transfer equation has been a standard model for predicting temperature distributions in living tissues. The model was formed by conducting a sequence of experiments in measuring temperatures of tissue and arterial blood flow in the resting human forearm. The equation has a special term

that explains the heat exchange between blood flow and solid tissues. The blood temperature is assumed to be constant arterial blood temperature. Tissue thermal equations can be explained concisely by considering the Pennes Bioheat Transfer Equation in its general formulation written as:

$$\nabla.k\nabla T + q_p + q_m - Wc_b(T - T_a) = \rho c_p \frac{\partial T}{\partial t} \quad (2.2)$$

Where,

T is the local tissue temperature

T_a is the arterial temperature

c_b is the blood specific heat

c_p is the tissue specific heat

W is the local tissue blood perfusion rate

k is the tissue thermal conductivity

ρ is the tissue density

q_p is the energy deposition rate

q_m is the metabolism

The term q_m in equation (2.2) is always very small compared to the external power deposition term q_p (Roemer *et al*., 1988). The term $Wc_b(T - T_a)$ accounts for the effects of blood perfusion and can be the dominant form of energy removal whenever you are considering heating processes. It authenticates that the blood enters the control volume at some arterial temperature and comes to the equilibrium at the tissue temperature. Therefore, as the blood is being carried away from the control volume, it carries away the energy and act as an energy sink in hyperthermia treatment. Pennes equation does

not have a physically dependable theoretical basis because it is an approximation equation. Indeed, this mathematical model predicts temperature fields very well in most applications. Pennes Bioheat Transfer Equation is widely used in the hyperthermia modeling because: it can predict the temperature field very well in applications and it is mathematically simple. The limitations of Pennes Bioheat Transfer Equation is that, it does not handle most physical effects, it does not put into consideration the direction of blood flow and does not portly any convective heat transfer mechanism.

Many researchers have developed alternative models to predict temperatures in living tissues. Chen and Holmes (1980) formulated another model with a very strong physical and physiological basis. The model equation can be written as:

$$\nabla.\left(k + k_p\right)\nabla T + q_p + q_m - Wc_b\left(T - T_a\right) - \rho_b c_b u.\nabla T = \rho c_p \frac{\partial T}{\partial t} \qquad (2.3)$$

Comparing equation (2.2) with equation (2.1), you will observe that additional terms have been added as follows: the term $-\rho_b c_b u.\nabla T$ is the convective heat transfer term which takes care of the thermal interactions between tissues and blood vessels and the term $\nabla.k_p \nabla T$ which takes care of the enhanced tissue conductive heat transfer due to blood perfusion term in tissues, where k_p is the perfusion conductivity which is a function of the blood perfusion rate. The blood perfusion term $-Wc_b\left(T - T_a\right)$ in the Chen and Holmes Model takes care of the effects of the large number of capillary structures with small dimensions relative to the macroscopic phenomenon under their study. Therefore, it needs detailed knowledge of the vascular anatomy and blood flow pattern to provide solution to it with increase in the accuracy.

Weinbaum and Jiji (1985) proposed an alternative mathematical model of the Bioheat Transfer Equation. Their model is based on their observations from the vascular

network of rabbit thighs; they observed that blood vessels that are important for heat transfer in tissues always happen in countercurrent pairs. Therefore, the main heat transfer mechanism between tissues and blood is the incomplete countercurrent heat exchanger between thermal arteries and veins. They used tensor notation in their model which can be written as:

$$\frac{w_0 \rho_t c_t \alpha T_a}{R_0} \frac{\partial \theta}{\partial \tau} = \frac{2kt_0 \alpha T_a}{R_0^2} \frac{\partial}{\partial \eta}\left((1+\alpha\theta)\frac{\partial \theta}{\partial \eta}\right) - w_b c_b \alpha T_a \theta + Q_{t_0} \frac{\pi}{2} \sin\left(\frac{\pi_t}{t_h}\right) \qquad (2.4)$$

Where,

θ is the local temperature

ρ is the volume of average tissue density

c is the specific heat product

a is the local blood vessel radius

σ is the shape factor for the thermal conduction resistance between adjacent counter current vessels

n is the number density of blood vessels

k_b is the blood thermal conductivity

pe is the local peclet number

u is the average blood flow velocity in the vessels

l_i is the direction cosine of the pair of countercurrent vessels

The conductivity tensor element $(k_{ij})_{eff}$ is given as:

$$(k_{ij})_{eff} = k\left(\lambda\delta_{ij} + \frac{\pi^2 n a^2 k_b^2}{4\sigma k^2} pe^2 l_i l_j\right) \qquad (2.5)$$

Where,

δ_{ij} is the kronecker delta function

k is the tissue thermal conductivity.

This equation is one of the most important contributions to the bioheat transfer model. Though, in practical conditions, this equation requires detailed understanding of the sizes, orientations and blood flow velocities in the countercurrent vessels in order to solve it which requires a difficult task. Moreover, there are several issues connected to the Weinbaum and Jiji model listed as follows: the comparisons for both predicted temperatures and macroscopic experiments are needed; the formulation was developed for superficial normal tissues in which counter-current heat transfer happens. When considering tumors, the vascular anatomy is different from the superficial normal tissues, and therefore a new model should be formulated for tumors. Wissler (1987) has questioned the two basic assumptions of the Weinbaum and Jiji model as follows: the arithmetic mean of the arteriole and blood temperature can be approximated by the mean tissue temperature and there is negligible heat transfer between the thermal arteriole-venule pairs and its surrounding tissue.

Weinbaum *et al*. (1984) tried to portray the effect of blood flow in the heat transfer process when it is limited to small vessels. Keller and Seiler (1971) described the effective conductivity of the non-isothermal region which is ascertained under different blood flow conditions. The Weinbaum, Jiji and Lemons model's approach is similar to that of Keller and Seiler(1971) mathematically in its use of three equations, but the Weinbaum, Jiji and Lemons model is basically on entirely different vascular generations, the Weinbaum, Jiji and Lemons equations apply to thermally important small vessels but not to major supply blood vessels.

Baish *et al*. (1986) believed that one of the noted assumptions in deriving the Weinbaum and Jiji model was that, as a result of the closeness of the vessels in a

countercurrent pair, most of the heat conducted through the arterial wall get to the venous wall. They criticised this hypothesis by assuming that some of the heat going out of the wall of a small arteriole will still remain within the tissue. They recommended that the heat transfer between the countercurrent vessels does not depend only on $T_a - T_v$ but also depend on the difference between the tissue temperatures T and the average blood temperature $\frac{T_a + T_v}{2}$, where T_a is the arterial temperature and T_v is the venous temperature.

Going by the publication of the Chen and Holmes Model, Weinbaum and Jiji models, many researches were performed to know the authenticity of these new approaches. Here, we present some arguments and approximations in order to study the blood flow impacts on bio thermal modeling.

Wissler (1987) strongly faults the Weinbaum and Jiji model because of the assumption made on the blood temperature at the arterial and venous vessels as well as the nearby tissue temperature. He proposed a new model that described tissue-blood vessels heat exchange that differs from the equations in the Weinbaum, Jiji and Lemons model by adding more perfusion term such as temperature profiles along the artery-vein which is approximated as $T \approx \frac{T_a + T_v}{2}$ in the Weinbaum and Jiji model. He denied the hypothesis that blood and tissue temperatures are closely joined which was mainly used for the formulation of the thermal conductivity tensor earlier defined in the Weinbaum, Jiji and Lemons equation. The thermal conductivity tensor formed in the Weinbaum, Jiji and Lemons equation is to eliminate the blood flow term. Charny *et al*. (1990) modified the Weinbaum, Jiji and Lemons model for the blood vessels by changing the governing equation with the tissue energy conservation equation. Based on their analysis of both

the steady state and transient temperature fields in the limb under hyper thermic and normothermic conditions, the tissue temperature profiles predicted by the model were very similar to those predicted by Penne's model in the tissue regions with large vessels. Craciunescu and Clegg (2001) solved the fully coupled Navier-Stokes and energy equations in order to secure the temperature distribution of pulsatile blood flow within a rigid blood vessel. They were able to found that the reversed flow improves as the Womersley number becomes larger which results to a smaller temperature difference between forward and reverse flows. However, in their model equations, they only concentrated on the temperature distribution in blood vessels without putting into cognizance the surrounding tissue. Khanafer *et al*. (2007) and Horng *et al*. (2015) further studied the effect of pulsatile blood flow on temperature distributions during hyperthermia by considering the pulsatile blood flow in a blood vessel with the model equation given as:

$$\left.\begin{aligned} \rho_t c_t \frac{\partial T_t}{\partial t} &= k_t \left[\frac{1}{r} \frac{\partial}{\partial r} \left(r \frac{\partial T_t}{\partial r} \right) + \frac{\partial^2 T_t}{\partial z^2} \right] - W_b c_b \left(T_t - T_a \right) + Q_t \left(r, z, t \right) \\ \rho_b c_b \left(\frac{\partial T_b}{\partial t} + w \frac{\partial T_b}{\partial z} \right) &= k_b \left[\frac{1}{r} \frac{\partial}{\partial r} \left(r \frac{\partial T_b}{\partial r} \right) + \frac{\partial^2 T_b}{\partial z^2} \right] + Q_b \left(r, z, t \right) \end{aligned}\right\} \tag{2.6}$$

2.3 Hyperthermia

This is a highly interesting topic in medicine. Several studies have been conducted on the use of heat transmission to living tissues for cancer treatment (Andreozzi *et al*., 2019) as well as to enhance treatment procedures and create more sophisticated and precise technologies for forecasting temperature in biological tissues. Such studies have led to the development and use of hyperthermia therapy, also known as "thermal medicine" or "thermotherapy," a kind of treatment in which the body's immunity and ability to self-heal are stimulated by exposing the body to high temperatures.

Hyperthermia can be used to treat a specific area of the body or the entire body. It is used in conjunction with standard treatments and is available only through referral and under the supervision of a healthcare practitioner (Das *et al*., 2019). In recent years, hyperthermia therapy has been shown to be useful in treating cancer. Its goal is to increase the heat of diseased tissues to beyond cytotoxic levels (41 ◦C to 45 ◦C) while avoiding overexposure of healthy tissues (Fan *et al*., 2017). In the treatment of some kinds of cancer, like liver metastases, radiation combined with traditional hyperthermia is more successful than radiation alone (Hooshmand *et al*., 2015). Several studies have been conducted on the use of heat transmission into living tissues, particularly for cancer treatment Lin and Li (2016). In addition, various studies have been applied over the years with the goal of forecasting temperature in biological tissues. One hyperthermia technique for treating tumors is Magnetic Fluid Hyperthermia (MFH). It is a non-invasive approach in which magnetic nano particles are injected into the tumor as heat mediators, after which the tumor is exposed to an external Alternating Magnetic Field (AMF) Zhang *et al*. (2021). MFH has various advantages. Its magnetic targeting method for cancer therapy achieves greater magnetic field penetration into tissues and increased accumulation of magnetic nano particles in tumors (Fan *et al*., 2017). Its most important advantages are that magnetic fluid hyperthermia-based multimodal cancer treatments are more successful for cancer treatment due to their synergistic action, particularly when combined with chemotherapy (Fan *et al*., 2017). Hyperthermia treatment can also be performed using a radiofrequency (RF) generator with electrodes and antennas (Lagendijk, 2000) as well as ultrasonic, microwave, and laser irradiance Hooshmand *et al*. (2015). These diverse techniques highlight the complexity of heat transmission in biological systems because many physiological functions rely on the spatiotemporal temperature differences in live biological tissues Zhang *et al*. (2021).

Thus, the success of the treatment is determined not only by the technology used but also by a thorough examination of the complex bio heat transfer process and the pattern of temperature increase in biological tissues during hyperthermia treatment Gupta *et al*. (2013).

An accurate explanation of the thermal relationships between blood vessels and tissues is required for the use of medical technology to be used in the treatment of deadly diseases such as cancer Andreozzi *et al*. (2019). To provide a therapeutic temperature while avoiding overheating and damage to surrounding healthy tissue, the temperature distribution within and outside the target area must be understood as a function of the exposure duration (Lagendijk 2000). The study of temporal and geographical variations in temperature is required while investigating bioheat transportation concerns because many physiological functions rely on the spatiotemporal temperature differences in live biological tissues (Roemer *et al*., 1988). Many biologists, physicians, mathematicians, and engineers have developed mathematical models of heat transfer in biological tissues Mathematical models are now often used in the study of hyperthermia in tumor treatment, oncology, cryosurgery, and many other applications (Gupta *et al*., 2013). There have been several models developed to regulate such heat transfer (Sarkar *et al*., 2015). An empirical law of thermal conductivity known as "Fourier's law" describes heat transfer in a continuous medium. Unfortunately, since the Fourier formula produces an infinite speed of heat spread due to the parabolic form of the diffusion equation, it has not been used in cases of fast transient heat transfer such as pulsed laser irradiation. As a result, a finite heat diffusion velocity must be determined. The Pennes model of bioheat transfer is widely used in modern engineering and medical therapy because of its simplicity, although it must be adjusted to account for the particular

characteristics of the tissue under investigation. It is based on the Fourier equation for thermal conductivity, which predicts the propagation of thermal disturbances at an infinite rate. As a result, a restricted heat transfer rate must be established. The Pennes bioheat equation incorporates the effects of diffusion, advection, volumetric heat production from metabolism, and spatial heating on heat transfer in a biological organism. The thermo physical characteristics of tissues, such as thermal conductivity, density, and specific heat, determine the diffusion and transitory thermal impacts. According to Kundu (2016), Pennes' explanation of the vascular contribution to heat transmission in perfused tissues fails to explain the real thermal equilibration process between streams of flowing blood. Consequently, for effective hyperthermia treatment, accurate thermal modeling is required. Khanafer *et al*. (2008) used physiological velocity waveforms to compute and analyse how the pulsatile laminar flow and heating protocol affect temperature variation in a single blood artery and tumor tissue that are undergoing hyperthermia therapy. They found that the existence of big vessels has an important impact on temperature variations, which must be considered when planning hyperthermia therapy. They further found that a uniform heating system has a wider temperature spread than the pulsed heating scheme, which may cause overheating in areas that may damage normal tissues. Several computational and experimental approaches have been developed to solve the bio thermal equation since it is critical to make an accurate calculation of the temperature range across the entire affected region. Kundu (2016) used the variable separation method to express exactly the temperature sensitivity in biological tissues based on the Fourier and non-Fourier heat transfer conditions during therapeutic settings. Kumar *et al*. (2015) studied the Dual-Phase-Lag (DPL) concept of bio heat transport with a Gaussian distribution source term under the most generalized boundary condition during hyperthermia treatment. To approximate an

analytical solution to the current problem, the finite element wavelet Galerkin approach, which uses the Legendre wavelet as a basic function, was employed. Liu *et al*. (2012) developed the bio heat transfer equation based on the DPL model to address the effect of micro structural interaction. They investigated the bio heat transfer problem in the skin, which was considered a three-layer composite, using the appropriate equation. Lin and Li (2016) proposed an analytical solution to bio heat transport in skin tissue with broad boundary conditions using the Pennes, Cattaneo-Vernotte, and DPL models. They looked at the heat transfer of skin that has been subjected to pulse laser heating and fluid cooling. Jaunich *et al*. (2008) investigated the temperature change and the heat-affected area after treating a skin tissue medium with a collimated or focused laser beam from a pulsed laser source. Experiments were conducted on multilayer tissue phantoms that resembled skin tissue, and on freshly excised mouse skin tissue samples with implanted heterogeneities that simulated subsurface tumors. Maamoun *et al*. (2021) described their use of microwave antennas for microwave imaging of tumors inside the liver and predicted the temperature profile in the liver and inside and outside the tumor throughout hyperthermia with and without nano particles, using a computer simulation of a genuine human model. Majchrzak and Stryczyski (2021) investigated the heat transmission between blood vessels and biological tissue using the DPL theory. The impact of the heating method is described by maintaining a consistent temperature for the tumor that is higher than the blood and tissue temperatures. To evaluate a Local Thermal Non-Equilibrium (LTNE) bio heat model, Dutta and Kundu (2021) presented an analytical hybrid scheme that consisted of a shift of variables and a finite integral transform. This system may be used to improve transient temperature prediction in the treatment of cancer patients using Localized Hyperthermia Treatment (LHT). The use of frameworks based on extended irreversible thermodynamics provides correspondences

of the proposed model with experimental models characterized by matching reduced computational loads. In the context of Extended Irreversible Thermodynamics (EIT), Chen and Yeh (2001) proposed a phenomenological theory for MR fluids that connects the dynamics of flows to a non-equilibrium-state equation and naturally includes the elasticity of Magnetic Resonance (MR) fluids. Versaci and Palumbo (2020) confirmed the association of the underlying shear flow and dilution behavior of the Herschel-Buckley plastic component from a known experimental model with elasto-viscoplastic generalization under the generalised standard materials. Magnetic nano particles have the potential to be magnetic contrast agents in biomedical magnetic imaging. Their interference in cellular biological systems such as those of a cell (10–100 nm), virus (20–450 nm), protein (5–50 nm), or gene (2 nm wide-ranging and 10–100 nm) due to their size can be adjusted from a few nanometers to tens of nanometers (Blanc-Beguin *et al*., 2009). Their existence in the biological systems under investigation may be determined using appropriate sensitive components (biosensors), which are attractive for magnetic bio-detection due to their high sensitivity, compact size, low power consumption, rapid response, and low cost (Blanc-Beguin *et al.*,2009). The potential of magnetic nano particle internalization has been illustrated by different in vitro studies. Internalization of magnetite (Fe2O3) or magnetite (Fe3O4) nano particles by cells have been demonstrated for diverse cellular types (Jiang *et al.*, 2016). Nanotechnology has the potential to improve the selectivity and efficacy of chemical, physical, and biological methods of killing cancer cells while reducing damage to noncancerous cells. Magnetic nano particles have also been used in numerous biomedical applications, such as hyperthermia treatment, radio immunotherapy, and magnetic resonance imaging. Nanotechnology can detect changes in a small number of cells due to their small size. It can distinguish between cancerous and normal cells. It can do these in the early stages

of cancer when the cancer cells are just starting to divide, and thus when the disease is easier to treat. Nanotechnology may also make it easier to detect tumors in imaging tests. Tumor targeting is one of the main potential advantages of nanotechnology for cancer treatment. The ability to distinguish between malignant and nonmalignant cells and selectively eliminate malignant cells is critical to the purpose of nanotechnology in cancer treatment. Malignant and non-malignant cell differentiation procedures fall into two categories: passive and active targeting (Chen *et al*., 2019). Nano particles coated with antibodies or other chemicals are likely to identify and stick to cancer cells. If the particles come into contact with cancer, they can be coated with compounds that send a signal (Blyakhman *et al*., 2018). Nano materials are increasingly being targeted at highly sensitive cancer cells, both actively and passively (Grossman and McNeil 2012). Cancer treatments can be made safer and more accurate with nanotechnology. Specially designed nano particles administer chemotherapy directly to tumors. Their small size enables them to transport drugs to hard-to-reach parts of the body. They only give drugs after they reach their destination. This prevents the drugs from causing damage to healthy tissue around the tumor, or other side effects as a result of injury. The design, safety, and extraction of geothermal energy from deep subterranean areas are based on research into the interaction of fluids and heat in the surrounding deep fissured rock. To generate an unstable 3D model of fluid-heat coupling heat transfer in the surrounding fractured rock, fractured media and heat transfer hypotheses were used (Kennedy *et al.*, 2018).

Ragab *et al*. (2021) presented a paper on Heat Transfer in Biological Spherical Tissues during Hyperthermia of Magnetoma. His model examines heat transport in biological tissues as forming an infinite concentric spherical region during magnetic fluid

hyperthermia. This model was able to explain the effects of different therapeutic approaches such as cryotherapy sessions, laser therapy, and physical occurrences, transfer, metabolism support, and blood perfusion with the following equation

$$\left(1+\tau_0\frac{\partial}{\partial t}\right)\left[\rho_1 C_1\frac{\partial^2\theta_1}{\partial t^2}+W_{b1}\rho_b C_b\frac{\partial\theta_1}{\partial t}+\frac{q_0}{t_p}e^{-\frac{t}{t_p}}\right]+P=\left(K_1\frac{\partial}{\partial t}+K_1^*\right)\left(\frac{\partial^2\theta_1}{\partial r^2}+\frac{2}{r}\frac{\partial\theta_1}{\partial r}\right) \quad (2.7)$$

2.4 Olayiwola's Generalized Polynomial Approximation Method (OGPAM)

Polynomial approximation methods are in wide use today for approximately solving partial differential equations of mathematical physics. An evolution of the polynomial approximation methods has led to the development of generalized polynomial approximation method, which can be applied to solve parabolic equations with constant or variable coefficients in the cases of considering slab, cylindrical or spherical geometries (Olayiwola, 2022). Different problems have been solved using the OGPAM.

The generalized polynomial approximation method is one of the simplest, and in some cases, accurate methods used to solve parabolic equations. The method involves five steps. The steps are applied to the dimensionless governing equation as follows:

The parabolic equations are defined by

$$\frac{\partial\phi}{\partial t}=\frac{k}{r^n}\frac{\partial}{\partial r}\left(r^n\frac{\partial\phi}{\partial r}\right)+F(r,t,\phi), \quad t>0, \quad r\in\Omega \ \left(\Omega\subset R^1,R^2 or R^3\right) \quad (2.8)$$

with the initial condition

$$\phi(r,0)=f(r) \quad (2.9)$$

and the boundary conditions

$$\alpha_1 \left.\frac{\partial \phi}{\partial r}\right|_{r=a} + \beta_1 \phi|_{r=a} = g_1(t), \qquad \alpha_2 \left.\frac{\partial \phi}{\partial r}\right|_{r=b} + \beta_2 \phi|_{r=b} = g_2(t) \tag{2.10}$$

where $F(r,t,\phi)$ are the other terms in equation (2.8), $n=0$ for a slab, $n=1$ for cylinder, $n=2$ for sphere, $f(r)$, $g_1(t)$, $g_2(t)$ are three known functions, $n, k, \alpha_1, \alpha_2, \beta_1, \beta_2$ are constants, and $a \le r \le b$ is the boundary of Ω.

To obtain an approximate solution of the partial differential equation (2.8) satisfying (2.9) and (2.10), the following steps are involved:

Step 1: Compare the equation to be solved with equations (2.8) – (2.10) and obtain A, B, C and $F(r,t,\phi)$, where

$$A = \begin{pmatrix} \dfrac{b(b-2a)}{b(b-2a)+a^2}\left(1+\dfrac{a}{\alpha_1}\left(1+\dfrac{a}{(b-2a)}\right)\beta_1\right) - \\ \dfrac{(n+1)\left(b^{n+2}-a^{n+2}\right)}{(n+2)\left(b^{n+1}-a^{n+1}\right)}\left(\dfrac{\beta_1}{\alpha_1}+\dfrac{2a}{(b-2a)}\dfrac{\beta_1}{\alpha_1}-\dfrac{2a}{b(b-2a)+a^2}\left(1+\dfrac{a}{\alpha_1}\left(1+\dfrac{a}{(b-2a)}\right)\beta_1\right)\right)+ \\ \dfrac{(n+1)\left(b^{n+3}-a^{n+3}\right)}{(n+3)\left(b^{n+1}-a^{n+1}\right)}\left(\dfrac{\beta_1}{(b-2a)\alpha_1}-\dfrac{1}{b(b-2a)+a^2}\left(1+\dfrac{a}{\alpha_1}\left(1+\dfrac{a}{(b-2a)}\right)\beta_1\right)\right) \end{pmatrix} \tag{2.11}$$

$$B = \begin{pmatrix} -\dfrac{ab(b-2a)}{\left(b(b-2a)+a^2\right)\alpha_1}\left(1+\dfrac{a}{(b-2a)}\right)+ \\ \dfrac{(n+1)\left(b^{n+2}-a^{n+2}\right)}{(n+2)\left(b^{n+1}-a^{n+1}\right)}\left(\dfrac{1}{\alpha_1}+\dfrac{2a}{(b-2a)\alpha_1}-\dfrac{2a^2}{\left(b(b-2a)+a^2\right)\alpha_1}\left(1+\dfrac{a}{(b-2a)}\right)\right)+ \\ \dfrac{(n+1)\left(b^{n+3}-a^{n+3}\right)}{(n+3)\left(b^{n+1}-a^{n+1}\right)}\left(\dfrac{a}{\left(b(b-2a)+a^2\right)\alpha_1}\left(1+\dfrac{a}{(b-2a)}\right)-\dfrac{1}{(b-2a)\alpha_1}\right) \end{pmatrix} \tag{2.12}$$

$$C = \begin{pmatrix} \dfrac{a^2}{\left(b(b-2a)+a^2\right)}-\dfrac{(n+1)\left(b^{n+2}-a^{n+2}\right)}{(n+2)\left(b^{n+1}-a^{n+1}\right)}\dfrac{2a}{b(b-2a)\beta_2}\left(1-\dfrac{a^2}{\left(b(b-2a)+a^2\right)}\right)+ \\ \dfrac{(n+1)\left(b^{n+3}-a^{n+3}\right)}{(n+3)\left(b^{n+1}-a^{n+1}\right)}\dfrac{1}{b(b-2a)\beta_2}\left(1-\dfrac{a^2}{\left(b(b-2a)+a^2\right)}\right) \end{pmatrix} \tag{2.13}$$

Step 2: Assumed generalized polynomial solution:

$$\phi(r,t)=\left(\begin{array}{l}\left(\dfrac{b(b-2a)}{b(b-2a)+a^2}\right)\left(\begin{array}{l}\left(\left(1+\dfrac{a}{\alpha_1}\left(1+\dfrac{ab}{b(b-2a)}\right)\beta_1\right)\phi\big|_{r=a}-\dfrac{a}{\alpha_1}\left(1+\dfrac{ab}{b(b-2a)}\right)g_1\right)+\\ +\left(\dfrac{a^2}{b(b-2a)\beta_2}\right)g_2\end{array}\right)+\\ \left(\begin{array}{l}\left(\dfrac{2a}{b(b-2a)}\left(\dfrac{b(b-2a)}{b(b-2a)+a^2}\right)\left(1+\dfrac{a}{\alpha_1}\left(1+\dfrac{ab}{b(b-2a)}\right)\beta_1\right)-\right)\phi\big|_{r=a}+\\ \dfrac{2a\beta_1}{(b-2a)\alpha_1}-\dfrac{\beta_1}{\alpha_1}\end{array}\right)\\ \left(\begin{array}{l}\left(\dfrac{1}{\alpha_1}+\dfrac{2a}{(b-2a)\alpha_1}-\dfrac{2a^2}{b(b-2a)\alpha_1}\left(\dfrac{b(b-2a)}{b(b-2a)+a^2}\right)\left(1+\dfrac{ab}{b(b-2a)}\right)\right)g_1\\ +\left(\dfrac{2a}{b(b-2a)}\left(\dfrac{b(b-2a)}{b(b-2a)+a^2}\right)\left(\dfrac{a^2}{b(b-2a)\beta_2}\right)-\left(\dfrac{2a}{b(b-2a)\beta_2}\right)\right)g_2\end{array}\right)r+\\ \dfrac{1}{b(b-2a)}\left(\begin{array}{l}\left(\left(\dfrac{b\beta_1}{\alpha_1}-\left(\dfrac{b(b-2a)}{b(b-2a)+a^2}\right)\left(1+\dfrac{a}{\alpha_1}\left(1+\dfrac{ab}{b(b-2a)}\right)\beta_1\right)\right)\phi\big|_{r=a}+\\ \left(\left(\dfrac{b(b-2a)}{b(b-2a)+a^2}\right)\dfrac{a}{\alpha_1}\left(1+\dfrac{ab}{b(b-2a)}\right)-\dfrac{b}{\alpha_1}\right)g_1+\\ \left(\dfrac{1}{\beta_2}-\left(\dfrac{b(b-2a)}{b(b-2a)+a^2}\right)\left(\dfrac{a^2}{b(b-2a)\beta_2}\right)\right)g_2\end{array}\right)r^2\end{array}\right) \tag{2.14}$$

Step 3: By using (2.14), evaluate

$$\frac{(n+1)}{\left(b^{n+1}-a^{n+1}\right)}\int_a^b r^n F(r,t,\phi)dr \tag{2.15}$$

and express the result in the form:

$$p_1\phi\big|_{r=b}+q_1(t) \tag{2.16}$$

Step 4: Obtain p_1 and $q_1(t)$

Step 5: Obtain

$$\phi\big|_{r=a} = e^{-\int p(t)dt}\int_0^t q(x)e^{\int p(x)dx}dx + f(r)e^{-\int p(t)dt} \tag{2.17}$$

where

$$p(t) = \frac{1}{A}\left(\frac{k(n+1)}{\left(b^{n+1}-a^{n+1}\right)}\left(\begin{array}{l}\dfrac{\left(b^n-a^n\right)\beta_1}{\alpha_1}+\dfrac{2b^n(a-b)}{(b-2a)\alpha_1}+\dfrac{2b^n(b-a)}{\left(b(b-2a)+a^2\right)}+\\ \dfrac{2ab^n(b-a)(b(b-2a)+a)\beta_1}{\left(b(b-2a)+a^2\right)b(b-2a)\alpha_1}\end{array}\right)-p_1\right) \tag{2.18}$$

$$q(t) = \frac{1}{A}\left(\begin{array}{l}\dfrac{k(n+1)}{\left(b^{n+1}-a^{n+1}\right)}\left(\dfrac{\left(b^n-a^n\right)}{\alpha_1}+\dfrac{2b^n(a-b)}{(b-2a)\alpha_1}+\dfrac{2ab^n(b-a)(b(b-2a)+a)}{\left(b(b-2a)+a^2\right)b(b-2a)\alpha_1}\right)g_1+\\ \dfrac{k(n+1)}{\left(b^{n+1}-a^{n+1}\right)}\dfrac{2b^n(b-a)}{b(b-2a)\beta_2}\left(1+\dfrac{a^2}{\left(b(b-2a)+a^2\right)}\right)g_2+q_1(t)-B\dfrac{\partial g_1}{\partial t}-C\dfrac{\partial g_2}{\partial t}\end{array}\right) \tag{2.19}$$

2.5 Summary of Review and Gaps to fill

In reviewing the literatures, several works have been carried out on a theoretical study of blood flow through arteries (stenosis). Some authors worked on blood flow through a tampered and overlapping stenosed artery under the action of an externally applied magnetic field and steady state condition with the blood medium assumed to be porous in nature and considered variable viscosity of blood without considering heat transfer. Most authors that considered heat transfer, considered the effect of pulsatile blood flow on temperature distributions during hyperthermia but do not take into account the temperature dependent blood and tissue thermal conductivities. In view of these, the present study aimed at establishing an approximate analytical solution capable of predicting effect of unsteadiness, variable viscosity and variable thermal conductivity on blood flow and heat transfer in the human cardiovascular system.

CHAPTER THREE

3.0 MATERIALS AND METHODS

3.1 Mathematical Formulation

We extend the work of Shit and Roy (2017) with the equation governing the blood flow under a closed watch of an external magnetic field via blood as follow:

$$\rho\frac{\partial w}{\partial t}=-\frac{\partial p}{\partial z}+\frac{1}{r}\frac{\partial}{\partial r}\left(r\mu(r)\frac{\partial w}{\partial r}\right)-\sigma B_0^2 w-\frac{\mu(r)}{\bar{k}}w \tag{3.1}$$

We assumed that blood is incompressible and has uniform dense throughout but the viscosity $\mu(r)$ varies in the radial direction. According to Einstein's formula for the variable viscosity of blood taken to be

$$\mu(r)=\mu_0(1+\beta h(r)) \tag{3.2}$$

Where μ_0 is the coefficient of viscosity of plasma, β is a constant whose value for blood is equal to 2.5 and $h(r)$ stands for hematocrit. The analysis will be carried out by using the following empirical formula for hematocrit given by

$$h(r)=H\left(1-\left(\frac{r}{R_0}\right)^m\right) \tag{3.3}$$

Where R_0 represents the radius of a normal arterial segment, H is the maximum hematocrit at the center of the artery and $m\geq 2$ a parameter that determines the exact shape of the velocity profile for blood.

We also extend the work of Horng *et al*. (2015) with the governing equations of the temperature evolution for the tissue and the energy transport for the blood vessels as:

$$\rho_t c_t \frac{\partial T_t}{\partial t} = k_t \frac{1}{r}\frac{\partial}{\partial r}\left(r\frac{\partial T_t}{\partial r}\right) + k_t \frac{\partial}{\partial z}\left(\frac{\partial T_t}{\partial z}\right) - W_b c_b \left(T_t - T_a\right) + Q_t\left(r,z,t\right) \tag{3.4}$$

$$\rho_b c_b \left(\frac{\partial T_b}{\partial t} + w\frac{\partial T_b}{\partial z}\right) = \left(\frac{1}{r}\frac{\partial}{\partial r}\left(k_b r\frac{\partial T_b}{\partial r}\right) + \frac{\partial}{\partial z}\left(k_b\frac{\partial T_b}{\partial z}\right)\right) + Q_b\left(r,z,t\right) \tag{3.5}$$

$$\left.\begin{aligned} Q_t\left(r,z,t\right) &= Q_{t0}\frac{\pi}{2}\sin\left(\frac{\pi_t}{t_h}\right) \\ Q_b\left(r,z,t\right) &= Q_{b0}\frac{\pi}{2}\sin\left(\frac{\pi_t}{t_h}\right) \end{aligned}\right\} \tag{3.6}$$

The dependence of blood thermal conductivity on tissue temperature is given by the expression:

$$k_b = k_{b0}\left(\frac{T_t}{T_a}\right) \tag{3.7}$$

To solve equations (3.1) – (3.7), we adopt no-slip boundary condition at the vessel wall and we put into consideration the axis-symmetric boundary condition of axial velocity at the mid line of the vessel with the assumptions that the blood vessel segment is straight, that the vessel wall is rigid and porous. Also, we assume that the flow is laminar, incompressible and Newtonian. Thus, the initial and boundary conditions are formulated as:

$$\left.\begin{array}{lllll} w(r,z,0)=0, & \left.\dfrac{\partial w}{\partial r}\right|_{r=0}=0, & \left.\dfrac{\partial w}{\partial z}\right|_{r=0}=0, & w(R_0,z,t)=0, & w(r,L,t)=0 \\ T_t(r,z,0)=T_a, & \left.\dfrac{\partial T_t}{\partial r}\right|_{r=0}=0, & \left.\dfrac{\partial T_t}{\partial z}\right|_{r=0}=0, & T_t(R_0,z,t)=T_a, & T_t(r,L,t)=T_a \\ T_b(r,z,0)=T_a, & \left.\dfrac{\partial T_b}{\partial r}\right|_{r=0}=0, & \left.\dfrac{\partial T_b}{\partial z}\right|_{r=0}=0, & T_b(R_0,z,t)=T_a, & T_b(r,L,t)=T_a \end{array}\right\} \quad (3.8)$$

Where,

z is the axial distance

r is the radial distance

ρ is the density

w is the axial velocity of blood flow

w_0 is the initial axial velocity of blood flow

p is the blood pressure

$\mu(r)$ is the blood viscosity at a radial distance r

$h(r)$ is the hematocrit at a distance r

H is the maximum hematocrit at the center of the artery

μ_0 is the coefficient of viscosity of plasma

R_0 is the radius of a normal arterial segment

β is a constant whose value for blood which is equal to 2.5

σ is the electrical conductivity

B_0 is the applied magnetic field strength

k is the permeability of the porous medium

k_t is the thermal conductivity of tissue

k_b is the thermal conductivity of blood

c_t is the specific heat capacity of tissue

c_b is the specific heat capacity of blood

T_t is the tissue temperature

T_b is the blood temperature

T_a is the ambient temperature that is normally assumed to be $37^0 C$

W_b is the perfusion mass flow rate

$Q_t(r,z,t)$ is the tissue power of heat added axis symmetrically

$Q_b(r,z,t)$ is the blood power of heat added axis symmetrically

α is the ratio of blood temperature to that of tissue temperature

η is the new space variable introduced

L is the length of vessel wall

3.2 Dimensional Analysis

Equations (3.1) – (3.8) are non–dimensionalized using the following dimensionless variables:

$$\left\{\begin{array}{lllll} r' = \dfrac{r}{R_0}, & \tau = \dfrac{w_0 t}{R_0}, & z' = \dfrac{z}{L}, & \phi = \dfrac{w}{w_0}, & \alpha = \dfrac{T_b}{T_t} \\ \theta = \dfrac{T_t - T_a}{\alpha T_a}, & \psi = \dfrac{T_b - T_a}{\alpha T_a}, & p' = \dfrac{p}{\rho w_0^2} & & \end{array}\right\} \tag{3.9}$$

Then equation (3.1) becomes

$$\frac{\rho w_0^2}{R_0}\frac{\partial \phi}{\partial \tau} = -\frac{\rho w_0^2}{L}\frac{\partial p'}{\partial z'} + \frac{w_0 \mu_0}{R_0^2 r'}\frac{\partial}{\partial r'}\left(r'\left(1+\beta H\left(1-r'^m\right)\right)\frac{\partial \phi}{\partial r'}\right) - \sigma B_0^2 w_0 \phi - \frac{w_0 \mu_0}{\bar{k}}\left(1+\beta H\left(1-r'^m\right)\right)\phi \tag{3.10}$$

Multiplying equation (3.10) by $\dfrac{R_0}{\rho w_0^2}$ gives

$$\frac{\partial \phi}{\partial \tau} = -\frac{R_0}{L}\frac{\partial p'}{\partial z'} + \frac{\mu_0}{\rho w_0 R_0}\frac{1}{r'}\frac{\partial}{\partial r'}\left(r'\left(1+\beta H\left(1-r'^m\right)\right)\frac{\partial \phi}{\partial r'}\right) - \frac{\sigma B_0^2 R_0}{\rho w_0}\phi - \frac{\mu_0 R_0}{\rho w_0 \bar{k}}\left(1+\beta H\left(1-r'^m\right)\right)\phi \tag{3.11}$$

Dropping prime, we have,

$$\frac{\partial \phi}{\partial \tau} = -D + \frac{1}{\mathrm{Re}}\frac{1}{r}\frac{\partial}{\partial r}\left(r\left(1+\beta H\left(1-r^m\right)\right)\frac{\partial \phi}{\partial r}\right) - \frac{M^2}{\mathrm{Re}}\phi - k_p\frac{k_p}{\mathrm{Re}}\left(1+\beta H\left(1-r^m\right)\right)\phi \tag{3.12}$$

Where,

$$a=\frac{R_0}{L},\ \mathrm{Re}=\frac{\rho w_0 R_0}{\mu_0},\ M^2=\frac{\sigma B_0^2 R_0^2}{\mu_0},\ k_p=\frac{R_0^2}{\bar{k}}=\frac{1}{k},\ D=a\frac{\partial p}{\partial z} \tag{3.13}$$

Also, equation (3.4) becomes

$$\frac{\rho_t c_t \alpha T_a w_0}{R_0}\frac{\partial\theta}{\partial\tau}=\left(\frac{k_t \alpha T_a}{R_0^2}\frac{1}{r'}\frac{\partial}{\partial r'}\left(r'\frac{\partial\theta}{\partial r'}\right)+\frac{k_t \alpha T_a}{L^2}\frac{\partial}{\partial z'}\left(\frac{\partial\theta}{\partial z'}\right)\right)-w_b c_b \alpha T_a \theta+$$
$$Q_{t_0}\frac{\pi}{2}\sin\left(\frac{\pi_t}{t_h}\right) \tag{3.14}$$

$$\frac{\partial\theta}{\partial\tau}=\left(\frac{k_t}{\rho_t c_t R_0 w_0}\frac{1}{r'}\frac{\partial}{\partial r'}\left(r'\frac{\partial\theta}{\partial r'}\right)+\frac{k_t R_0}{\rho_t c_t R_0 w_0 L^2}\frac{\partial}{\partial z'}\left(\frac{\partial\theta}{\partial z'}\right)\right)-\frac{w_b c_b R_0}{\rho_t c_t w_0}\theta$$
$$-\frac{w_b c_b R_0}{\rho_t c_t w_0}\theta+\frac{Q_{t_0} R_0}{\rho_t c_t \alpha T_a w_0}\frac{\pi}{2}\sin\left(\frac{\pi_t}{t_h}\right) \tag{3.15}$$

Dropping prime, we have

$$\frac{\partial\theta}{\partial\tau}=\frac{1}{Pe_1}\frac{1}{r}\frac{\partial}{\partial r}\left(r\frac{\partial\theta}{\partial r}\right)+\frac{1}{Pe_2}\frac{\partial}{\partial z}\left(\frac{\partial\theta}{\partial z}\right)-\alpha_1\theta+\frac{\gamma_1\pi}{2}\sin\left(\frac{\pi_t}{t_h}\right) \tag{3.16}$$

$$\frac{1}{Pe_1}=\frac{k_t}{\rho_t c_t R_0 w_0},\ \frac{1}{Pe_2}=\frac{k_t R_0}{\rho_t c_t w_0 L^2},\ \alpha_1=\frac{w_b c_b R_0}{\rho_t c_t R_0 w_0},\ \gamma_1=\frac{Q_{t_0} R_0}{\rho_t c_t \alpha T_a w_0} \tag{3.17}$$

Also, equation (3.5) becomes

$$\frac{\rho_b c_b \alpha T_a w_0}{R_0}\frac{\partial\psi}{\partial\tau}+\frac{\rho_b c_b \alpha T_a w_0}{L}\phi\frac{\partial\psi}{\partial z^1}=\frac{k_{b_0}\alpha T_a}{R_0^2}\frac{1}{r'}\frac{\partial}{\partial r'}\left(r'(1+\alpha\theta)\frac{\partial\psi}{\partial r'}\right)+$$
$$\frac{k_{b_0}\alpha T_a}{L^2}\frac{\partial}{\partial z'}\left((1+\alpha\theta)\frac{\partial\psi}{\partial z'}\right)+Q_{b_0}\frac{\pi}{2}\sin\left(\frac{\pi_t}{t_h}\right) \tag{3.18}$$

i.e

$$\frac{\partial \psi}{\partial \tau}+\frac{R_0}{L}\varphi\frac{\partial \psi}{\partial z^1}=\frac{k_{b_0}}{\rho_b c_b R_0 w_0}\frac{1}{r'}\frac{\partial}{\partial r'}\left(r'\left(1+\alpha\theta\right)\frac{\partial \psi}{\partial r'}\right)+\frac{k_{b_0}R_0}{\rho_b c_b w_0 L^2}\frac{\partial}{\partial z}\left(\left(1+\alpha\theta\right)\frac{\partial \psi}{\partial z'}\right)+\frac{Q_{b_0}R_0}{\rho_b c_b \alpha T_a w_0}\frac{\pi}{2}\sin\left(\frac{\pi_t}{t_h}\right) \tag{3.19}$$

Dropping prime, we have

$$\frac{\partial \psi}{\partial \tau}+a\varphi\frac{\partial \psi}{\partial z}=\frac{1}{Pe_3}\frac{1}{r}\frac{\partial}{\partial r}\left(r\left(1+\alpha\theta\right)\frac{\partial \psi}{\partial r}\right)+\frac{1}{Pe_4}\frac{\partial}{\partial z}\left(\left(1+\alpha\theta\right)\frac{\partial \psi}{\partial z}\right)+\frac{\gamma_2\pi}{2}\sin\left(\frac{\pi_t}{t_h}\right) \tag{3.20}$$

where

$$Pe_3=\frac{\rho_b c_b R_0 w_0}{k_{b_0}},\quad Pe_4=\frac{\rho_b c_b w_0 H^2}{k_{b_0}R_0},\quad \gamma_2=\frac{Q_{b_0}R_0}{\rho_b c_b \alpha T_a w_0} \tag{3.21}$$

Also, equation (3.8) can be expressed as

$$w\left(r,z,0\right)=w_0\phi\left(r',z',0\right)=0\Rightarrow\phi\left(r,z,0\right)=0 \tag{3.22}$$

$$\left.\frac{\partial w}{\partial r}\right|r=0=\frac{w_0}{R}\left.\frac{\partial \phi}{\partial r'}\right|r'=0=0\Rightarrow\left.\frac{\partial \phi}{\partial r}\right|r=0=0 \tag{3.23}$$

$$\left.\frac{\partial w}{\partial z}\right|z=0=\frac{w_0}{L}\left.\frac{\partial \phi}{\partial z'}\right|z'=0=0\Rightarrow\left.\frac{\partial \phi}{\partial z}\right|z=0=0 \tag{3.24}$$

$$w\left(R_0,z,t\right)=w_0\phi\left(1,z',t\right)=0\Rightarrow\phi\left(1,z,t\right)=0 \tag{3.25}$$

$$w\left(r,L,t\right)=w_0\phi\left(r',1,t'\right)=0\Rightarrow\varphi\left(r,1,t\right)=0 \tag{3.26}$$

$$T_t\left(r,z,0\right)=\alpha T_a\theta\left(r',z',0\right)+T_a=T_a\Rightarrow\theta\left(r,z,0\right)=0 \tag{3.27}$$

$$\left.\frac{\partial T_t}{\partial r}\right|r=0=\frac{\alpha T_a}{R}\left.\frac{\partial \theta}{\partial r'}\right|r'=0=0\Rightarrow\left.\frac{\partial \theta}{\partial r}\right|r=0=0 \tag{3.28}$$

$$\left.\frac{\partial T_t}{\partial z}\right|_{z=0} = \frac{\alpha T_a}{L}\left.\frac{\partial \theta}{\partial z'}\right|_{z'=0} = 0 \Rightarrow \left.\frac{\partial \theta}{\partial z}\right|_{z=0} = 0 \tag{3.29}$$

$$T_t(R_0, z, t) = \alpha T_a \theta(1, z', t') + T_a = T_a \Rightarrow \theta(1, z, t) = 0 \tag{3.30}$$

$$T_t(r, H, t) = \alpha T_a \theta(r', 1, t') + T_a = T_a \Rightarrow \theta(r, 1, t) = 0 \tag{3.31}$$

$$T_b(r, z, 0) = \alpha T_a \psi(r', z', 0) + T_a = T_a \Rightarrow \psi(r, z, 0) = 0 \tag{3.32}$$

$$\left.\frac{\partial T_b}{\partial r}\right|_{r=0} = \frac{\alpha T_a}{R}\left.\frac{\partial \psi}{\partial r'}\right|_{r'=0} = 0 \Rightarrow \left.\frac{\partial \psi}{\partial r}\right|_{r=0} = 0 \tag{3.33}$$

$$\left.\frac{\partial T_b}{\partial z}\right|_{z=0} = \frac{\alpha T_a}{L}\left.\frac{\partial \psi}{\partial z'}\right|_{z'=0} = 0 \Rightarrow \left.\frac{\partial \psi}{\partial z}\right|_{z=0} = 0 \tag{3.34}$$

$$T_b(R_0, z, t) = \alpha T_a \psi(1, z', t') + T_a = T_a \Rightarrow \psi(1, z, t) = 0 \tag{3.35}$$

$$T_b(r, L, t) = \alpha T_a \psi(r', 1, t') + T_a = T_a \Rightarrow \psi(r, 1, t) = 0 \tag{3.36}$$

Therefore, the dimensionless equations with their initial and boundary conditions are

$$\frac{\partial \phi}{\partial \tau} = D + \frac{1}{\mathrm{Re}}\frac{1}{r}\frac{\partial}{\partial r}\left(r\left(1+\beta H\left(1-r^m\right)\right)\frac{\partial \phi}{\partial r}\right) - \frac{M^2}{\mathrm{Re}}\phi - \frac{k_p}{\mathrm{Re}}\left(1+\beta H\left(1-r^m\right)\right)\phi \tag{3.37}$$

$$\frac{\partial \theta}{\partial \tau} = + \frac{1}{Pe_1}\frac{1}{r}\frac{\partial}{\partial r}\left(r\left(1+\alpha\theta\right)\frac{\partial \theta}{\partial r}\right) + \frac{1}{Pe_2}\frac{\partial}{\partial z}\left(\frac{\partial \theta}{\partial z}\right) - \alpha_1\theta + \gamma_1\frac{\pi}{2}\sin\left(\frac{\pi_t}{t_h}\right) \tag{3.38}$$

$$\frac{\partial \psi}{\partial \tau} + a\phi\frac{\partial \psi}{\partial z} = \frac{1}{Pe_3}\frac{1}{r}\frac{\partial}{\partial r}\left(r\left(1+\alpha\theta\right)\frac{\partial \psi}{\partial r}\right) + \frac{1}{Pe_4}\frac{\partial}{\partial z}\left(\left(1+\alpha\theta\right)\frac{\partial \theta}{\partial z}\right) + \gamma_2\frac{\pi}{2}\sin\left(\frac{\pi_t}{t_h}\right) \tag{3.39}$$

$$\left\{\begin{array}{l}\phi(r,\ z,\ 0)=0,\ \left.\dfrac{\partial\phi}{\partial r}\right|_{r=0}=0,\ \left.\dfrac{\partial\phi}{\partial z}\right|_{z=0}=0,\ \ \phi(1,\ z,\ t)=0,\ \phi(r,\ 1,\ t)=0\\ \theta(r,\ z,\ 0)=0,\ \left.\dfrac{\partial\theta}{\partial r}\right|_{r=0}=0,\ \left.\dfrac{\partial\theta}{\partial z}\right|_{z=0}=0,\ \ \theta(1,\ z,\ t)=0,\ \theta(r,\ 1,\ t)=0\\ \psi(r,\ z,\ 0)=0,\ \left.\dfrac{\partial\psi}{\partial r}\right|_{r=0}=0,\ \left.\dfrac{\partial\psi}{\partial z}\right|_{z=0}=0,\ \ \psi(1,\ z,\ t)=0,\ \psi(r,\ 1,\ t)=0\end{array}\right\} \quad (3.40)$$

3.3 Method of Solution

We introduce a new space variable as

$$2\eta = r + z \quad (3.41)$$

Then

$$r = 2\eta - z = \varepsilon \quad (3.42)$$

$$\Rightarrow 2\eta = \varepsilon + z \quad (3.43)$$

Then

$$\frac{\partial}{\partial r} = \frac{1}{2}\frac{\partial}{\partial \eta} \quad \textit{and} \quad \frac{\partial}{\partial z} = \frac{1}{2}\frac{\partial}{\partial \eta} \quad (3.44)$$

Therefore, equations (3.37) – (3.40) reduce to

$$\frac{\partial\phi}{\partial\tau} = -D + \frac{1}{4\,\mathrm{Re}}\frac{1}{\varepsilon}\frac{\partial}{\partial\eta}\left(\varepsilon\left(1+\beta H\left(1-\varepsilon^{m}\right)\right)\frac{\partial\phi}{\partial\eta}\right) - \frac{M^{2}}{\mathrm{Re}}\phi - \frac{k_{p}}{\mathrm{Re}}\left(1+\beta H\left(1-\varepsilon^{m}\right)\right)\phi \quad (3.45)$$

$$\frac{\partial\theta}{\partial\tau} = \frac{1}{4Pe_{1}}\frac{1}{\varepsilon}\frac{\partial}{\partial\eta}\left(\varepsilon\frac{\partial\theta}{\partial\eta}\right) + \frac{1}{4Pe_{2}}\frac{\partial}{\partial\eta}\left(\frac{\partial\theta}{\partial\eta}\right) - \alpha_{1}\theta + \gamma_{1}\frac{\pi}{2}\sin\left(\frac{\pi_{t}}{t_{h}}\right) \quad (3.46)$$

$$\frac{\partial\psi}{\partial\tau} + \frac{a}{2}\phi\frac{\partial\psi}{\partial\eta} = \frac{1}{4Pe_{3}}\frac{1}{\varepsilon}\frac{\partial}{\partial\eta}\left(\varepsilon\left(1+\alpha\theta\right)\frac{\partial\psi}{\partial\eta}\right) + \frac{1}{4Pe_{4}}\frac{\partial}{\partial\eta}\left(\left(1+\alpha\theta\right)\frac{\partial\psi}{\partial\eta}\right) + \gamma_{2}\frac{\pi}{2}\sin\left(\frac{\pi_{t}}{t_{h}}\right) \quad (3.47)$$

$$\left.\begin{aligned}
&\phi(\eta,0)=0,\ \left.\frac{\partial\phi}{\partial\eta}\right|_{\eta=0}=0,\ \ \phi(1,\tau)=0\\
&\theta(\eta,0)=0,\ \left.\frac{\partial\theta}{\partial\eta}\right|_{\eta=0}=0,\ \ \theta(1,\tau)=0\\
&\psi(\eta,0)=0,\ \left.\frac{\partial\psi}{\partial\eta}\right|_{\eta=0}=0,\ \ \psi(1,\tau)=0
\end{aligned}\right\} \tag{3.48}$$

Here, equations (3.45) – (3.48) will be considered in two forms as follows:

Case 1: When $\alpha \neq 0$ *and* $\beta \neq 0$.

When $\alpha \neq 0$ *and* $\beta \neq 0$. Then equations (3.45) – (3.48) reduced to:

$$\frac{\partial\phi}{\partial\tau}=\frac{1+\beta H}{4\,\mathrm{Re}}\frac{\partial^2\phi}{\partial\eta^2}-\frac{\beta H}{4\,\mathrm{Re}}\varepsilon^m\frac{\partial^2\phi}{\partial\eta^2}+\frac{1}{4\,\mathrm{Re}}\frac{1}{\varepsilon}\frac{\partial}{\partial\eta}\left(\varepsilon\left(1+\beta H\left(1-\varepsilon^m\right)\right)\frac{\partial\phi}{\partial\eta}\right)-$$
$$\frac{M^2}{\mathrm{Re}}\phi-\frac{k_p}{\mathrm{Re}}\left(1+\beta H\left(1-\varepsilon^m\right)\right)\phi-D \tag{3.49}$$

$$\frac{\partial\theta}{\partial\tau}=\left(\frac{1}{4Pe_1}+\frac{1}{4Pe_2}\right)\frac{\partial^2\theta}{\partial\eta^2}+\frac{1}{4Pe_1}\frac{1}{\varepsilon}\frac{\partial\theta}{\partial\eta}+\alpha_1\theta+\gamma_1\frac{\pi}{2}\sin\left(\frac{\pi_t}{t_h}\right) \tag{3.50}$$

$$\frac{\partial\psi}{\partial\tau}=\left(\frac{1}{4Pe_3}+\frac{1}{4Pe_4}\right)\frac{\partial^2\psi}{\partial\eta^2}+\alpha\left(\frac{1}{4Pe_3}+\frac{1}{4Pe_4}\right)\theta\frac{\partial^2\psi}{\partial\eta^2}+\alpha\left(\frac{1}{4Pe_3}+\frac{1}{4Pe_4}\right)\frac{\partial\theta}{\partial\eta}\frac{\partial\psi}{\partial\eta}+$$
$$\frac{1}{4Pe_3}\frac{1}{\varepsilon}(1+\alpha\theta)\frac{\partial\psi}{\partial\eta}-\frac{a}{2}\phi\frac{\partial\psi}{\partial\eta}+\gamma_2\frac{\pi}{2}\sin\left(\frac{\pi_t}{t_h}\right) \tag{3.51}$$

Case 2: When $\alpha = 0$ *and* $\beta = 0$.

When $\alpha = 0$ *and* $\beta = 0$. Then equations (3.45) – (3.48) reduced to:

$$\frac{\partial\phi}{\partial\tau}=\frac{1}{4\,\mathrm{Re}}\frac{\partial^2\phi}{\partial\eta^2}+\frac{1}{4\,\mathrm{Re}}\frac{1}{\varepsilon}\frac{\partial\phi}{\partial\eta}-\frac{M^2}{\mathrm{Re}}\phi-\frac{k_p}{\mathrm{Re}}\phi-D \tag{3.52}$$

$$\frac{\partial\theta}{\partial\tau}=\left(\frac{1}{4Pe_1}+\frac{1}{4Pe_2}\right)\frac{\partial^2\theta}{\partial\eta^2}+\frac{1}{4Pe_1}\frac{1}{\varepsilon}\frac{\partial\theta}{\partial\eta}+\alpha_1\theta+\gamma_1\frac{\pi}{2}\sin\left(\frac{\pi_t}{t_h}\right) \tag{3.53}$$

$$\frac{\partial \psi}{\partial \tau} = \left(\frac{1}{4Pe_3} + \frac{1}{4Pe_4} \right) \frac{\partial^2 \psi}{\partial \eta^2} + \frac{1}{4Pe_3} \frac{1}{\varepsilon} \frac{\partial \psi}{\partial \eta} - \frac{a}{2} \phi \frac{\partial \psi}{\partial \eta} + \gamma_2 \frac{\pi}{2} \sin\left(\frac{\pi_t}{t_h} \right) \tag{3.54}$$

3.3.1 Solution of Case 1 via OGPAM

Consider (3.49) satisfying (3.48) and compare with equations (2.8) – (2.10), we have

$$k = \frac{1+\beta H}{4\,\mathrm{Re}},\ n = 0,\ \phi = \phi,\ t = \tau,\ r = \eta \tag{3.55}$$

$$F(r,t,\phi) = -\frac{\beta H}{4\,\mathrm{Re}} \varepsilon^m \frac{\partial^2 \phi}{\partial \eta^2} + \frac{1}{4\,\mathrm{Re}} \frac{1}{\varepsilon} \frac{\partial}{\partial \eta} \left(\varepsilon \left(1 + \beta H \left(1 - \varepsilon^m \right) \right) \right) \frac{\partial \phi}{\partial \eta} - \frac{M^2}{\mathrm{Re}} \phi - \frac{k_p}{\mathrm{Re}} \left(1 + \beta H \left(1 - \varepsilon^m \right) \right) \phi - D \tag{3.56}$$

$$f(r) = 0, \alpha_1 = 1, \beta_1 = 0, g_1(t) = 0, \alpha_2 = 0, \beta_2 = 1, g_2(t) = 0, a = 0, b = 1 \tag{3.57}$$

Then

$$A = \left(1 - \frac{1}{3} \right) = \frac{2}{3}, B = \left(1 - \frac{2}{3} \right) = \frac{1}{3}, C = \frac{1}{3} \tag{3.58}$$

Assumed a polynomial solution of the form (2.14) as:

$$\phi(\eta,t) = \phi \Big|_{\eta=0} - \phi \Big|_{\eta=0} \eta^2 \tag{3.59}$$

Then

$$\int_0^1 r^n F(r,t,\phi)\, dr = \int_0^1 \left(\begin{array}{l} \left(\frac{-\beta H}{4\,\mathrm{Re}} (2\eta - z)^m \frac{\partial^2 \phi}{\partial \eta^2} + \frac{1}{4\,\mathrm{Re}} \frac{1}{(2\eta - z)} \frac{\partial}{\partial \eta} \left((2\eta - z) \left(1 + \beta H \left(1 - (2\eta - z)^m \right) \right) \right) \right) \frac{\partial \phi}{\partial \eta} - \\ \frac{M^2}{\mathrm{Re}} \phi - \frac{k_p}{\mathrm{Re}} \left(1 + \beta H \left(1 - (2\eta - z)^m \right) \right) \phi - D \end{array} \right) d\eta \tag{3.60}$$

$$\int_0^1 \left(\begin{array}{l} \dfrac{2\beta H}{4\,\mathrm{Re}}\phi\Big|_{\eta=0}(2\eta-z)^m + \dfrac{4m\beta H}{4\,\mathrm{Re}}\phi\Big|_{\eta=0}\eta(2\eta-z)^{m-1} \\ -\dfrac{4(1+\beta H)}{4\,\mathrm{Re}}\phi\Big|_{\eta=0}\dfrac{\eta}{(2\eta-z)} + \dfrac{4\beta H}{4\,\mathrm{Re}}\phi\Big|_{\eta=0}\eta(2\eta-z)^{m-1} \\ -\dfrac{M^2}{\mathrm{Re}}\phi\Big|_{\eta=0}(1-\eta^2) - D - \dfrac{k_p}{\mathrm{Re}}(1+\beta H)\phi\Big|_{\eta=0} + \dfrac{k_p}{\mathrm{Re}}\beta H\phi\Big|_{\eta=0}(2\eta-z)^m + \\ \dfrac{k_p}{\mathrm{Re}}(1+\beta H)\phi\Big|_{\eta=0}\eta^2 - \dfrac{k_p}{\mathrm{Re}}\beta H\phi\Big|_{\eta=0}\eta^2(2\eta-z)^m \end{array} \right) d\eta \quad (3.61)$$

$$= \left(\begin{array}{l} \left(\dfrac{(2-z)^{m+1}}{2(m+1)} - \dfrac{z^{m+1}}{2(m+1)}\right)\left(\dfrac{2}{4\,\mathrm{Re}} + \dfrac{k_p}{\mathrm{Re}}\right)\beta H - \dfrac{4(1+\beta H)}{4\,\mathrm{Re}}\left(\dfrac{1}{2} + \dfrac{\ln\left(\dfrac{z-2}{z}\right)z}{4}\right) - \\ \dfrac{2M^2}{3\mathrm{Re}} - \dfrac{2}{3}\dfrac{k_p}{\mathrm{Re}}(1+\beta H) + \dfrac{4\beta H}{4\,\mathrm{Re}}(m+1)\left(\dfrac{2^{m-1}}{m+1} - \dfrac{(m-1)2^{m-2}z}{m} + \right. \\ \left.(m-2)2^{m-2}z^2\right) - \\ \dfrac{k_p}{\mathrm{Re}}\beta H\left(\dfrac{2^m}{m+3} - \dfrac{2^{m-1}mz}{m+2} + \dfrac{2^{m-3}m(m-1)z^2}{(m+1)}\right) \end{array} \right)\phi\Big|_{\eta=0} - D \quad (3.62)$$

$\Rightarrow$

$$p_1 = \left(\begin{array}{l} \left(\dfrac{(2-z)^{m+1}}{2(m+1)} - \dfrac{z^{m+1}}{2(m+1)} \right) \left(\dfrac{2}{4\,\mathrm{Re}} + \dfrac{k_p}{\mathrm{Re}} \right) \beta H - \\ \dfrac{4(1+\beta H)}{4\,\mathrm{Re}} \left(\dfrac{1}{2} + \dfrac{\ln\left(\dfrac{z-2}{z} \right) z}{4} \right) - \\ \dfrac{2M^2}{3\,\mathrm{Re}} - \dfrac{2}{3} \dfrac{k_p}{\mathrm{Re}} (1+\beta H) + \dfrac{4\beta H}{4\,\mathrm{Re}} (m+1) \left(\dfrac{2^{m-1}}{m+1} - \dfrac{(m-1)2^{m-2} z}{m} + \right) - \\ (m-2)2^{m-2} z^2 \\ \dfrac{k_p}{\mathrm{Re}} \beta H \left(\dfrac{2^m}{m+3} - \dfrac{2^{m-1} mz}{m+2} + \dfrac{2^{m-3} m(m-1) z^2}{(m+1)} \right) \end{array} \right) = B_0 \tag{3.63}$$

$$q_1(t) = -D \tag{3.64}$$

Then,

$$P(t) = \frac{3}{2} \left(\frac{1+\beta H}{4\,\mathrm{Re}} (-2+2) - B_0 \right) = -\frac{3}{2} (B_0) = -B_1 \tag{3.65}$$

$$q(t) = \frac{3}{2} (-D) = -\frac{3D}{2} = -B_2 \tag{3.66}$$

Then,

$$\phi \Big|_{\eta = 0} = e^{B_1 t} \int_0^t -B_2 e^{-B_1 x} dx + 0 \cdot e^{B_1 t} \tag{3.67}$$

$$= e^{B_1 t} \left(\frac{B_2}{B_1} e^{-B_1 x} \Big|_0^t \right) + 0 \tag{3.68}$$

$$= e^{B_1 t}\left(\frac{B_2}{B_1}\left(e^{-B_1 t}-1\right)\right) = \frac{B_2}{B_1}\left(1-e^{-B_1 t}\right) \tag{3.69}$$

Thus,

$$\phi(\eta,t) = \frac{B_2}{B_1}\left(1-e^{B_1 t}\right)\left(1-\eta^2\right) \tag{3.70}$$

Consider (3.50) satisfying (3.48), let $p = \left(\frac{1}{4Pe_1}+\frac{1}{4Pe_2}\right)$ and compare with equations (2.8) - (2.10), we have,

$$\begin{pmatrix} k=p,\ n=0,\ \phi=\theta,\ t=\tau,\ r=\eta,\ F\left(r,t,\phi\right)=\dfrac{1}{4Pe_1}\dfrac{1}{\varepsilon}\dfrac{\partial\theta}{\partial\eta}+\alpha_1\theta+\gamma_1\dfrac{\pi}{2}\sin\left(\dfrac{\pi_t}{t_h}\right), \\ f\left(r\right)=0,\ \alpha_1=1,\ \beta_1=0,\ g_1\left(t\right)=0,\ \alpha_2=0,\ \beta_2=1,\ g_2\left(t\right)=0, a=0,\ b=1 \end{pmatrix} \tag{3.71}$$

Then,

$$A=\frac{2}{3},\quad B=\frac{1}{3},\quad C=\frac{1}{3} \tag{3.72}$$

Assume a polynomial solution of the form (2.14) as:

$$\theta(\eta,t) = \theta\Big|_{\eta=0} - \theta\Big|_{\eta=0}\eta^2 \tag{3.73}$$

Then,

$$\int_0^1 r^n F\left(r,t,\phi\right)dr = \int_0^1\left(\frac{1}{4Pe_1}\frac{1}{\eta-z}\frac{\partial\theta}{\partial\eta}+\alpha_1\theta+\gamma_1\frac{\pi}{2}\sin\left(\frac{\pi_t}{t_h}\right)\right)d\eta \tag{3.74}$$

$$\int_0^1\left(-\frac{2}{4Pe_1}\theta\Big|_{\eta=0}\frac{\eta}{\left(2\eta-z\right)}+\alpha_1\theta\Big|_{\eta=0}\left(1-\eta^2\right)+\gamma_1\frac{\pi}{2}\sin\left(\frac{\pi_t}{t_h}\right)\right)d\eta \tag{3.75}$$

$$= -2\left(\frac{1}{4Pe_1}\left(\frac{1}{2} + \frac{\ln\left(\frac{z-2}{z}\right)z}{4} \right) - \frac{\alpha_1}{3} \right)\theta\Big|_{\eta=0} + \gamma_1 \frac{\pi}{2}\sin\left(\frac{\pi_t}{t_h}\right) \tag{3.76}$$

$$P_1 = -2\left(\frac{1}{4Pe_1}\left(\frac{1}{2} + \frac{\ln\left(\frac{z-2}{z}\right)z}{4} \right) - \frac{\alpha_1}{3} \right) = -B_3 \tag{3.77}$$

$$q_1(t) = \gamma_1 \frac{\pi}{2}\sin\left(\frac{\pi_t}{t_h}\right) = B_4 \tag{3.78}$$

Then,

$$P(t) = \frac{3}{2}\left(\frac{p}{2}(-2+2) + B_3 \right) = B_5 \tag{3.79}$$

$$q(t) = \frac{3}{2}B_4 = B_6 \tag{3.80}$$

Then,

$$\theta\Big|_{\eta=0} = e^{-B_5 t}\int_0^t B_6 e^{B_5 x}dx + 0\cdot e^{-B_5 t} \tag{3.81}$$

$$= e^{-B_5 t}\left(\frac{B_6}{B_5} e^{B_5 x}\Big|_0^t \right) + 0 \tag{3.82}$$

$$\theta\Big|_{\eta=0} = \frac{B_6}{B_5}\left(1 - e^{-B_5 t}\right) \tag{3.83}$$

Thus,

$$\theta(\eta,t)=\frac{B_6}{B_5}\left(1-e^{-B_5 t}\right)\left(1-\eta^2\right) \tag{3.84}$$

Consider (3.51) satisfying (3.48), let $q=\left(\frac{1}{4Pe_3}+\frac{1}{4Pe_4}\right)$ and compare with equations (2.8)-(2.10), we have,

$$\left(\begin{array}{l} k=q,\ n=0,\ \phi=\psi,\ t=\tau,\ r=\eta,\ F\left(r,t,\phi\right)=\alpha q\theta\frac{\partial^2\psi}{\partial\eta^2}+ \\ \alpha q\frac{\partial\theta}{\partial\eta}\frac{\partial\psi}{\partial\eta}+\frac{1}{4Pe_3}\frac{1}{\varepsilon}\left(1+\alpha\theta\right)\frac{\partial\psi}{\partial\eta}+\frac{a}{2}\phi\frac{\partial\psi}{\partial\eta}+\gamma_2\frac{\pi}{2}\sin\left(\frac{\pi_t}{t_h}\right), \\ f\left(r\right)=0,\ \alpha_1=1,\ \beta_1=0,\ g_1\left(t\right)=0,\ \alpha_2=0,\ \beta_2=1,\ g_2\left(t\right)=0, a=0,\ b=1 \end{array}\right) \tag{3.85}$$

Then,

$$A=\frac{2}{3},\quad B=\frac{1}{3},\quad C=\frac{1}{3} \tag{3.86}$$

Assume a polynomial solution of the form (2.14) as:

$$\psi\left(\eta,t\right)=\psi\Big|_{\eta=0}-\psi\Big|_{\eta=0}\eta^2 \tag{3.87}$$

Then,

$$\int_0^1 r^n F\left(r,t,\phi\right)dr=$$
$$\int_0^1\left(\begin{array}{l}\alpha q\theta\frac{\partial^2\psi}{\partial\eta^2}+\alpha q\frac{\partial\theta}{\partial\eta}\frac{\partial\psi}{\partial\eta}+\frac{1}{4Pe_3}\frac{1}{\left(2\eta-z\right)}\left(1+\alpha\theta\right)\frac{\partial\psi}{\partial\eta}+\frac{a}{2}\phi\frac{\partial\psi}{\partial\eta}+ \\ \gamma_2\frac{\pi}{2}\sin\left(\frac{\pi_t}{t_h}\right)\end{array}\right)d\eta \tag{3.88}$$

$$\int_0^1 \begin{pmatrix} \alpha q\left(-2\psi\Big|_{\eta=0}\right)\theta\Big|_{\eta=0}\left(1-\eta^2\right)+4\alpha q\theta\Big|_{\eta=0}\psi\Big|_{\eta=0}\eta^2- \\ \frac{2}{4Pe_3}\frac{\eta}{(2\eta-z)}\psi\Big|_{\eta=0}-\frac{2}{4Pe_3}\alpha\theta\Big|_{\eta=0}\psi\Big|_{\eta=0}\frac{\eta\left(1-\eta^2\right)}{(2\eta-z)}- \\ a\phi\Big|_{\eta=0}\psi\Big|_{\eta=0}\eta\left(1-\eta^2\right)+\gamma_2\frac{\pi}{2}\sin\left(\frac{\pi_t}{t_h}\right) \end{pmatrix} d\eta \qquad (3.89)$$

$$= \begin{pmatrix} \begin{pmatrix} \alpha\left(-\frac{2}{4Pe_3}\left(\frac{1}{16}ln(-z)z^3-\frac{1}{4}zln(-z)+\frac{1}{3}-\frac{1}{8}z-\frac{1}{8}z^3-\right.\right.\right. \\ \left.\left.\left.\frac{1}{16}ln(2-z)z^3+\frac{1}{4}z\ln(2-z)\right)\right)\theta\Big|_{\eta=0}- \\ \frac{a}{4}\phi\Big|_{\eta=0}-\frac{2}{4Pe_3}\left(\frac{1}{2}+\frac{\ln\left(\frac{z-2}{z}\right)z}{4}\right) \end{pmatrix}\psi\Big|_{\eta=0}+ \\ \gamma_2\frac{\pi}{2}\sin\left(\frac{\pi_t}{t_h}\right) \end{pmatrix} \qquad (3.90)$$

$\Rightarrow$

$$P_1 = \begin{pmatrix} \begin{pmatrix} -\frac{2\alpha B_6}{4Pe_3}\left(\frac{1}{16}ln(-z)z^3-\frac{1}{4}zln(-z)+\frac{1}{3}-\frac{1}{8}z-\frac{1}{8}z^3-\right.\right. \\ \left.\left.\frac{1}{16}ln(2-z)z^3+\frac{1}{4}z\ln(2-z)\right)+\frac{aB_2}{4}\end{pmatrix}t- \\ \frac{2}{4Pe_3}\left(\frac{1}{2}+\frac{\ln\left(\frac{z-2}{z}\right)z}{4}\right) \end{pmatrix} = \left(B_7t-B_8\right) \qquad (3.91)$$

$$q_1(t)=\gamma_2\frac{\pi}{2}\sin\left(\frac{\pi_t}{t_h}\right)=B_9 \qquad (3.92)$$

Then,

$$P(t)=\frac{3}{2}\left(\left(-\frac{q}{2}(-2+2)+B_8\right)-B_7t\right)=\frac{3}{2}\left(B_{10}-B_7t\right) \qquad (3.93)$$

$$q(t)=\frac{3}{2}B_9=B_{11} \tag{3.94}$$

Then,

$$\psi\Big|_{\eta=0}=e^{-\frac{3}{2}\int(B_{10}-B_7t)dt}\int_0^t B_{11}e^{\frac{3}{2}\int(B_{10}-B_7x)dx}dx+0e^{-\int(B_{10}-B_7t)dt} \tag{3.95}$$

$$=e^{-\frac{3}{2}\left(B_{10}t-\frac{1}{2}B_7t^2\right)}\int_0^t B_{11}e^{\frac{3}{2}\left(B_{10}x-\frac{1}{2}B_7x^2\right)}dx+0 \tag{3.96}$$

$$\psi\Big|_{\eta=0}=e^{-\frac{3}{2}\left(B_{10}t-\frac{1}{2}B_7t^2\right)}\left(\sqrt{\frac{\pi}{3B_7}}B_{11}e^{\frac{3}{4}\frac{B_{10}^2}{B_7}}\left(erf\left(\frac{B_{10}}{2}\sqrt{\frac{3}{B_7}}\right)+erf\left(\frac{\sqrt{3}\left(B_7t-B_{10}\right)}{2\sqrt{B_7}}\right)\right)\right) \tag{3.97}$$

Thus,

$$\psi(\eta,t)=\psi\Big|_{\eta=0}\left(1-\eta^2\right) \tag{3.98}$$

3.3.2 Solution of Case 2 via OGPAM

Consider (3.52) satisfying (3.48) and compare with equations (2.8) – (2.10), we have

$$k=\frac{1}{4\,\mathrm{Re}},\ n=0,\ \phi=\phi,\ t=\tau,\ r=\eta \tag{3.99}$$

$$F(r,t,\phi)=\frac{1}{4\,\mathrm{Re}}\frac{1}{\varepsilon}\frac{\partial}{\partial\eta}(\varepsilon)\frac{\partial\phi}{\partial\eta}-\frac{M^2}{\mathrm{Re}}\phi-\frac{k_p}{\mathrm{Re}}\phi-D \tag{3.100}$$

$$f(r)=0,\alpha_1=1,\beta_1=0,g_1(t)=0,\alpha_2=0,\beta_2=1,g_2(t)=0,a=0,b=1 \tag{3.101}$$

Then,

$$A=\left(1-\frac{1}{3}\right)=\frac{2}{3}, B=\left(1-\frac{2}{3}\right)=\frac{1}{3}, C=\frac{1}{3} \tag{3.102}$$

Assumed a polynomial solution of the form (2.14) as:

$$\phi(\eta,t)=\phi\Big|_{\eta=0}-\phi\Big|_{\eta=0}\eta^2 \tag{3.103}$$

Then,

$$\int_0^1 r^n F(r,t,\phi)\,dr=\int_0^1\left(\left(\frac{1}{4\,\mathrm{Re}}\frac{1}{(2\eta-z)}\frac{\partial}{\partial\eta}\left((2\eta-z)\right)\right)\frac{\partial\phi}{\partial\eta}-\frac{M^2}{\mathrm{Re}}\phi-\frac{k_p}{\mathrm{Re}}\phi-D\right)d\eta \tag{3.104}$$

$$=\int_0^1\left(-\frac{1}{\mathrm{Re}}\phi\Big|_{\eta=0}\frac{\eta}{(2\eta-z)}-\frac{M^2}{\mathrm{Re}}\phi\Big|_{\eta=0}\left(1-\eta^2\right)-D-\frac{k_p}{\mathrm{Re}}\phi\Big|_{\eta=0}+\frac{k_p}{\mathrm{Re}}\phi\Big|_{\eta=0}\eta^2\right)d\eta \tag{3.105}$$

$$=\left(-\frac{1}{\mathrm{Re}}\left(\frac{1}{2}+\frac{\ln\left(\frac{z-2}{z}\right)z}{4}\right)-\frac{2M^2}{3\mathrm{Re}}-\frac{2}{3}\frac{k_p}{\mathrm{Re}}\right)\phi\Big|_{\eta=0}-D \tag{3.106}$$

$\Rightarrow$

$$p_1=\left(-\frac{1}{\mathrm{Re}}\left(\frac{1}{2}+\frac{\ln\left(\frac{z-2}{z}\right)z}{4}\right)-\frac{2M^2}{3\mathrm{Re}}-\frac{2}{3}\frac{k_p}{\mathrm{Re}}\right)=B_{12} \tag{3.107}$$

$$q_1(t)=-D \tag{3.108}$$

Then,

$$P(t)=\frac{3}{2}\left(\frac{1}{4\,\mathrm{Re}}(-2+2)-B_{12}\right)=-\frac{3}{2}(B_{12})=-B_{13} \tag{3.109}$$

$$q(t)=\frac{3}{2}(-D)=-\frac{3D}{2}=-B_2 \tag{3.110}$$

Then,

$$\phi\Big|_{\eta=0}=e^{B_{13}t}\int_0^t -B_2e^{-B_{13}x}dx+0\cdot e^{B_{13}t} \tag{3.111}$$

$$=e^{B_{13}t}\left(\frac{B_2}{B_{13}}e^{-B_{13}x}\Big|_0^t\right)+0 \tag{3.112}$$

$$=e^{B_{13}t}\left(\frac{B_2}{B_{13}}\left(e^{-B_{13}t}-1\right)\right)=\frac{B_2}{B_{13}}\left(1-e^{-B_{13}t}\right) \tag{3.113}$$

Thus,

$$\phi(\eta,t)=\frac{B_2}{B_{13}}\left(1-e^{B_{13}t}\right)\left(1-\eta^2\right) \tag{3.114}$$

Consider (3.53) satisfying (3.48), let $p=\left(\frac{1}{4Pe_1}+\frac{1}{4Pe_2}\right)$ and compare with equations (2.8) - (2.10), we have,

$$\begin{pmatrix} k=p,\ n=0,\ \phi=\theta,\ t=\tau,\ r=\eta,\ F\left(r,t,\phi\right)=\dfrac{1}{4Pe_1}\dfrac{1}{\varepsilon}\dfrac{\partial\theta}{\partial\eta}+\alpha_1\theta+\gamma_1\dfrac{\pi}{2}\sin\left(\dfrac{\pi_t}{t_h}\right), \\ f\left(r\right)=0,\ \alpha_1=1,\ \beta_1=0,\ g_1\left(t\right)=0,\ \alpha_2=0,\ \beta_2=1,\ g_2\left(t\right)=0, a=0,\ b=1 \end{pmatrix} \tag{3.115}$$

Then,

$$A=\frac{2}{3},\quad B=\frac{1}{3},\quad C=\frac{1}{3} \tag{3.116}$$

Assumed a polynomial solution of the form (2.14) as:

$$\theta(\eta,t)=\theta\Big|_{\eta=0}-\theta\Big|_{\eta=0}\eta^2 \tag{3.117}$$

Then,

$$\int_0^1 r^n F(r,t,\phi)\,dr=\int_0^1\left(\frac{1}{4Pe_1}\frac{1}{\eta-z}\frac{\partial\theta}{\partial\eta}+\alpha_1\theta+\gamma_1\frac{\pi}{2}\sin\left(\frac{\pi_t}{t_h}\right)\right)d\eta \tag{3.118}$$

$$\int_0^1\left(-\frac{2}{4Pe_1}\theta\Big|_{\eta=0}\frac{\eta}{(2\eta-z)}+\alpha_1\theta\Big|_{\eta=0}\left(1-\eta^2\right)+\gamma_1\frac{\pi}{2}\sin\left(\frac{\pi_t}{t_h}\right)\right)d\eta \tag{3.119}$$

$$=-2\left(\frac{1}{4Pe_1}\left(\frac{1}{2}+\frac{\ln\left(\frac{z-2}{z}\right)z}{4}\right)-\frac{\alpha_1}{3}\right)\theta\Big|_{\eta=0}+\gamma_1\frac{\pi}{2}\sin\left(\frac{\pi_t}{t_h}\right) \tag{3.120}$$

$$P_1=-2\left(\frac{1}{4Pe_1}\left(\frac{1}{2}+\frac{\ln\left(\frac{z-2}{z}\right)z}{4}\right)-\frac{\alpha_1}{3}\right)=-B_3 \tag{3.121}$$

$$q_1(t)=\gamma_1\frac{\pi}{2}\sin\left(\frac{\pi_t}{t_h}\right)=B_4 \tag{3.122}$$

Then,

$$P(t)=\frac{3}{2}\left(\frac{p}{2}(-2+2)+B_3\right)=B_5 \tag{3.123}$$

$$q(t)=\frac{3}{2}B_4=B_6 \tag{3.124}$$

Then,

$$\theta\Big|_{\eta=0} = e^{-B_5 t}\int_0^t B_6 e^{B_5 x}dx + 0\cdot e^{-B_5 t} \tag{3.125}$$

$$= e^{-B_5 t}\left(\frac{B_6}{B_5}e^{B_5 x}\Big|_0^t\right) + 0 \tag{3.126}$$

$$\theta\Big|_{\eta=0} = \frac{B_6}{B_5}\left(1-e^{-B_5 t}\right) \tag{3.127}$$

Thus,

$$\theta(\eta,t) = \frac{B_6}{B_5}\left(1-e^{-B_5 t}\right)\left(1-\eta^2\right) \tag{3.128}$$

Consider (3.54) satisfying (3.48), let $q = \left(\frac{1}{4Pe_3}+\frac{1}{4Pe_4}\right)$ and compare with equations (2.8) - (2.10), we have,

$$\left(\begin{array}{l} k=q,\ n=0,\ \phi=\psi,\ t=\tau,\ r=\eta,\ F(r,t,\phi)=\dfrac{1}{4Pe_3}\dfrac{1}{\varepsilon}\dfrac{\partial\psi}{\partial\eta}+\dfrac{a}{2}\phi\dfrac{\partial\psi}{\partial\eta}+ \\ \gamma_2\dfrac{\pi}{2}\sin\left(\dfrac{\pi_t}{t_h}\right),\ f(r)=0,\ \alpha_1=1,\ \beta_1=0,\ g_1(t)=0,\ \alpha_2=0,\ \beta_2=1, \\ g_2(t)=0, a=0,\ b=1 \end{array}\right) \tag{3.129}$$

Then,

$$A=\frac{2}{3},\quad B=\frac{1}{3},\quad C=\frac{1}{3} \tag{3.130}$$

Assumed a polynomial solution of the form (2.14) as:

$$\psi(\eta,t) = \psi\Big|_{\eta=0} - \psi\Big|_{\eta=0}\eta^2 \tag{3.131}$$

Then,

$$\int_0^1 r^n F\left(r,t,\phi\right)dr = \int_0^1 \left(\frac{1}{4Pe_3}\frac{1}{\left(2\eta - z\right)}\frac{\partial \psi}{\partial \eta} + \frac{a}{2}\phi\frac{\partial \psi}{\partial \eta} + \gamma_2 \frac{\pi}{2}\sin\left(\frac{\pi_t}{t_h}\right)\right)d\eta \tag{3.132}$$

$$= \int_0^1 \left(\frac{2}{4Pe_3}\frac{\eta}{\left(2\eta - z\right)}\psi\Big|_{\eta=0} - a\phi\Big|_{\eta=0}\psi\Big|_{\eta=0}\eta\left(1-\eta^2\right) + \gamma_2\frac{\pi}{2}\sin\left(\frac{\pi_t}{t_h}\right)\right)d\eta \tag{3.133}$$

$$= \left(\left(-\frac{a}{4}\phi\Big|_{\eta=0} - \frac{2}{4Pe_3}\left(\frac{1}{2} + \frac{\ln\left(\frac{z-2}{z}\right)z}{4}\right)\right)\psi\Big|_{\eta=0} + \gamma_2\frac{\pi}{2}\sin\left(\frac{\pi_t}{t_h}\right)\right. \tag{3.134}$$

$\Rightarrow$

$$P_1 = \left(\frac{aB_2}{4}t - \frac{2}{4Pe_3}\left(\frac{1}{2} + \frac{\ln\left(\frac{z-2}{z}\right)z}{4}\right)\right) = \left(B_{14}t - B_8\right) \tag{3.135}$$

$$q_1\left(t\right) = \gamma_2\frac{\pi}{2}\sin\left(\frac{\pi_t}{t_h}\right) = B_9 \tag{3.136}$$

Then,

$$P\left(t\right) = \frac{3}{2}\left(\left(-\frac{q}{2}\left(-2+2\right) + B_8\right) - B_{14}t\right) = \frac{3}{2}\left(B_{10} - B_{14}t\right) \tag{3.137}$$

$$q\left(t\right) = \frac{3}{2}B_9 = B_{11} \tag{3.138}$$

Then,

$$\psi\Big|_{\eta=0} = e^{-\frac{3}{2}\int\left(B_{10}-B_{14}t\right)dt}\int_0^t B_{11}e^{\frac{3}{2}\int\left(B_{10}-B_{14}x\right)dx}dx + 0e^{-\int\left(B_{10}-B_{14}t\right)dt} \tag{3.139}$$

$$= e^{-\frac{3}{2}\left(B_{10}t-\frac{1}{2}B_{14}t^2\right)}\int_0^t B_{11}e^{\frac{3}{2}\left(B_{10}x-\frac{1}{2}B_{14}x^2\right)}dx+0 \tag{3.140}$$

$$\psi\Big|_{\eta=0} = e^{-\frac{3}{2}\left(B_{10}t-\frac{1}{2}B_{14}t^2\right)}\left(\sqrt{\frac{\pi}{3B_{14}}}B_{11}e^{\frac{3}{4}\frac{B_{10}^2}{B_{14}}}\left(erf\left(\frac{B_{10}}{2}\sqrt{\frac{3}{B_{14}}}\right)+erf\left(\frac{\sqrt{3}\left(B_{14}t-B_{10}\right)}{2\sqrt{B_{14}}}\right)\right)\right) \tag{3.141}$$

Thus,

$$\psi\left(\eta,t\right)=\psi\Big|_{\eta=0}\left(1-\eta^2\right) \tag{3.142}$$

$$B_{14}=\frac{a}{4}B_2 \tag{3.143}$$

CHAPTER FOUR

4.0 RESULTS AND DISCUSSION

4.1 Analysis of Results

In this analysis, we solved the equations governing the blood flow and heat transfer in the cardiovascular system of human undergoing tumor treatment analytically using OGPAM. This is to see the effect of parameters involved on the axial velocity of blood flow, tissue temperature and blood temperature. Two cases were considered.

Finally, we examined the effect of the Reynolds number (Re), Permeability parameter (k), Peclet numbers (P_{e1}, P_{e2}), Pressure gradient parameter (C), Hematocrit (H), Perfusion mass flow rate (α_1), Temperatures ratio (α), Tissue power of heat added (γ_1), Blood power of heat added (γ_2), Hartman number (M) on the velocity and temperatures. The computations were done using computer symbolic algebraic package MAPLE 17.

4.1.1 Graphs of case 1

Graphical illustrations of Case 1 problem are presented in Figures 4.1 to 4.24:

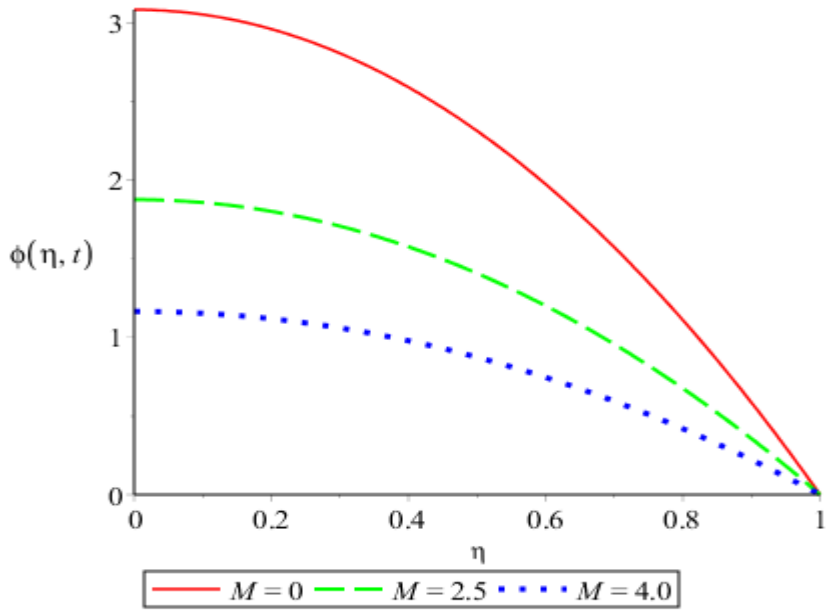

Figure 4.1: Graph of velocity profile against distance at M = 0, 2.5, and 4.0

Figure 4.1 shows the graph of velocity profile $\phi(\eta,t)$ against distance η with different values of Hartman number

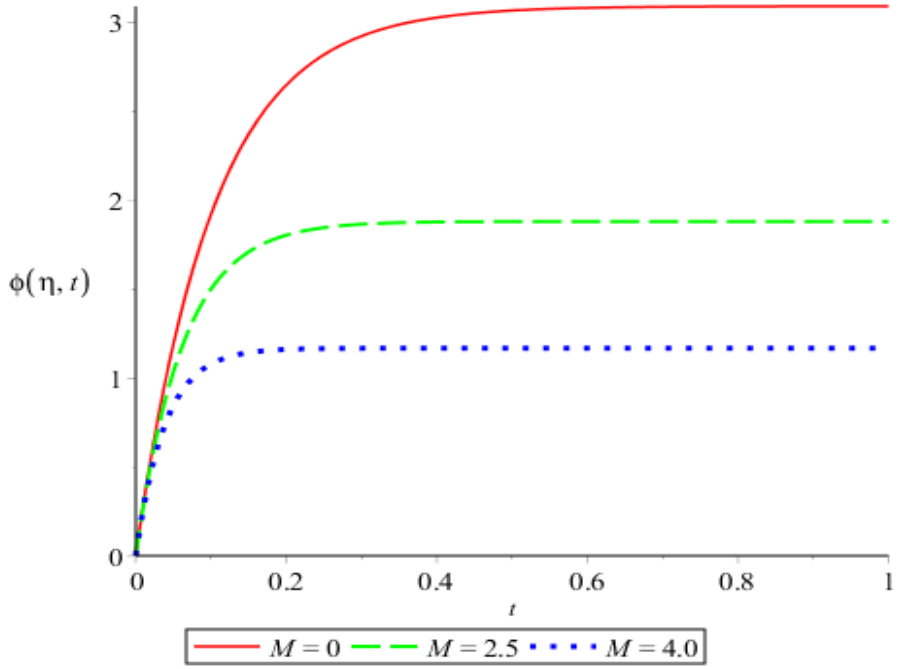

Figure 4.2: Graph of velocity profile against time at M = 0, 2.5, and 4.0

Figure 4.2 shows the graph of velocity profile $\phi(\eta,t)$ against time t for different values of Hartman number.

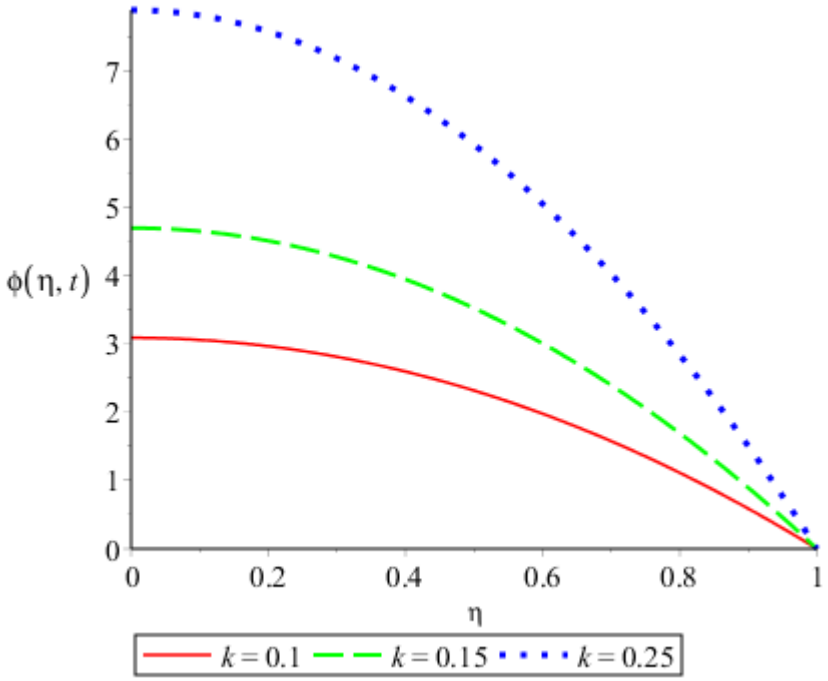

Figure 4.3: Graph of velocity profile against distance at k = 0.1, 0.15 and 0.25

Figure 4.3 shows the graph of velocity profile $\phi(\eta,t)$ against distance η for different values of permeability parameter.

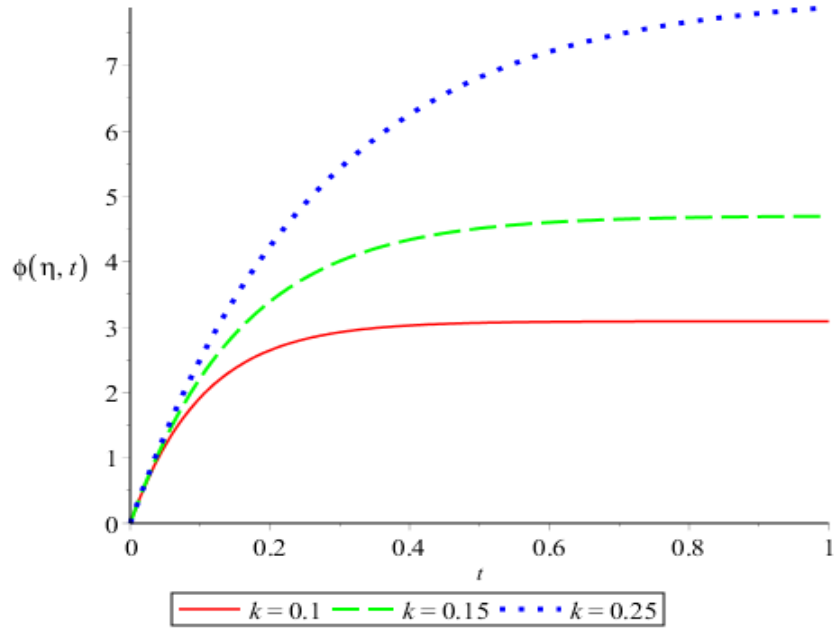

Figure 4.4: Graph of velocity profile against time at k = 0.1, 0.15 and 0.25

Figure 4.4 shows the graph of velocity profile $\phi(\eta,t)$ against time t for different values of permeability parameter.

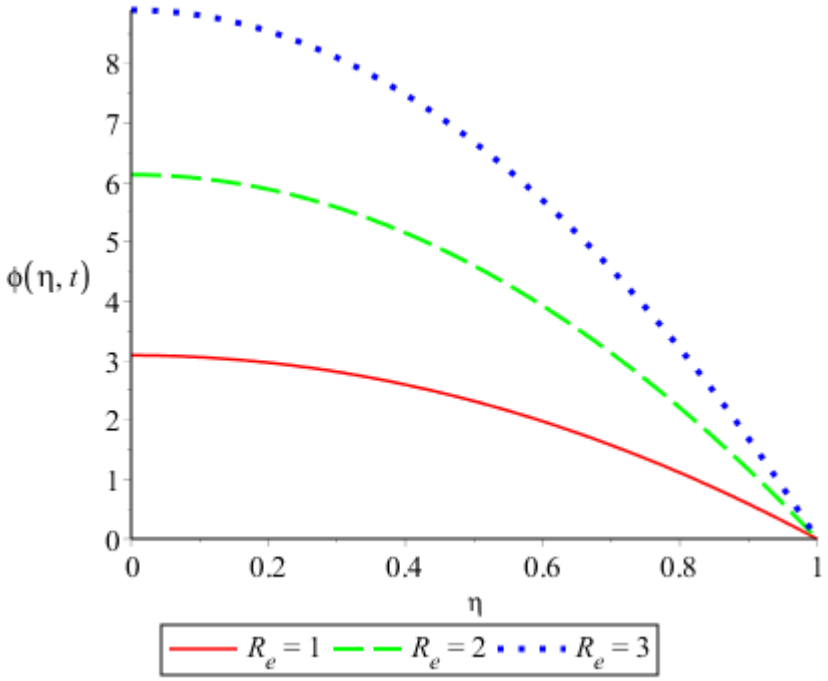

Figure 4.5: Graph of velocity profile against distance at R_e = 1, 2 and 3

Figure 4.5 shows the graph of velocity profile $\phi(\eta,t)$ against distance η for different values of Reynolds number

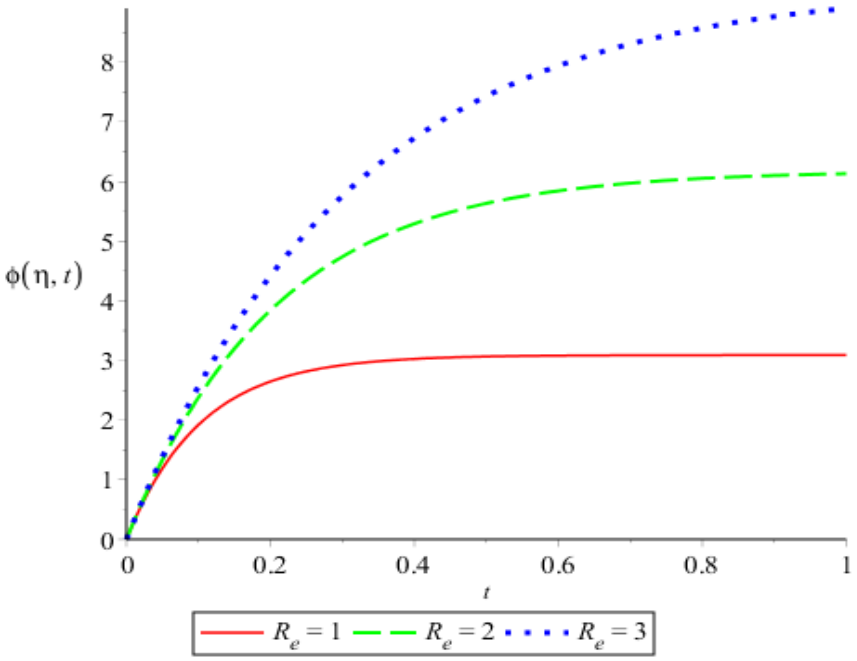

Figure 4.6: Graph of velocity profile against time at R_e =1, 2 and 3

Figure 4.6 shows the graph of velocity profile $\phi(\eta,t)$ against time t for different values of Reynolds number

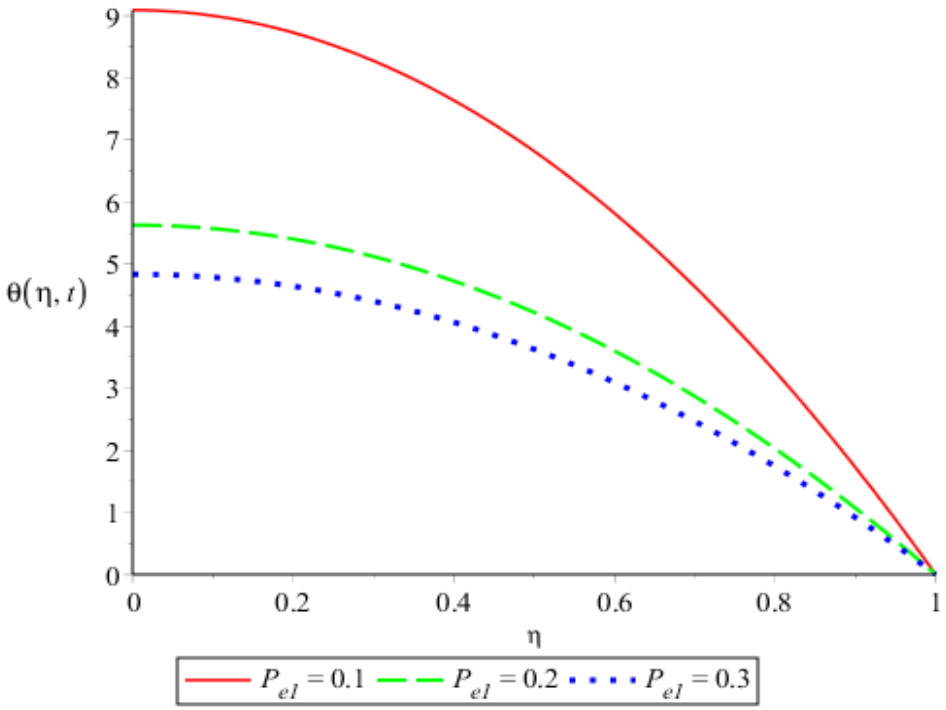

Figure 4.7: Graph of tissue temperature against distance at P_{e1} = 0.1, 0.2 and 0.3

Figure 4.7 shows the graph of tissue temperature $\theta(\eta,t)$ against distance η for different values of peclet number.

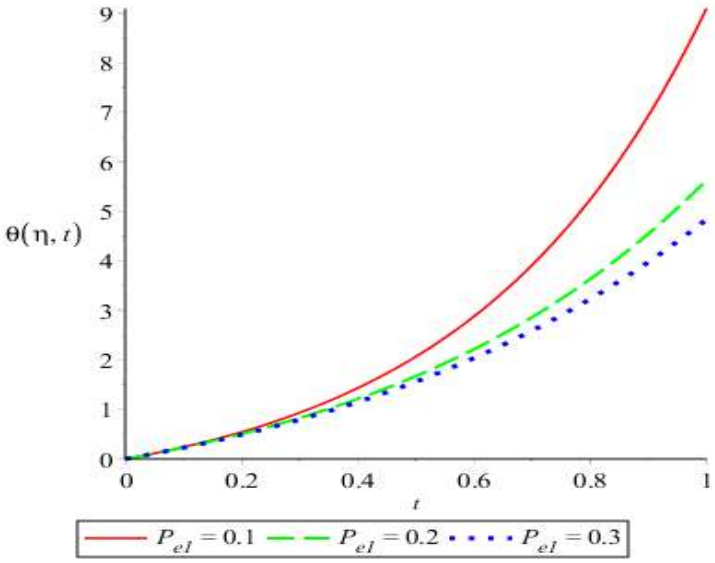

Figure 4.8: Graph of tissue temperature against time at P_{e1} = 0.1, 0.2 and 0.3

Figure 4.8 shows the graph of tissue temperature $\theta(\eta,t)$ against time t for different values of peclet number

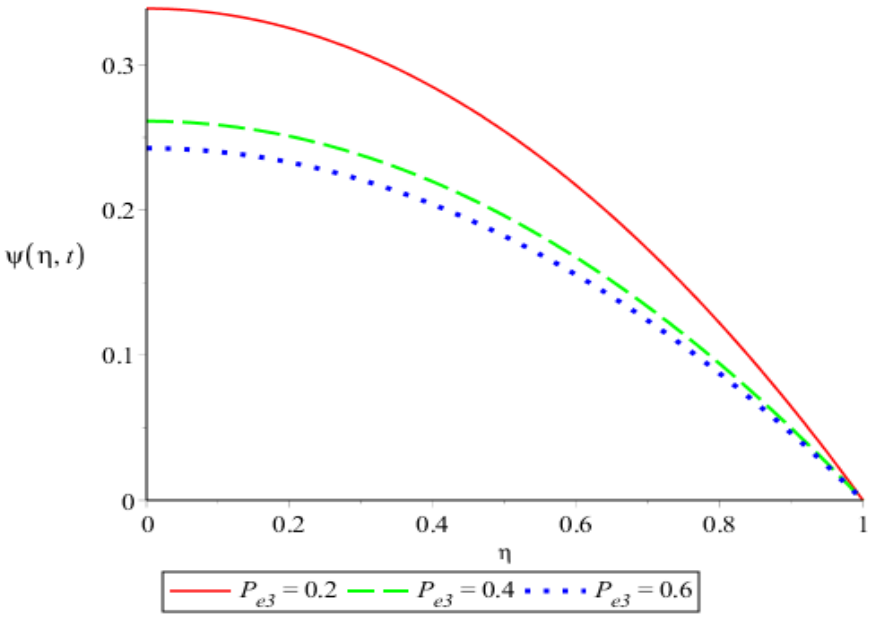

Figure 4.9: Graph of blood temperature against distance η at P_{e3} = 0.2, 0.4 and 0.6

Figure 4.9 shows the graph of blood temperature $\psi(\eta,t)$ against distance η for different values of peclet number.

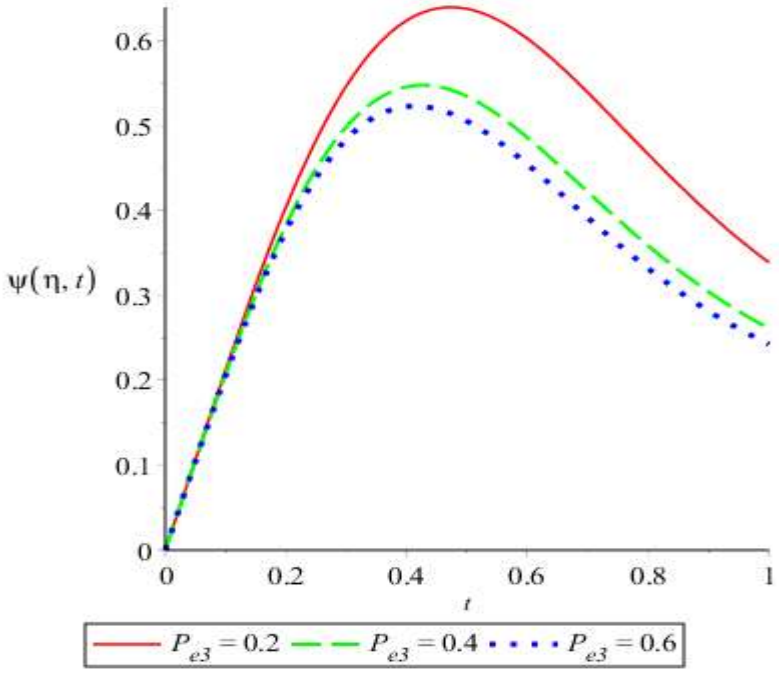

Figure 4.10: Graph of blood temperature against time at P_{e3} = 0.2, 0.4 and 0.6

Figure 4.10 shows the graph of blood temperature $\psi(\eta,t)$ against time t for different values of peclet number.

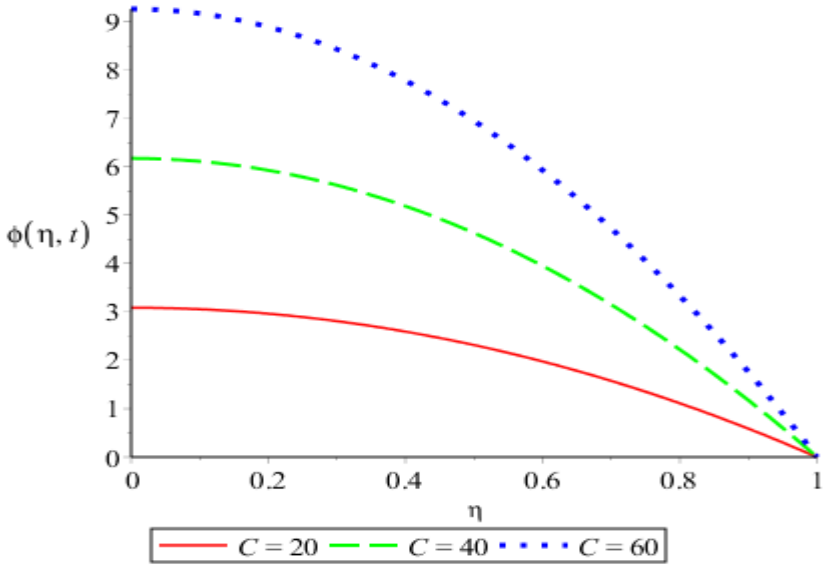

Fig 4.11: Graph of velocity profile against distance at C = 20, 40 and 60

Fig 4.11 shows the graph of velocity profile $\phi(\eta,t)$ against distance η for different values of pressure gradient parameter.

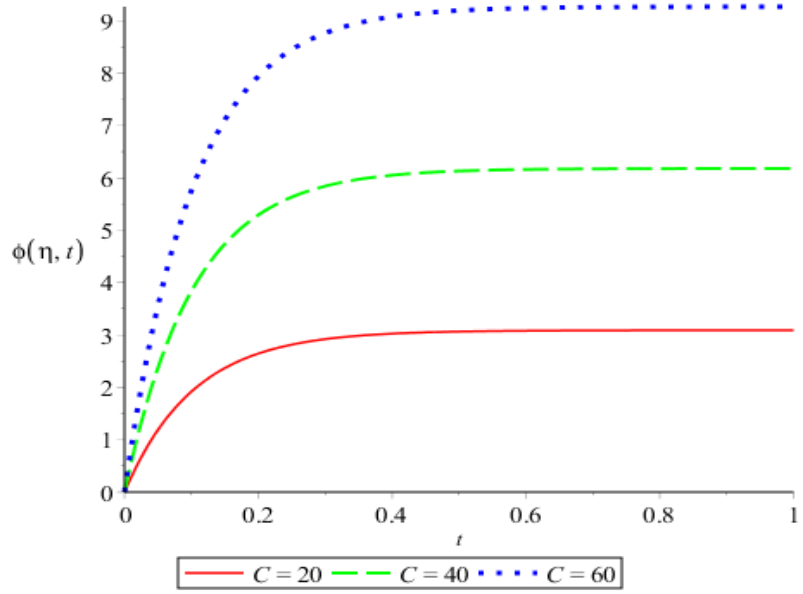

Figure 4.12: Graph of velocity profile against time at C = 20, 40 and 60

Fig 4.12 shows the graph velocity profile $\phi(\eta,t)$ against time t for different values of pressure gradient parameter.

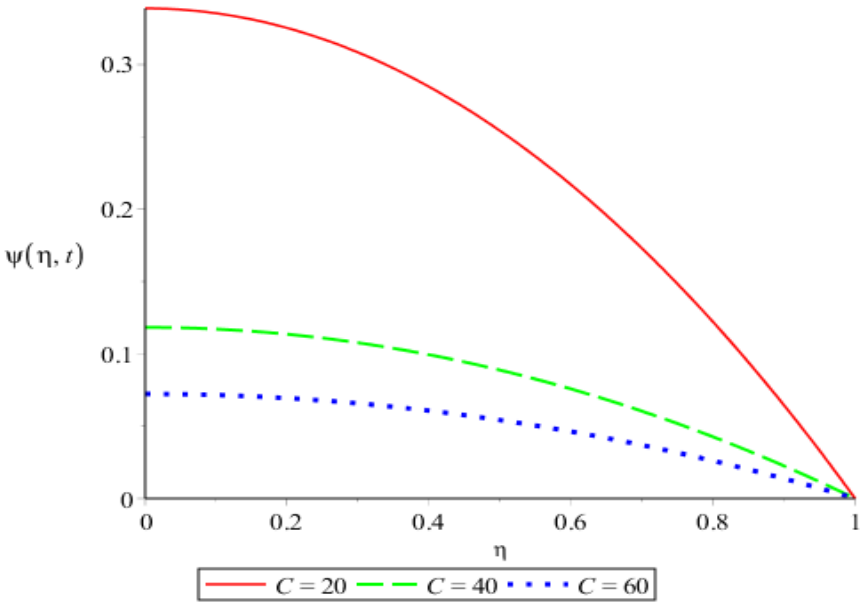

Figure 4.13: Graph of blood temperature against distance at C = 20, 40 and 60

Figure 4.13 shows the graph of blood temperature $\psi(\eta,t)$ against distance η for different values of pressure gradient parameter.

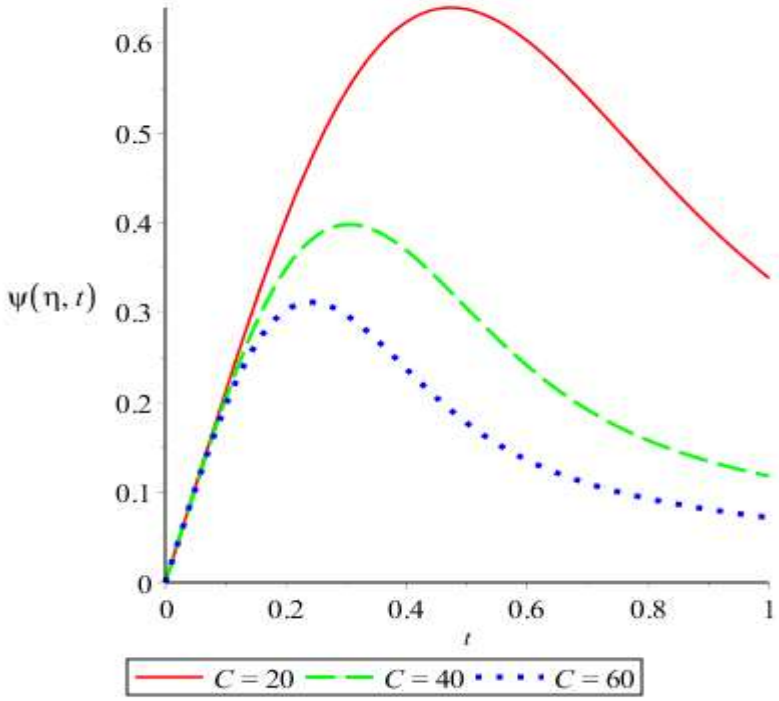

Figure 4.14: Graph of blood temperature against time at C = 20, 40 and 60

Figure 4.14 shows the graph of blood temperature $\psi(\eta,t)$ against time t for different values of pressure gradient parameter.

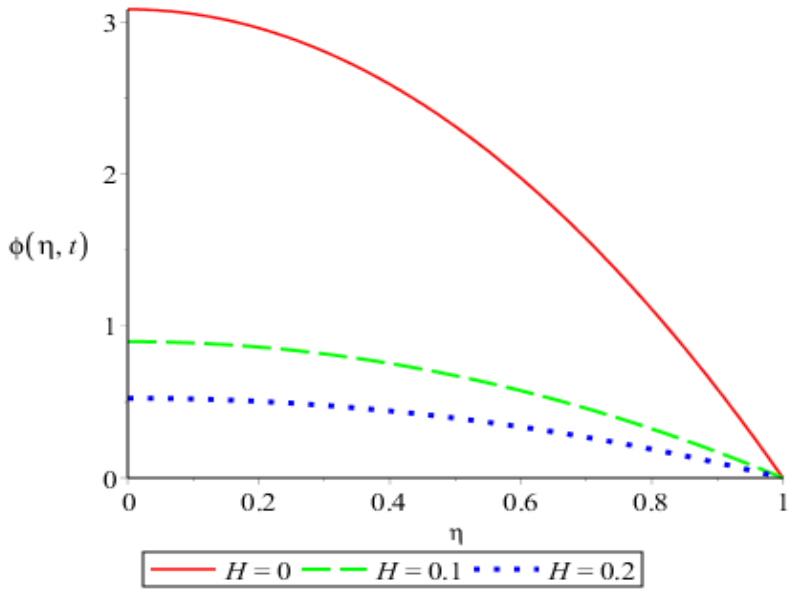

Figure 4.15: Graph of velocity profile against distance at H = 0, 0.1 and 0.2

Figure 4.15 shows the graph of velocity profile $\phi(\eta,t)$ against distance η for different values of Hematocrit.

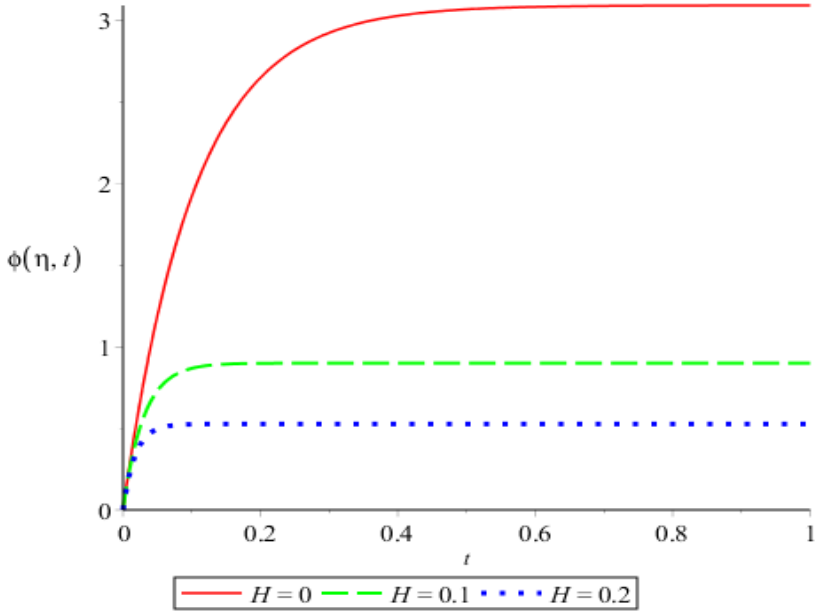

Figure 4.16: Graph of velocity profile against time at H = 0, 0.1 and 0.2

Figure 4.16 shows the graph of velocity profile $\phi(\eta,t)$ against time t for different values of Hematocrit.

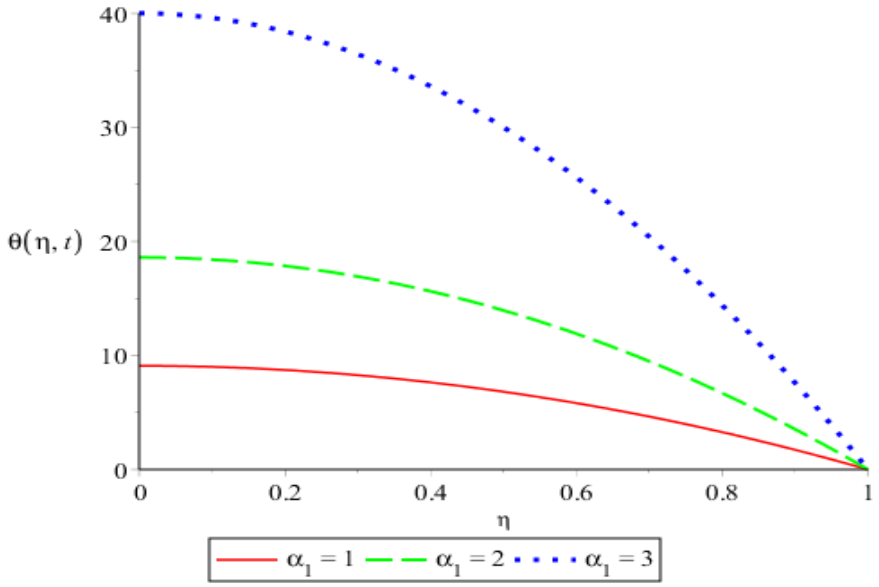

Figure 4.17: Graph of tissue temperature against distance at α_1 = 1, 2 and 3

Figure 4.17 shows the graph of tissue temperature $\theta(\eta,t)$ against distance η for different values of perfusion mass flow rate.

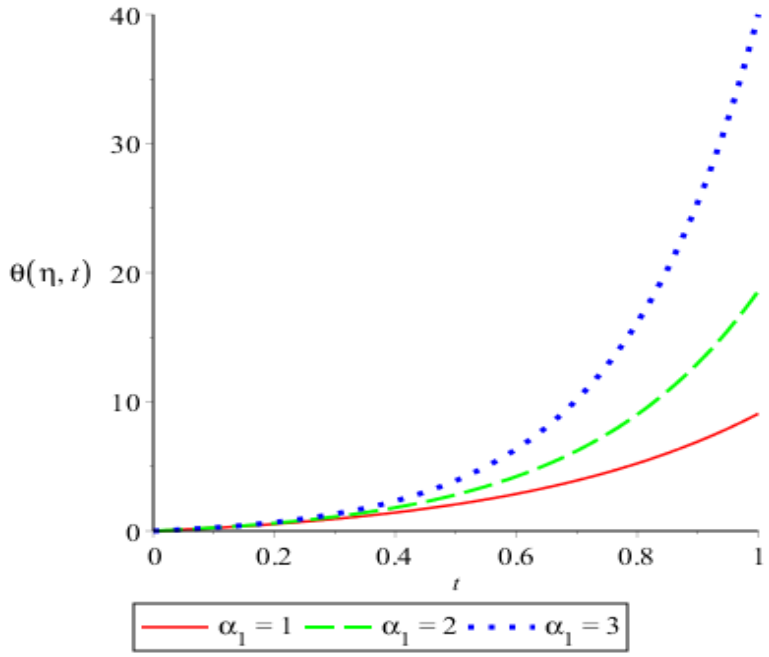

Figure 4.18: Graph of tissue temperature against time at α_1 = 1, 2 and 3

Figure 4.18 shows the graph of tissue temperature $\theta(\eta,t)$ against time t for different values of perfusion mass flow rate.

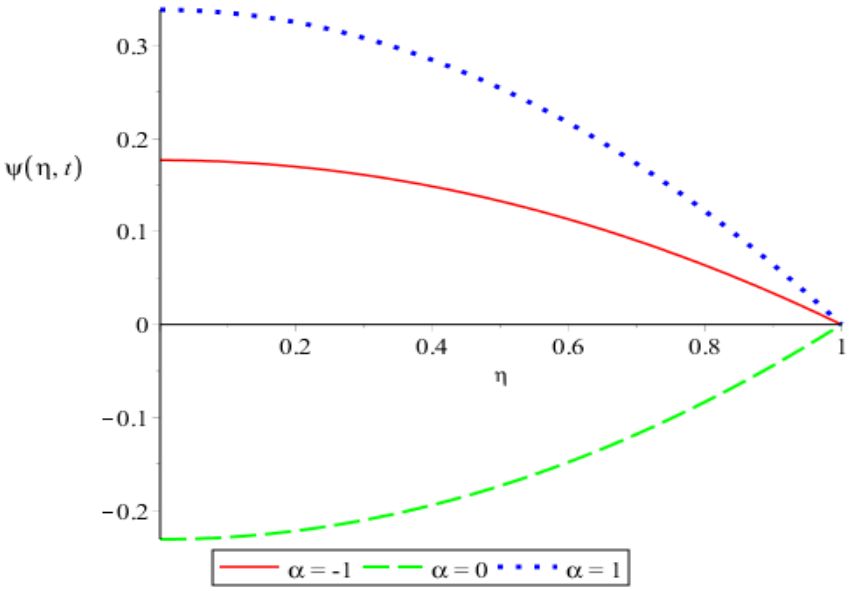

Figure 4.19: Graph of blood temperature against distance at α = -1, 0 and 1

Figure 4.19 shows the graph of blood temperature $\psi(\eta,t)$ against distance η for different values of perfusion mass flow rate.

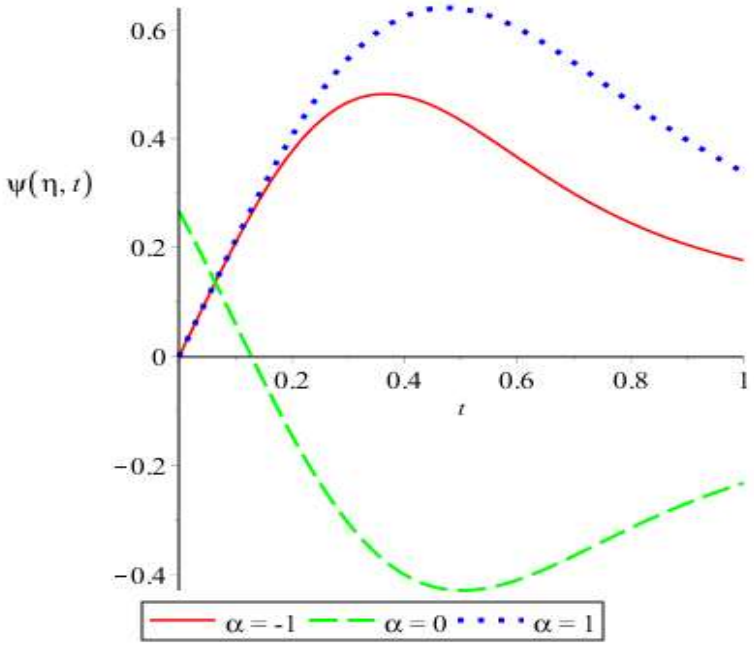

Figure 4.20: Graph of blood temperature against time at α = -1, 0 and 1

Figure 4.20 shows the graph blood temperature $\psi(\eta,t)$ against time t for different values of perfusion mass flow rate.

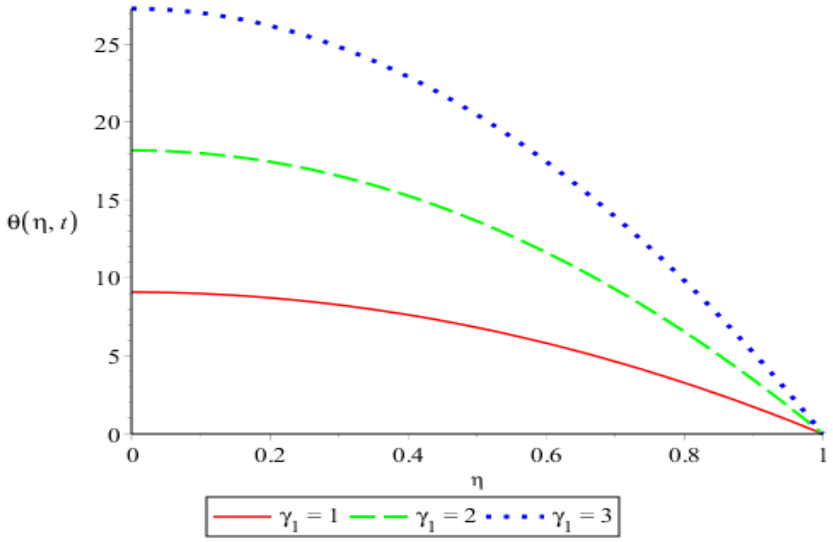

Figure 4.21: Graph of tissue temperature against distance at γ_1 = 1, 2 and 3

Figure 4.21 shows the graph of tissue temperature $\theta(\eta,t)$ against distance η for different values of tissue power of heat added.

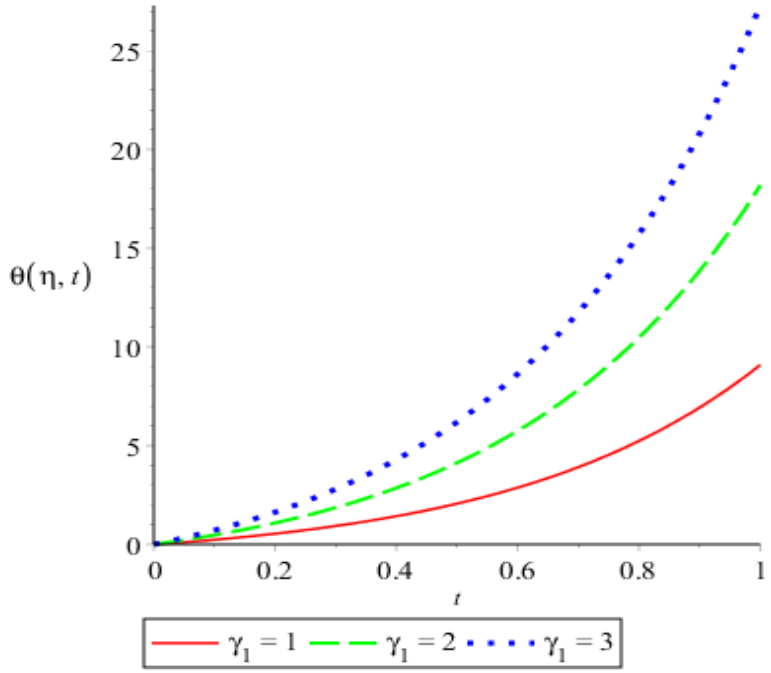

Figure 4.22: Graph of tissue temperature against time at γ_1 = 1, 2 and 3

Figure 4.22 is the graph of tissue temperature $\theta(\eta,t)$ against time t for different values of tissue power of heat added.

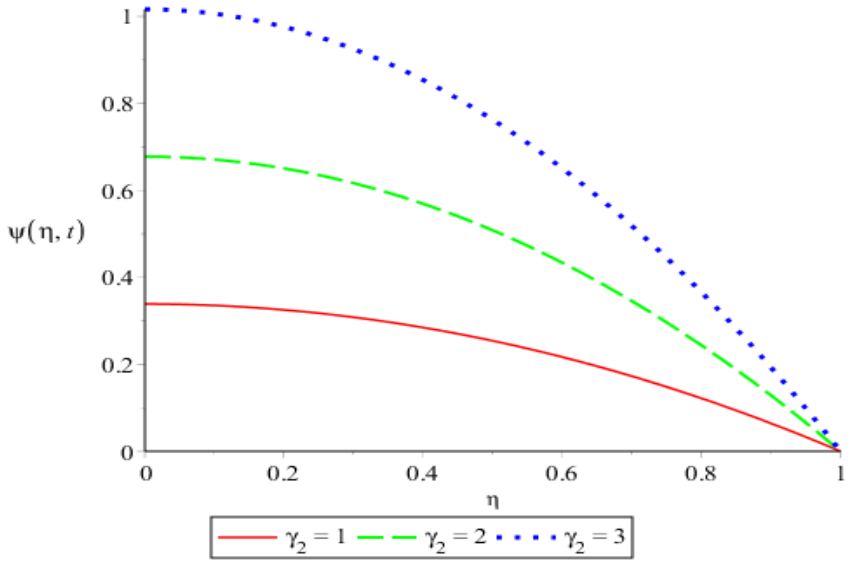

Figure 4.23: Graph of blood temperature against distance at γ_2 = 1, 2 and 3

Figure 4.23 is the graph of blood temperature $\psi(\eta,t)$ against distance η for different values of blood power of heat added.

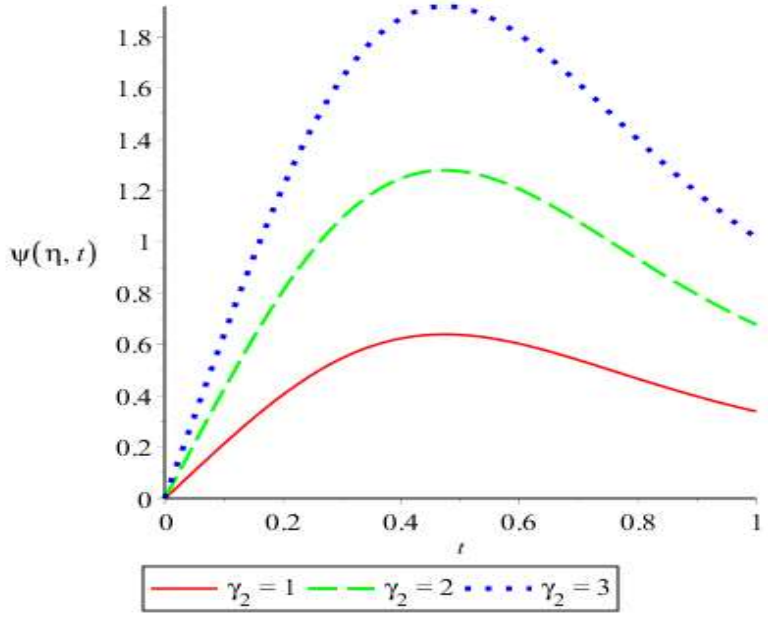

Figure 4.24: Graph of blood temperature against time at γ_2 = 1, 2 and 3

Figure 4.24 shows the graph of blood temperature $\psi(\eta,t)$ against time t for different values of blood power of heat added.

4.1.2 Discussion of results of case 1

Figure 4.1 displays the graph of velocity profile $\phi(\eta,t)$ for different values of Hartmann number (M). It is observed that velocity decrease along the distance and this velocity decreases as Hartmann number increases. Figure 4.2 shows the graph of velocity profile $\phi(\eta,t)$ for different values of Hartmann number (M). It is observed that velocity increase and later became steady with time and maximum velocity decreases as Hartmann number increases. Figure 4.3 depicts the graph of velocity profile $\phi(\eta,t)$ for different values of permeability parameter (k). It is observed that velocity decrease along the distance and this velocity increases as the values of permeability parameter increases. Figure 4.4 shows the graph of velocity profile $\phi(\eta,t)$ for different values of permeability parameter (k). It is observed that velocity increase and later became steady with time and maximum velocity increases as the value of permeability parameter increases. Figure 4.5 displays the graph of velocity profile $\phi(\eta,t)$ for different values of Reynolds number (R_e). It is observed that velocity decrease along the distance and this velocity increases as Reynolds number increases. Figure 4.6 depicts the graph of velocity profile $\phi(\eta,t)$ for different values of Reynolds number (R_e). It is observed that velocity increase and later became steady with time and maximum velocity increases as Reynolds number increases. Figure 4.7 shows the graph of tissue temperature profile $\theta(\eta,t)$ for different values of Peclet number (P_{e1}). It is observed that tissue temperature decrease along the distance and this temperature increases as Peclet number increases. Figure 4.8 depicts the graph of tissue temperature profile $\theta(\eta,t)$ for different values of Peclet number (P_{e1}). It is observed that tissue

temperature increase with time and maximum temperature decreases as Peclet number increases. Figure 4.9 shows the graph of blood temperature profile $\psi(\eta,t)$ for different values of Peclet number (P_{e3}). It is observed that blood temperature decrease along the distance and this temperature decreases as Peclet number increases. Figure 4.10 depicts the graph of blood temperature profile $\psi(\eta,t)$ for different values of Peclet number (P_{e3}). It is observed that blood temperature increase reached maximum and later decrease with time and maximum temperature decreases as Peclet number increases. Figure 4.11 displays the graph of velocity profile $\phi(\eta,t)$ for different values of pressure gradient parameter (C). It is observed that velocity decrease along the distance and this velocity increases as the values of pressure gradient parameter increases. Figure 4.12 shows the graph of velocity profile $\phi(\eta,t)$ for different values of pressure gradient parameter (C). It is observed that velocity increase and later became steady with time and maximum velocity increases as values of pressure gradient increases. Figure 4.13 shows the graph of blood temperature profile $\psi(\eta,t)$ for different values of pressure gradient parameter (C). It is observed that blood temperature decrease along the distance and this temperature decreases as values of pressure gradient increases. Figure 4.14 depicts the graph of blood temperature profile $\psi(\eta,t)$ for different values of pressure gradient parameter (C). It is observed that blood temperature increase reached maximum and later decrease with time and maximum temperature decreases as values of pressure gradient increases. Figure 4.15 displays the graph of velocity profile $\phi(\eta,t)$ for different values of hematocrit (H). It is observed that velocity decrease along the distance and this velocity decreases as the values of hematocrit increases. Figure 4.16

shows the graph of velocity profile $\phi(\eta,t)$ for different values of hematocrit (H). It is observed that velocity increase and later became steady with time and maximum velocity decreases as values of hematocrit increases. Figure 4.17 shows the graph of tissue temperature profile $\theta(\eta,t)$ for different perfusion mass flow rate (α_1). It is observed that tissue temperature decrease along the distance and this temperature increases as perfusion mass flow rate increases. Figure 4.18 depicts the graph of tissue temperature profile $\theta(\eta,t)$ for different perfusion mass flow rate (α_1). It is observed that tissue temperature increase with time and maximum temperature increases as perfusion mass flow rate increases. Figure 4.19 shows the graph of blood temperature profile $\psi(\eta,t)$ against distance for different values of temperature ratio (α). It is observed that we have positive blood temperature profile when $\alpha<0$ and $\alpha>0$ while we have negative blood temperature profile when $\alpha=0$. This by implication means that variable thermal conductivity brings about increase in blood temperature. Figure 4.20 depicts the graph of blood temperature profile $\psi(\eta,t)$ against time for different values of temperature ratio (α). It is observed that we have positive blood temperature profile when $\alpha<0$ and $\alpha>0$ while we have negative blood temperature profile when $\alpha=0$. This by implication means that variable thermal conductivity brings about increase in blood temperature. Figure 4.21 shows the graph of tissue temperature profile $\theta(\eta,t)$ for different values of tissue power of heat added (γ_1). It is observed that tissue temperature decrease along the distance and this temperature increases as tissue power of heat added increases. Figure 4.22 depicts the graph of tissue temperature profile $\theta(\eta,t)$ for different values of tissue power of heat added (γ_1). It is observed that tissue temperature

increase with time and maximum temperature increases as tissue power of heat added increases. Figure 4.23 shows the graph of blood temperature profile $\psi(\eta,t)$ for different values of blood power of heat added (γ_2). It is observed that blood temperature decrease along the distance and this temperature increases as blood power of heat added increases. Figure 4.24 depicts the graph of blood temperature profile $\psi(\eta,t)$ for different values of blood power of heat added (γ_2). It is observed that blood temperature increase reached maximum and later decrease with time and maximum temperature increases as values of blood power of heat added (γ_2) increases.

4.1.3 Graphs of case 2

Graphical illustrations of Case 2 problem are presented in Figures 4.25 to 4.46 as:

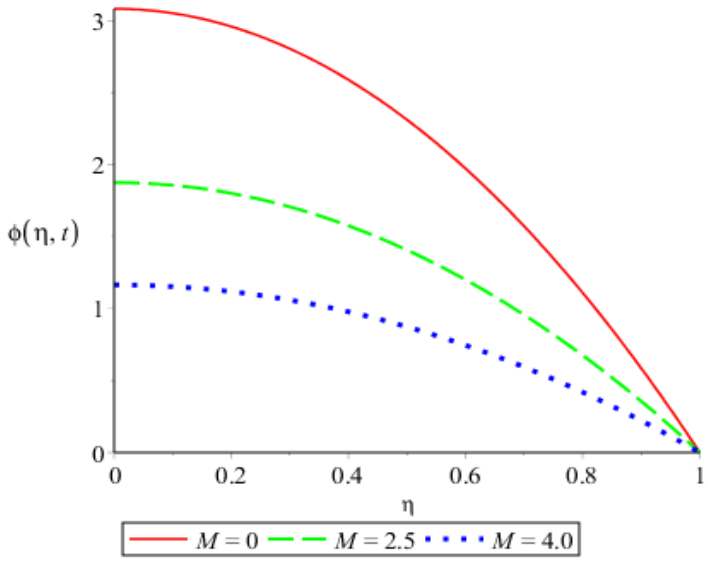

Figure 4.25: Graph of velocity profile against distance at M = 0, 2.5 and 4.0

Figure 4.25 shows the graph of velocity profile $\phi(\eta,t)$ against distance η for different values of Hartmann number.

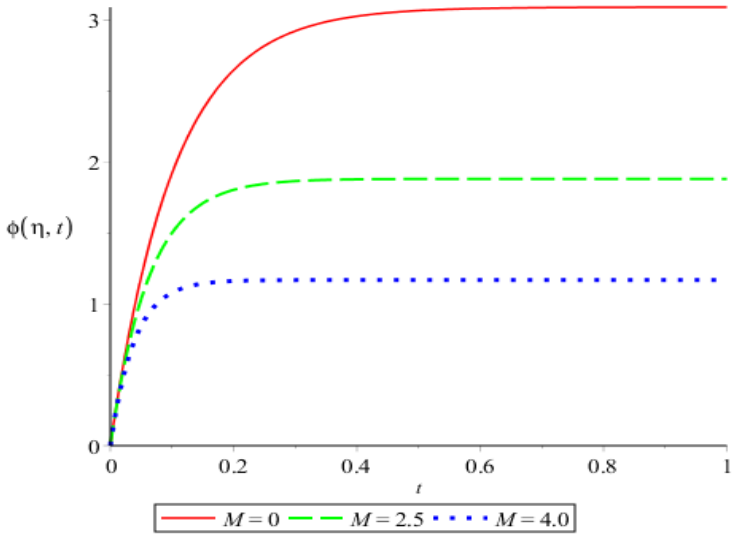

Figure 4.26: Graph of velocity profile against time at M = 0, 2.5 and 4.0

Figure 4.26 shows the graph of velocity profile $\phi(\eta,t)$ against time t for different values of Hartmann number.

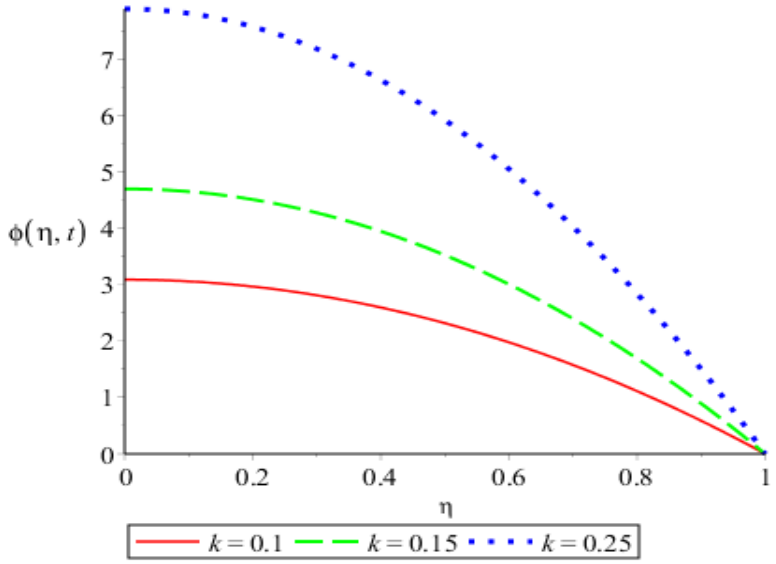

Figure 4.27: Graph of velocity profile against distance at k = 0.1, 0.15 and 0.25

Figure 4.27 shows the graph of velocity profile $\phi(\eta,t)$ against distance η for different values of permeability parameter

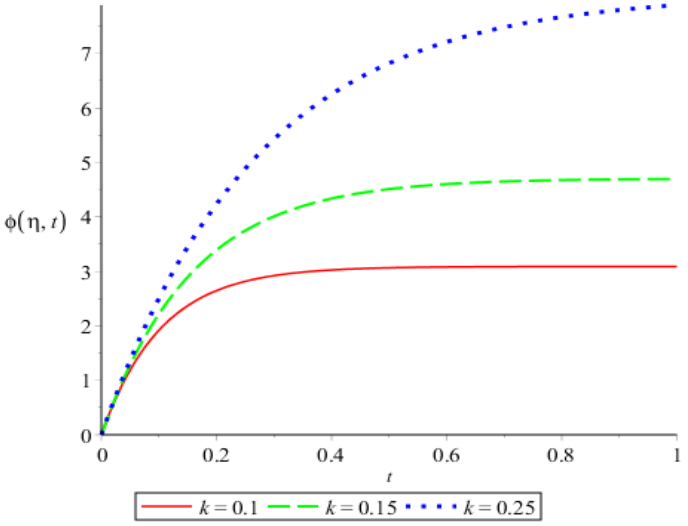

Figure 4.28: Graph of velocity profile against time at k = 0.1, 0.15 and 0.25

Figure 4.28 shows the graph of velocity profile $\phi(\eta,t)$ against time t for different values of permeability parameter.

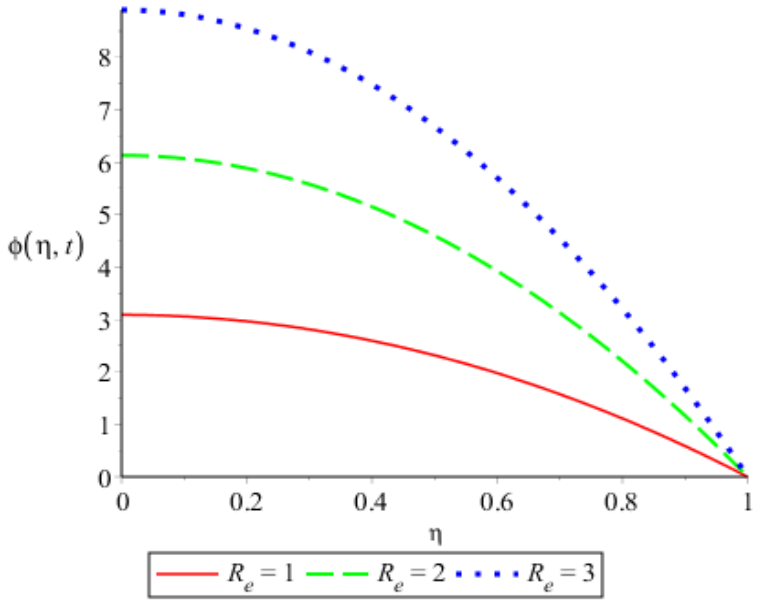

Figure 4.29: Graph of velocity profile against distance at R_e = 1, 2 and 3

Figure 4.29 shows the graph of velocity profile $\phi(\eta,t)$ against distance η for different values of Reynolds number

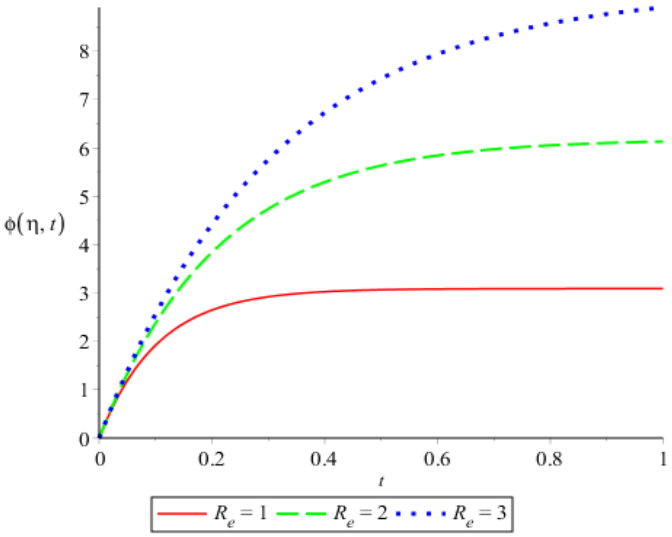

Figure 4.30: Graph of velocity profile against time at R_e = 1, 2 and 3

Figure 4.30 shows the graph of velocity profile $\phi(\eta,t)$ against time t for different values of Reynolds number.

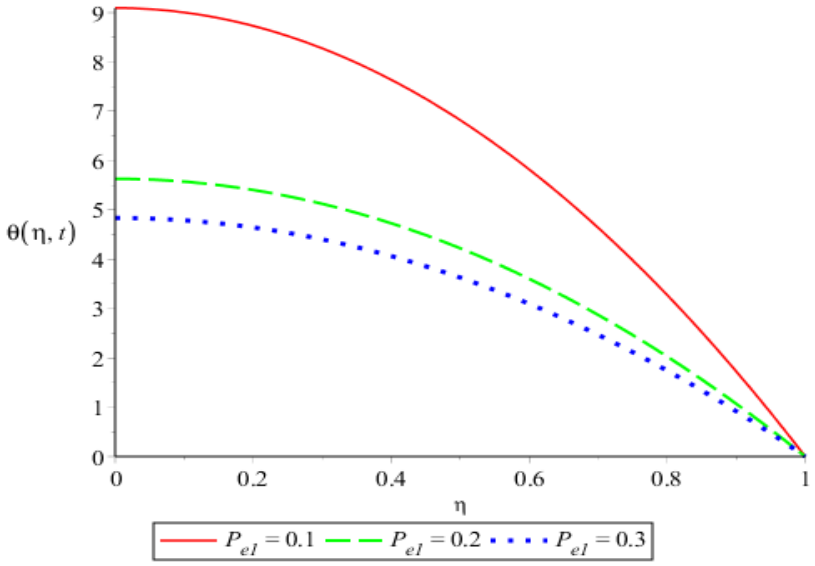

Figure 4.31: Graph of tissue temperature against distance at P_{e1} = 0.1, 0.2 and 0.3

Figure 4.31 shows the graph of tissue temperature profile $\theta(\eta,t)$ against distance η for different values of peclet number.

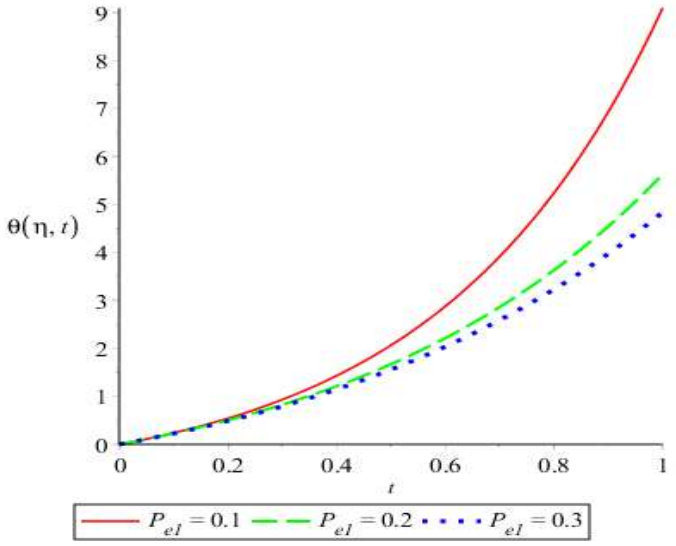

Figure 4.32: Graph of tissue temperature against time at P_{e1} = 0.1, 0.2 and 0.3

Figure 4.32 shows the graph of tissue temperature profile $\theta(\eta,t)$ against time t for different values of peclet number.

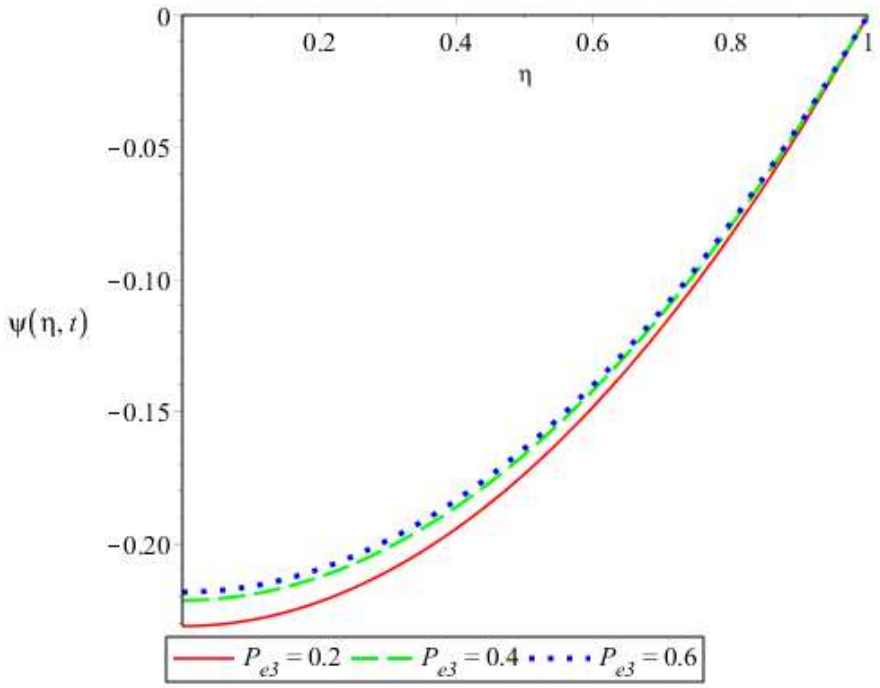

Figure 4.33: Graph of blood temperature against distance at P_{e3} = 0.2, 0.4 and 0.6

Figure 4.33 shows the graph of blood temperature profile $\psi(\eta,t)$ against distance η for different values of Peclet number

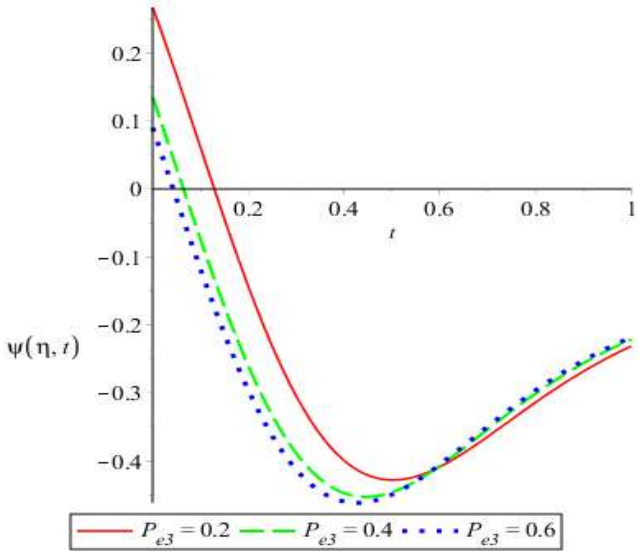

Figure 4.34: Graph of blood temperature against time at P_{e3} = 0.2, 0.4 and 0.6

Figure 4.34 shows the graph of blood temperature profile $\psi(\eta,t)$ against time t for different values of Peclet number

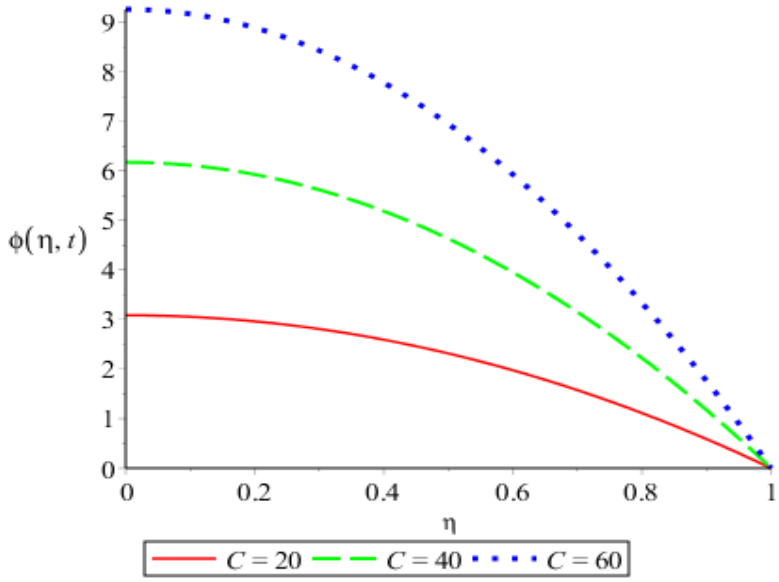

Figure 4.35: Graph of velocity profile against distance at C = 20, 40 and 60

Figure 4.35 shows the graph of velocity profile $\phi(\eta,t)$ against distance η for different values of pressure gradient parameter

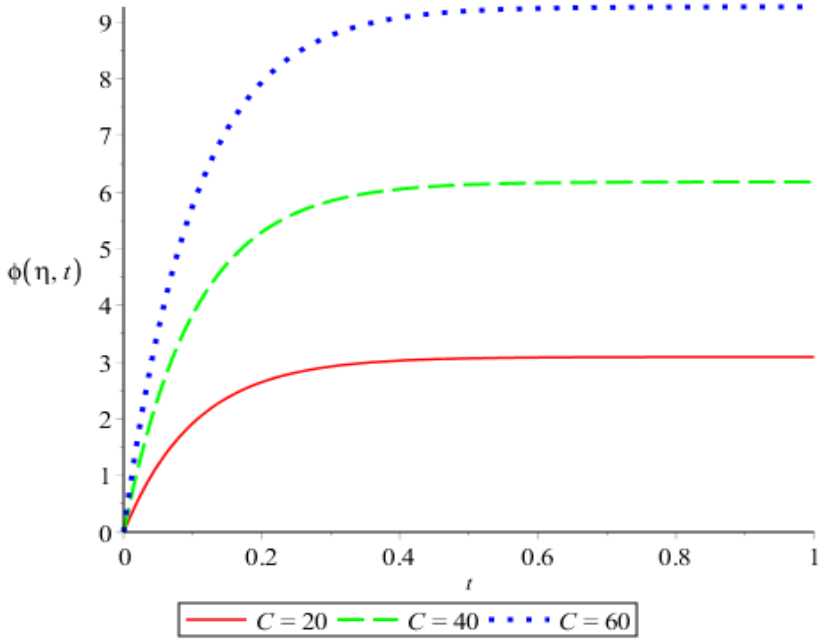

Figure 4.36: Graph of velocity profile against time at C = 20, 40 and 60

Figure 4.36 shows the graph of velocity profile $\phi(\eta,t)$ against time t for different values of pressure gradient parameter

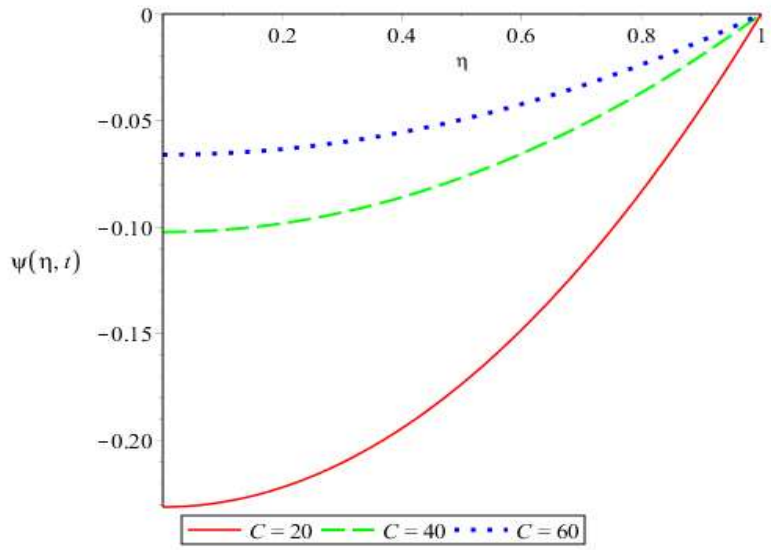

Figure 4.37: Graph of blood temperature against distance at C = 20, 40 and 60

Figure 4.37 shows the graph of blood temperature profile $\psi(\eta,t)$ against distance η for different values of pressure gradient parameter.

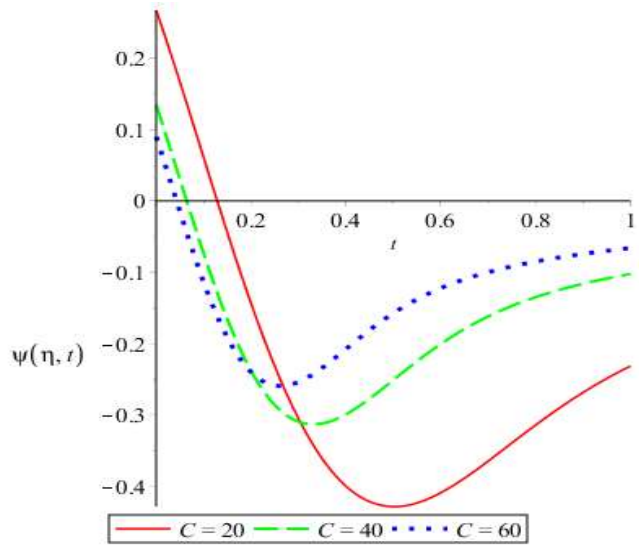

Figure 4.38: Graph of blood temperature against time at C = 20, 40 and 60

Figure 4.38 shows the graph of blood temperature profile $\psi(\eta,t)$ against time t for different values of pressure gradient parameter.

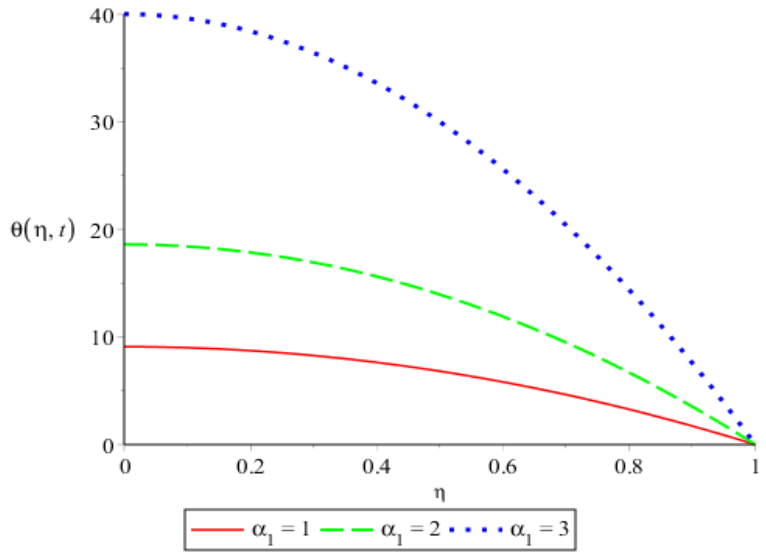

Figure 4.39: Graph of tissue temperature profile against distance at α_1 = 1, 2 and 3

Figure 4.39 shows the graph of tissue temperature profile $\theta(\eta,t)$ against distance η for different values of perfusion mass flow rate

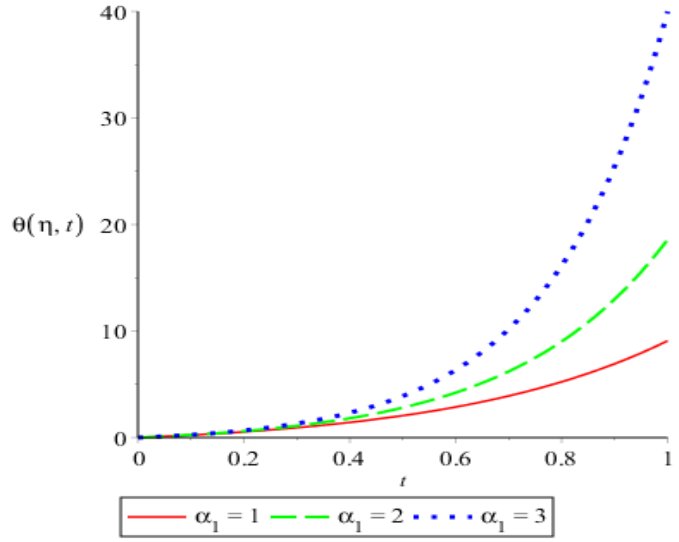

Figure 4.40: Graph of tissue temperature profile against time at α_1 = 1, 2 and 3

Figure 4.40 shows the graph of tissue temperature profile $\theta(\eta,t)$ against time for different values of perfusion mass flow rate

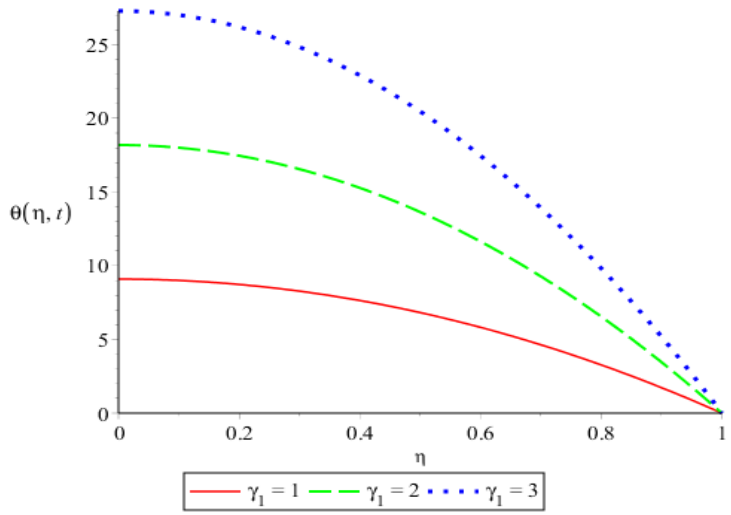

Figure 4.41: Graph of tissue temperature profile against distance at γ_1 = 1, 2 and 3

Figure 4.41 shows the graph of tissue temperature profile $\theta(\eta,t)$ against distance η for different values of tissue power of heat added

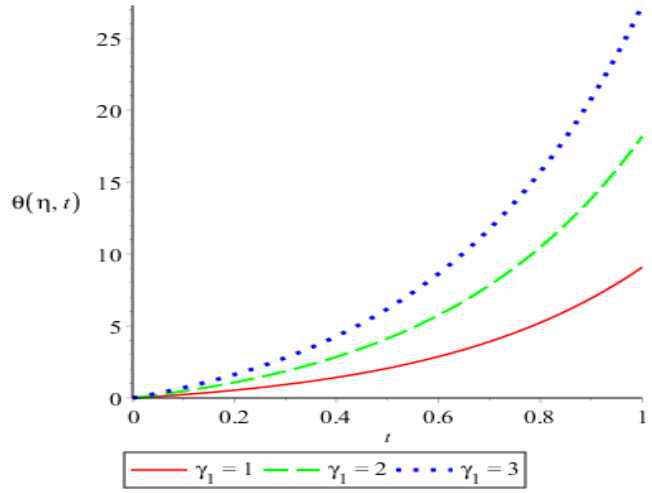

Figure 4.42: Graph of tissue temperature profile against time t at γ_1 = 1, 2 and 3

Figure 4.42 shows the graph of tissue temperature profile $\theta(\eta,t)$ against time t for different values of tissue power of heat added

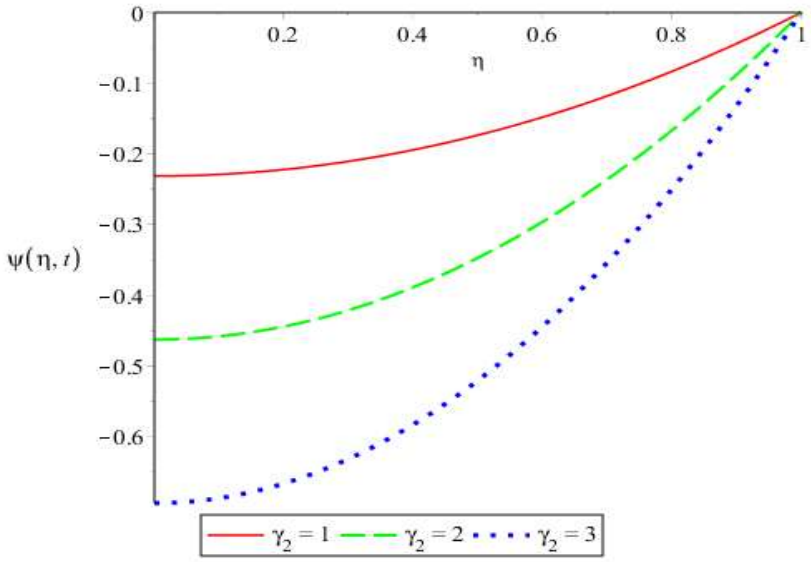

Figure 4.43: Graph of blood temperature profile against distance at γ_2 = 1, 2 and 3

Figure 4.43 shows the graph of blood temperature profile $\psi(\eta,t)$ against distance η for different values of blood power of heat added.

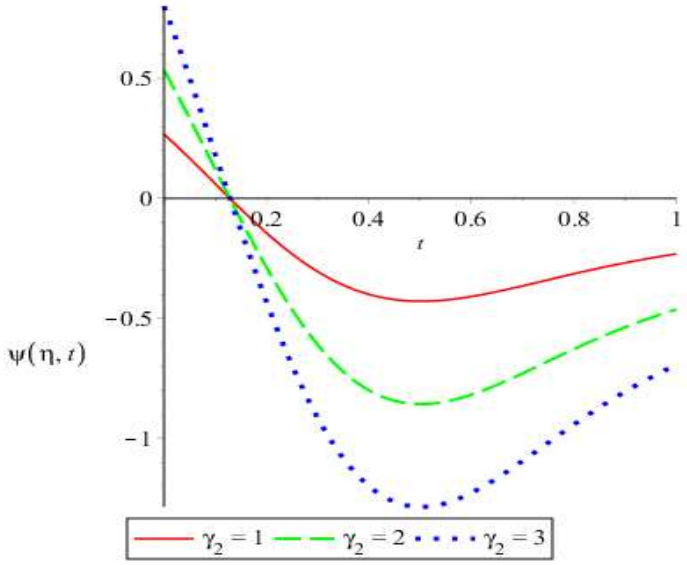

Figure 4.44: Graph of blood temperature profile against time at γ_2 = 1, 2 and 3

Figure 4.44 shows the graph of blood temperature profile $\psi(\eta,t)$ against time t for different values of blood power of heat added.

4.1.4 Discussion of results of case 2

Figure 4.25 displays the graph of velocity profile $\phi(\eta,t)$ for different values of Hartmann number (M). It is observed that velocity decrease along the distance and this velocity decreases as Hartmann number increases. Figure 4.26 shows the graph of velocity profile $\phi(\eta,t)$ for different values of Hartmann number (M). It is observed that velocity increase and later became steady with time and maximum velocity decreases as Hartmann number increases. Figure 4.27 depicts the graph of velocity profile $\phi(\eta,t)$ for different values of permeability parameter (k). It is observed that velocity decrease along the distance and this velocity increases as values of permeability parameter increases. Figure 4.28 shows the graph of velocity profile $\phi(\eta,t)$ for different values of permeability parameter (k). It is observed that velocity increase and later became steady with time and maximum velocity increases as value permeability parameter increases. Figure 4.29 displays the graph of velocity profile $\phi(\eta,t)$ for different values of Reynolds number (R_e). It is observed that velocity decrease along the distance and this velocity increases as Reynolds number increases. Figure 4.30 depicts the graph of velocity profile $\phi(\eta,t)$ for different values of Reynolds number (R_e). It is observed that velocity increase and later became steady with time and maximum velocity increases as Reynolds number increases. Figure 4.31 shows the graph of tissue temperature profile $\theta(\eta,t)$ for different values of Peclet number (P_{e1}). It is observed that tissue temperature decrease along the distance and this temperature decreases as Peclet number increases. Figure 4.32 depicts the graph of tissue temperature profile $\theta(\eta,t)$ for different values of Peclet number (P_{e1}). It is observed

that tissue temperature increase with time and maximum temperature decreases as Peclet number increases. Figure 4.33 shows the graph of blood temperature profile $\psi(\eta,t)$ for different values of Peclet number (P_{e3}). It is observed that blood temperature increases along the distance and this temperature increases as Peclet number increases. Figure 4.34 depicts the graph of blood temperature profile $\psi(\eta,t)$ for different values of Peclet number (P_{e3}). It is observed that blood temperature decrease reached minimum and later increase with time and minimum temperature decreases as Peclet number increases. Figure 4.35 displays the graph of velocity profile $\phi(\eta,t)$ for different values of pressure gradient parameter (C). It is observed that velocity decrease along the distance and this velocity increases as the values of pressure gradient parameter increases. Figure 4.36 shows the graph of velocity profile $\phi(\eta,t)$ for different values of pressure gradient parameter (C). It is observed that velocity increase and later became steady with time and maximum velocity increases as values of pressure gradient increases. Figure 4.37 shows the graph of blood temperature profile $\psi(\eta,t)$ for different values of pressure gradient parameter (C). It is observed that blood temperature increase along the distance and this temperature increases as values of pressure gradient increases. Figure 4.38 depicts the graph of blood temperature profile $\psi(\eta,t)$ for different values of pressure gradient parameter (C). It is observed that blood temperature increase reached minimum and later increase with time and minimum temperature increases as values of pressure gradient increases. Figure 4.39 shows the graph of tissue temperature profile $\theta(\eta,t)$ for different perfusion mass flow rate (α_1). It is observed that tissue temperature decrease along the distance and this

temperature increases as perfusion mass flow rate increases. Figure 4.40 depicts the graph of tissue temperature profile $\theta(\eta,t)$ for different perfusion mass flow rate (α_1). It is observed that tissue temperature increase with time and maximum temperature increases as perfusion mass flow rate increases. Figure 4.41 shows the graph of tissue temperature profile $\theta(\eta,t)$ for different values of tissue power of heat added (γ_1). It is observed that tissue temperature decrease along the distance and this temperature increases as tissue power of heat added increases. Figure 4.42 depicts the graph of tissue temperature profile $\theta(\eta,t)$ for different values of tissue power of heat added (γ_1). It is observed that tissue temperature increase with time and maximum temperature increases as tissue power of heat added increases. Figure 4.43 shows the graph of blood temperature profile $\psi(\eta,t)$ for different values of blood power of heat added (γ_2). It is observed that blood temperature increase along the distance and this temperature decreases as blood power of heat added increases. Figure 4.44 depicts the graph of blood temperature profile $\psi(\eta,t)$ for different values of blood power of heat added (γ_2). It is observed that blood temperature decrease reached minimum and later increase with time and minimum temperature decreases as values of blood power of heat added (γ_2) increases.

4.2 Validation of Result

To validate the present result, all introduced variable are made to be zero and compared to that of Shit and Roy (2017) results as shown in table 4.1.

Table 4.1: Comparison between present results and Shit and Roy (2017) results.

η	$\phi(\eta,t)$ **Polynomial Results**	$\phi(y,t)$ **Frobenius Results**	$\lvert\phi_{Fro}-\phi_{Pol}\rvert$
0	3.089322110	3.096264762	$6.94265\ x10^{-3}$
0.1	3.058428888	3.060160648	$1.73176x10^{-3}$
0.2	2.965749224	3.025482232	$5.973301x10^{-2}$
0.3	2.811283119	2.896357737	$8.507462\ x10^{-2}$
0.4	2.595030572	2.707927454	$1.128969x10^{-1}$
0.5	2.316991582	2.456533594	$1.395420x10^{-1}$
0.6	1.977166150	2.136702629	$1.595365x10^{-1}$
0.7	1.575554276	1.741228948	$1.656747x10^{-1}$
0.8	1.112155960	1.261065303	$1.489093x10^{-1}$
0.9	0.586971200	0.685122417	$9.815122x10^{-2}$
1.0	0	0	0

Table 4.1 shows comparison between the present results using generalized polynomial approximation method and Shit and Roy (2017) results using Frobenius method. Generally, the difference is of order 10^{-1}, 10^{-2} and 10^{-3}.

CHAPTER FIVE

5.0 CONCLUSION AND RECOMMENDATIONS

5.1 Conclusion

To check the validity of the present work, the numerical results are compared with that of Shit and Roy (2017). Thus the results are in good agreement with the mentioned literature review with the difference of order 10^{-1}, 10^{-2} and 10^{-3}. For constant and variable viscosity and blood thermal conductivity, the equations governing the blood flow and heat transfer in the cardiovascular system of human undergoing tumor treatment have been solved analytically using OGPAM.

The effects of the dimensionless parameters as shown on the graphs were analyzed. From the results obtained, all the parameters including Reynolds number, Peclet number, Hartman number, Hematocrit, Permeability parameter, Pressure gradient parameter, Temperature ratio, Perfusion mass flow rate, Tissue power of heat added and Blood power of heat added on the velocity and temperature have appreciable impact on the system. The main findings of the present study are listed as:

(i) Hartmann number reduces the flow velocity.

(ii) The flow velocity at the central region decreases gradually with the increase of magnetic field strength.

(iii) The permeability parameter k has an enhancing effect on the flow characteristics of blood.

(iv) Reynolds number and permeability parameter enhance flow velocity.

(v) Peclet number reduces both blood and tissue temperatures.

(vi) Pressure gradient enhances flow velocity while it reduces blood temperature.

(vii) Hematocrit reduces flow velocity.

(viii) The hematocrit and the pressure has a linear relationship as reported.

(ix) The lower range of hematocrit may leads to the further deposition of cholesterol at the endothelium of the vascular wall.

(x) Hematocrit contributes to the regulation of blood pressure.

(xi) Perfusion mass flow rate enhanced the tissue temperature.

(xii) Variable blood thermal conductivity enhances the blood temperature.

5.2 Recommendations

The present study brings out many interesting results on blood flow and heat transfer in the human cardiovascular system with variable viscosity dependent on red blood cells concentration (hematocrit). Since high blood pressure is very dangerous for cardiovascular system, the present models may be used by cardiologist as a tool for reducing the blood pressure. Also, since the Hartman number and the externally applied magnetic field gradually reduces the flow velocity, the present study is useful for the reduction of blood flow during surgery and magnetic resonance imaging (MRI).

In order to control blood pressure, it is suggested to vary viscosity of blood with red blood cell concentration (hematocrit). The results from this research work are recommended to form basis for further research on blood flow and heat transfer modeling. Since the hematocrit positively affects blood pressure, further study should examine the other factors such as diet, tobacco smoking, and overweight from a cardiovascular point of view.

5.3 Contributions to Knowledge

From our findings, the following are the achievements:

1. Model formulation by incorporating unsteadiness, variable viscosity and temperature-dependent blood thermal conductivity.
2. Analytical solution via OGPAM.
3. The flow velocity is at maximum value $\phi(\eta, t) = 3.1$ when $\eta = 0$.
4. Blood temperature attained maximum values when $\eta = 0$ and $t = 0.5$.

REFERENCES

Aiyesimi Y. M., & Salihu O. N. (2016). Effects of Pollutants and Atmospheric Temperature Rise on Agriculture. *Journal of the Nigerian Association of Mathematical Physics*, 35, 115 – 124.

Andreozzi, A., Brunese, L., Iasiello, M., Tucci, C., & Vanoli, G.P. (2019). Modelling Heat Transfer in Tumors: A Review of Thermal Therapies. *Ann. Biomed. Eng*., 47, 676–693.

Baish, J. W., Ayyaswamy, P. S., & Foster, K. R. (1986). Heat Transport Mechanism in Vascular Tissues: A Model Comparison. *Journal of Biomechanical Engineering,* 108(4), 324-331.

Bali, R., & Awasthi, U. (2011). Mathematical Model of blood Flow I Small Blood Vassel in the Presence of Magnetic Field. *Journal of Applied Mathematics,*2, 264-269.

Bessonov, N., Sequeira, A., Simakov, S., Vassilevskii, Y., & Volpert, V. (2016). Method of Blood Flow Modeling. *Journal of Math. Model Nat. Phenom.,* 11(1), 1-25.

Bhargava, R., Rawat, S., Takhar, H. S., & Beg, O. A. (2007). Pulsatile magneto-biofluid flow and mass transfer in a non-Darcian porous medium channels.*Meccanica,* 42(4), 247–262.

Blanc-Beguin, F., Nabily, S., Gieraltowski, J., Turzo, A., Querellou, S., & Salaun, P.Y. (2009). Cytotoxicity and GMI bio-sensor detection of maghemite nanoparticles internalized into cells. *J. Magn. Magn. Mater.*, 321, 192–197.

Blyakhman, F., Buznikov, N., Sklyar, T., Safronov, A., Golubeva, E., Svalov, A., & Kurlyandskaya, G. (2018). Mechanical, Electrical and Magnetic Properties of Ferrogels with Embedded Iron Oxide Nanoparticles Obtained by Laser Target Evaporation: Focus on Multifunctional Biosensor Applications. *Sensors* 2018, 18, 872.

Buchanan, J. R., Kleinstreuer, C. & Corner, J. K. (2000). Rheological effects on pulsatile hemodynamic in a stenosed tube, *Computers& Fluids,*29 (4), 695–724.

Caro, C. G. (2001). Vascular fluid dynamics and vascular biological and disease, *Mathematical Methods in the Applied Sciences,* 24(5), 1311–1324.

Caro, C. G., Pedley, T. J., Schroter, R. C. & Seed, W. A. (1978). *The Mechanis of the Circulation*, Oxford University Press, Oxford.

Chakeras, D. W., Kargarlu, A., Boundoulas, H., & Young, D. C. (2003). Effect of static magnetic field exposure of upto 8 Tesla on sequential human vital sign measurements. *Journal of Magnetic Resonance Imaging,* 18(21), 346–352.

Chakravarty, S. & Mondal, P. K. (1994). Mathematical modeling of blood flow through an overlapping stenosis. *Mathematical and Computer Modeling,* 19(4), 59–70.

Charny, C. K., Weinbaum, S., & Levin, U. L. (1990). An evaluation of the Weinbaum-Jiji bioheat equation for normal and hyperthermic conditions. *J Biomech Eng,* 1 (12), 80–7.

Chaturani, P., & Palanisamy, V. (1991). Pulsatile Flow of Blood with Periodic Body Acceleration," *International Journal of Engineering Science,* 29(1), 113-119.

Chen, I. H. (1985). Analysis of an Intensive Magnetic Field on Blood Flow: Part-2. *Journal of Bioelectronics*, 4(1), 55-61.

Chen, J., Lu, X. Y., & Wang, W. (2006). Non-Newtonian effects of blood flow on hemodynamic in distal vascular graft anastomoses. *Journal of Biomechanics* 39(2006), 1983–1995.

Chen, K.C., & Yeh, C. S. (2001) Extended Irreversible Thermodynamics Approach to Magnetorheological Fluids. *J. Non-Equilib. Thermodyn.*, 26, 355–372.

Chen, L., Chu, Y., Zhang, Y., Han, F., & Zhang, J. (2019). Analysis of Heat Transfer Characteristics of Fractured Surrounding Rock in Deep Underground Spaces. *Math. Probl. Eng*. 2019, 2019, 1926728.

Chen, M. M., & Holmes, K. R. (1980). Micro vascular contributions in tissue heat transfer. *Ann N Y Acad Sci*, 335, 137–50.

Craciunescu, O. I., & Clegg, S. T. (2001). Pulsatile blood flow effects on temperature distribution and heat transfer in rigid vessels. *J Biomech Eng*, 123, 500–5005.

Das, P., Colombo, M., & Prosperi, D. (2019). Recent advances in magnetic fluid hyperthermia for cancer therapy. *Colloids Surf. B Bio interfaces,* 174, 42–55.

Dash, R. K., Mehta, K. N., & Jayaraman, G. (1996). Casson fluid flowin a pipe filled with homogeneous porous medium, *International Journal of Engineering Science* 34(6), 1146–1156.

Dutta, J., & Kundu, B. (2021). An improved analytical model for heat flow in cancerous tumours to avoid thermal injuries during hyperthermia. *Proc. Inst. Mech. Eng. Part H J. Eng. Med.*, 235, 500–514.

Fan, W., Yung, B., Huang, P., & Chen, X. (2017). Nanotechnology for multimodal synergistic cancer therapy. *Chem. Rev.*, 117, 13566–13638.

Grossman, J.H., & McNeil, S.E. (2012). Nanotechnology in Cancer Medicine. *Phys. Today* 2012, 65, 38–42.

Gumez, R. C., Conejero, J. A., & Fernandez, I. G. (2017). Analysis of Blood Flow in One Dimensional Elastic Artery Using Navier-Stokes Conservation Law. arXiv: 1710.06258v2 (physics.flu-dyn) 19 Oct 2017.

Gupta, P. K., Singh, J., Rai, K.N., & Rai, S.K. (2013). Solution of the heat transfer problem in tissues during hyperthermia by finite difference–decomposition method. *Appl. Math. Comput.* 219, 6882–6892.

Haik, Y., Pai, V., & Chen, C. J. (2001). Apparent Viscosity of Human Blood in a High Statics Magnetic Field. *Journal of Magnetism and Magnetic Materials*, 225(1-2), 180-186.

Hooshmand, P., Moradi, A., & Khezry, B. (2015). Bioheat transfer analysis of biological tissues induced by laser irradiation. *Int. J. Therm. Sci.*, 90, 214–223.

Horng, T. L., Lin, W. L., Liauh, C. T., & Shih, T. C. (2015). Effects of pulsatile blood flow in large vessels on thermal dose distribution during thermal therapy. *American Association of Physicists in Medicine*, 34, 1312–1320.

Jaunich, M., Raje, S., Kim, K., Mitra, K., & Guo, Z. (2008). Bio-heat transfer analysis during short pulse laser irradiation of tissues. *Int. J. Heat Mass Transf.*, 51, 5511–5521.

Jiang, G., Li, W., Rao, S., Shi, Y., Tang, X., Zhu, C., Gao, P., Wang, Y., & Hu, S. (2016). Heat flow, depth–temperature, and assessment of the enhanced geothermal system (EGS) resource base of continental China. *Environ. Earth Sci*. 2016, 75, 1432.

Keller, K. H., & Seiler, L. (1971). An analysis of peripheral heat transfer in man. *J Appl Physiol*, 30, 779–86.

Kennedy, S., Roco, C., Deleris, A., Spoerri, P., Cezar, C., Weaver, J., Vandenburgh, H., & Mooney, D. (2018). Improved magnetic regulation of delivery profiles from ferrogels. *Biomaterials* 2018, 161, 179–189.

Khanafer, K. M., Bull, J. L., Pop, I., & Berguer, R. (2008). Influence of pulsatile blood flow and heating scheme on the temperature distribution during hyperthermia treatment. *Int. J. Heat Mass Transf.*, 50, 4883–4890.

Khanafer, K.M., Bull, J.L., Pop, I., & Berguer, R. (2007). Effects of pulsatile blood flow and heat transfer on the temperature sharing during hyperthermia treatment. *Int. J. Heat Mass Transf*. 2007, 90, 2733–2740.

Khushboo, T., Agrawal, A. K., Upadhyay, V., & Harish C. (2017). A Mathematical Study of Two Phase Pulmonary Blood Flow in Artery with Special Special Reference to Tuberculosis. *International Journal of Mathematics and Statistics Invention*, 45, 14 – 22.

Kinouchi, Y., Yamaguchi, H., & Tenforde, T. S. (1996). Theoretical analysis of magnetic field interactions with aortic blood flow, *Bioelectromagnetics*, 17(5), 21–32.

Kumar, P., Kumar, D., & Rai, K. N. (2015). A numerical study on dual-phase-lag model of bio-heat transfer during hyperthermia treatment. *J. Therm. Biol.*, 49(50), 98–105.

Kundu, B. (2016). Exact analysis for propagation of heat in a biological tissue subject to different surface conditions for therapeutic applications. *Appl. Math. Comput*, 285, 204–216.

Labadin, L., & Ahmadi, A. (2006). Mathematical Modeling of the Arterial Blood Flow. *Proceeding of the 2nd IMT-GT Regional Conference on Mathematics, Statistics and Applications at Universiti Sains Malaysia, Penang*, 13-15.

Lagendijk, J. W. (2000). Hyperthermia treatment planning. *Phys. Med. Biol*., 45, R61–R76.

Layek, G. C., Mukhopadhaya, S., & Gorla, R. S. R. (2009). Unsteady viscous flow with variable viscosity in a vascular tube with a double constriction. *International Journal of Engineering Science*, 47(29), 649–659.

Liepsch, D. W. (1986). Flow in tubes and arteries - A comparison, *Biorheology* 23(1986), 395–433.

Liepsch, D. W. (2002). An introduction to biofluid mechanics–basic models and applications, *Journal of Biomechanics* 35(2002), 415–435.

Lightfoot, E. N. (1974). Transport Phenomenon in Living System. Wiley, New York, 1974.

Lin, S. M., & Li, C.Y. (2016). Analytical solutions of non-Fourier bio-heat conductions for skin subjected to pulsed laser heating. *Int. J. Therm. Sci.*, 110, 146–158.

Liu, K. C., Wang, Y. N., & Chen, Y. S. (2012). Investigation on the bio-heat transfer with the dual-phase-lag effect. *Int. J. Therm. Sci.*, 58, 29–35.

Liu, X., Chen, X., Zhang, Y., Xie, J., Jia, X., Deng T., Zheng, Y., Davood, T., & Majid, Z. (2022). The thermal behavior of blood flow in the arteries with various radii and various stenosis angles using non-Newtonian Sisko model. *Alexandria Engineering Journal*, 61(9), 45, 7195-7201.

Maamoun, W., Badawi, M.I., Aly, A. A., & Khedr, Y. (2021). Nanoparticles in enhancing microwave imaging and microwave Hyperthermia effect for liver cancer treatment. *Rev. Adv. Mater. Sci.*, 60, 223–236.

MacDonald, D. A. (1979). On steady flow through modeled vascular stenoses. *Journal of Biomechanics*, 12(6), 13–20.

Majchrzak, E., & Stryczyski, M. (2021). Dual-phase lag model of heat transfer between blood vessel and biological tissue. *Math. Biosci. Eng.*, 18, 1573–1589.

Malatos, S., Raptis, A., & Xenos, M. (2016). Advances in Low-Dimensional Mathematical Modeling of the Human Cardiovascular System. *Journal of Hypertension and Management*, 2(2) 2474-3690.

Mishra, B. K., & Verma, N. (2007). Magnetic Effect on Blood Flow in a Multi-Stenosed Artery. *Applied Mathematics and Computation*, 20, 31 - 59.

Misra, J. C., & Chakravorty, S. (1986). Flow in arteries in the presence of stenosis, *Journal of Biomechanics* 19(1), 907–918.

Misra, J. C., & Shit, G. C. (2006). Blood flow through arteries in a pathological state: A theoretical study, *International Journal of Engineering Science* 44(6), 662–671.

Misra, J. C., & Shit, G. C. (2007). Role of slip velocity in blood flow through stenosed arteries: A non-Newtonian model, *Journal of Mechanics in Medicine and Biology* 7(2007), 337–353.

Misra, J. C., & Shit, G. C. (2009). Flow of a biomegnetic fluid in a channel with stretching walls, *ASME J ApplMech*, 7(4), 061006 (9 pages).

Misra, J. C., Shit, G. C., & Rath, H. J. (2008a). Flow and heat transfer of a MHD viscoelastic fluid in a channel with stretching walls: Some applications to hemodynamics, *Computers & Fluids*, 37 (7), 1–11.

Misra, J. C., Sinha, A., & Shit, G. C. (2008b). Theoretical analysis of blood flow through an arterial segment having multiple stenosis, *Journal of Mechanics in Medicine and Biology*, 8(2), 265–279.

Misra, J. C., Sinha, A., & Shit, G. C. (2011). Mathematical modeling of blood flow in a porous vessel having double stenoses in the presence of an external magnetic field, *International Journal of Biomathematics*, 4(2), 207–225.

Mohan, V., Prasad, V., Singh, J., & Varshney, N. K. (2012). Blood Flow in Arterioles: A Mathematical Study. *International Journal of Mathematical Archive*. 3(1), 113-117.

Muhammad, S. J., & Zuhaila, I. (2019). Simulation of Heat Transfer on Blood Flow through a Stenosed Bifurcated Artery. *Journal of Advanced Research in Fluid Mechanics and Thermal Sciences,* 60(2), 310-323.

Nayfeh, A. H. (1966). Oscillatory Two-Phase Flow Through a Rigid Pipe," *AIAA Journal*, 4(5), 1868-1871.

Olayiwola, R. O. (2022). Solving parabolic equations by Olayiwola's generalized polynomial approximation method. *International Journal of Mathematical Analysis and Modelling,* 5(3), 24 – 43.

Pennes, H. H. (1948). Analysis of tissue and arterial blood temperature in the resting human forearm. *J ApplPhys,* 23(3), 193–122.

Perez, G. C., Roy, M., & Sinha, A. (2017). Mathematical modelling of blood flow through a tapered overlapping stenosed artery with variable viscosity. Department of Mathematics, Jadavpur University, Kolkata, India.

Pries, A. R., Neuhaus, D., & Gaehtegnes, P. (1992). Blood Viscosity in Tube Flow: Dependence on Diameter and Hematocrit. *American Journal of Physiology*, 263, 1170-1778.

Ragab, M., Abouelregal, A.E., AlShaibi, H.F., & Mansouri, R.A. (2021). Heat Transfer in Biological Spherical Tissues during Hyperthermia of Magnetoma. *Biology,* 10, 1259.

Roemer, R. B., Forsyth, K., Oleson, J. R., Clegg, S. T., & Sim, D. A. (1988). The effect of hydralazine dose on blood perfusion changes during hyperthermia. *Int J Hyperthermia,* 4(4), 401–15.

Saffman, P. G. (1962). On the Stability of Laminar Flow of a Dusty Gas. *The Journal of Fluid Mechanics,* 13, 120-128.

Sankar, D. S., & Lee, U. (2008). Two-Fluid Herchel-Bilkey Model for Blood Flow in Catheterized Arteries. *Journal of Mechanical Sciences and Technology*, 22(5), 1008-1018.

Sanyal, D. C., Das, K., & Debnath, S. (2007). Effect of Magnetic Field on Pulsatile Blood Flow through an Inclined Circular Tube with Periodic Body Acceleration. *The Journal of Physiological Sciences*, 11(7), 43-56.

Sarkar, D., Haji-Sheikh, A., & Jain, A. (2015). Temperature distribution in multi-layer skin tissue in presence of a tumor. *Int. J. Heat Mass Transf*, 91, 602–610.

Sharan, M., & Popel, A. S. (2001). A Two-Phase Model for Flow of Blood in Narrow Tubes with Increased Effective Viscosity Near the Wall. *Biorheology,* 38(5-6), 415-428.

Shih, T. C., Kou, H. S., & Lin, W. L. (2006). Cooling Effect of Thermally Significant Blood Vessel in Perfused Tumor Tissue During Thermal Therapy. *International Commune Heat Mass*, 33, 135 – 141.

Shit, G. C., & Roy, M. (2012). Hydromagnetic pulsating flow of blood in a constricted porous channel: A theoretical study, in: *Proceedings of the world congress on Engineering*, London, UK, 1. 83–88.

Shit, G. C., & Roy, M. (2017). Pulsatile flow and heat transfer of a magneto micropolar fluid through a stenosed artery under the influence of body acceleration, *Journal of Mechanics in Medicine and Biology*, 11 (5), 643–661.

Song, C. W., Lokshina, A., Rhee, J. G., Paten, M., & Levitt, S. H. (1984). Implication of blood flow in hyperthermia treatments of tumors. *IEEE Trans Biomed Eng*, 31, 9–16.

Srivastava, H., Pet, M. A. & Horng, T. (2007). Bioheat Transfer and Thermal Heating for Tumor Treatment. *ApplTherm Eng*, 50, 837–847.

Srivastava, M., Upadhyay, V., Agrawal, A. K., & Pandey, P. N. (2012). A Generalized Mathematical Study of Two Phase Pulmonary Blood Flow in Lungs with Special Reference to Asthma. *Journal of Mathematics*, 1(6), 10-06.

Srivastava, V. P & Rivastava, R. (2009). Particulate Suspension Blood Flow Through a Narrow Catheterized Artery. *Computers & Mathematics with Applications*, 58(2), 227-238.

Sud, V. K., & Sekhon, G. S. (1985). Arterial Flow under Periodic Body Acceleration. *Bulletin of Mathematical Biology*, 47(1), 35-52.

Talukder, N., Karayannacos, P. E., Narem, R. M., & Vasco, J. S. (1977). An experimental study of fluid mechanics of arterial stenosis. *ASME Journal of Biomechanical Engineering*, 99(4), 74–82.

Taura, L. S., Ishiyaku, I. B., & Kawo, A. H. (2012). The use of continuity equation of fluid mechanics to reduce the abnormality of the cardiovascular system: A control mechanics of the human heart. *Journal of Biophysics and Structural Biology*, 4(1), 1-12.

Tian, F. B., Zhu, L., Fok, P. W., & Lu, X. Y. (2013). Simulation of a pulsatile non-Newtonian flow past a stenosed 2D artery with atherosclerosis. *Computers in Biology and Medicine* 43(5), 1098–1113.

Tripathi, K., Agrawal, A. K., Upadhyay, V., & Chandra, H. (2017). A Mathematical Study of Two Phase Pulmonary Blood Flow in Artery with Special Reference to Tuberculosis. *International Journal of Mathematics and Statistics Invention*, 1(5), 14-22.

Tu, C. & Deville, M. (1996). Pulsatile flow of non-Newtonian fluid through arterial stenosis. *Journal of Biomechanics,* 29(7), 899–908.

Urquiza, S. A., Blanco, P. J., Venere, M. J., & Feijoo, R. A. (2005). Multidimensional Modeling for the Carotid Artery Blood Flow. *Elsevier Science Direct*, 45, 131 – 149.

Varshney, G., Katiyar, V. K. & Kumar, S. (2010). Effect of magnetic field on the blood flow in artery having multiple stenosis: A numerical study. *International Journal of Engineering Science and Technology*, 2 (2), 67–82.

Versaci, M., & Palumbo, A. (2020). Magnetorheological Fluids: Qualitative and details comparison between a mixture model in the extended irreversible principle of a Thermodynamics framework and a Herschel–Bulkley experimental work on the elastoviscoplastic model. *Int. J. Non-Linear Mech.*, 118, 103 - 288.

Wagh, D. K., & Wagh, S. D. (1992). Blood Flow Considered as Magnetic Flow. *Proceeding of Physiology of Fluid Dynamics*, 45, 311-315.

Weinbaum, S., & Jiji, L. M. (1985). A new simplified bioheat equation for the effect of blood flow on local average tissue temperature. *JBiomech Eng*, 107, 131–139.

Weinbaum, S., Jiji, L. M., & Lemons, D. E. (1984). Theory and experiment for the effect of svascular temperature on surface tissueheat transfer—part 11: model formulation and solution. *J Biomech Eng*, 106, 331–341.

Whitemore, R. L. (1959). *Rheology of the circulation*, Pergaman Press, London, UK. 84–102.

Wissler, E. H. (1987). Comments on the new bioheat equation proposed by Weinbaum and Jiji. *J Biomech Eng*, 109, 131–139.

Womersley, J. R. (1955). Method for the Calculation of Velocity Rate of Flow and Viscous Dragin Arteries When the Pressure Gradient is known. *The Journal of Physiology*, 127(3), 533-563.

Young, D. F. (1979). Fluid mechanics of arterial stenoses, *ASME Journal of Biomechanical Engineering,* 101(5), 157–175.

Young, D. F., & Tsai, F. Y. (1973). Flow characteristics in models of arterial stenoses-I, Steady flow. *Journal of Biomechanics,* 6(4), 395–410.

Zhang, Q., Sun, Y., & Yang, J. (2021). Bio-heat transfer analysis based on fractional derivative and memory-dependent derivative heat conduction models. Case Study. *Therm. Eng*., 27, 101 - 211.